A THEORETICAL STUDY OF STRUCTURAL, ELECTRONIC, MAGNETIC AND OPTICAL PROPERTIES OF FILLED SKUTTERUDITES

By

Amit Shankar

Submitted

in fulfilment for the requirements of the

Degree of Doctor of Philosophy in Physics of

Mizoram University, Aizawl

Department of Physics

Mizoram University, Aizawl

Mizoram, India

July 2014

मिज़ोरम विश्वविद्यालय
भौतिक विज्ञान विद्यालय
आइजोल ७९६००४ मिज़ोरम
फोन : ०३८९-२३२८०४४(ङ),९४३६१४०५२३(मो०)
फैक्स : ०३८९-२३३०५२२
प्रोफेशर राम कुमार थापा
संकाय प्रमुख

MIZORAM UNIVERSITY
SCHOOL OF PHYSICAL SCIENCES
AIZAWL 796 004 MIZORAM
Phones : 0389 - 2328044(R), 9436140523(M)
FAX : 0389 - 2330522
E-mail : r.k.thapa@gmail.com
Prof. R. K. Thapa
Dean

Dated: 1st July, 2014

Certificate

*Certify that Sri Amit Shankar has carried out research work under my personal supervision and guidance in the Department of Physics, Mizoram University. The results of research work by Sri Amit Shnakar have been presented in this thesis entitled "**A theoretical study of structural, electronic, magnetic and optical properties of filled skutterudites**" and the same has been submitted to the Mizoram University, Aizawl, Mizoram, for the degree of Doctor of Philosophy.*

Sri Amit Shankar has fulfilled all the requirements under the Ph.D. regulations of the Mizoram University. To the best of my knowledge, this thesis as a whole or any part, thereof has not been submitted to this University or any other institution for any degree of diploma.

(Prof. R. K. Thapa)
Supervisor

Declaration of the Candidate

I, Amit Shankar, a Ph. D. scholar in Physics Department, Mizoram University, Aizawl, do hereby solemnly declare that the subject matter of this thesis is the record of the work done by me. I have duly worked on my Ph.D. thesis under the supervision of Prof. R. K. Thapa, Department of Physics, Mizoram University. This is being submitted to Mizoram University for the degree of Doctor of Philosophy in Physics and that I have not submitted this work to any other University or Institute for any other degree.

I also declare that the present investigations relate to bonafide research works undertaken by me and the title of the thesis is ***"A Theoretical Study of Structural, Electronic, Magnetic and Optical Properties of Filled Skutterudites".***

Dated: 1st July, 2014 *(Amit Shankar)*

Candidate

Acknowledgement

Writing the acknowledgement is something I have looked forward to for the last four years of my learning process. It gives me an opportunity to express my deep sense of gratitude and immense respect to the people who have directly or indirectly, knowingly or unknowingly, encouraged and assisted me in this episode of my academic development. This thesis would never have come about without the constant interaction I have had with lots of wonderful people around.

The journey of my academic development is commemorated with meeting of innumerable personality, the real architecture of my success. I fell that I was really fortunate to have the guidance and encouragement from my supervisor ***Prof. R. K. Thapa****, Dean, School of Physical Science, Mizoram University. I have been indebted to him, for his patience and kindness as well as academic experience, which enabled me to solve problems that I faced during this period of my academic development. Despite being busy with his academic and administrative work, he was always willing to drop everything to help me in every respect. I owe my every achievement to him and shall remain obliged to him forever.*

This work was supported by research fellowship from ***UGC, New Delhi*** *and I am grateful ever. I am also grateful to the teaching faculty of Department of Physics, Mizoram University, for useful discussion and their valuable suggestion during the course of my work. My heartfelt thanks go to* ***Prof. R. C. Tiwari****,* ***Prof. Zaithanzauva Pachuau****,* ***Prof. Suman Rai****,* ***Dr. V. Madhurima****,* ***Dr. Hranghmingthanga****,* ***Dr. Lalremruata and Dr. Lalthakimi Zadeng****. My thanks go to all the* ***non-teaching staff***

***members** of **Department of Physics** and **Dean's Office** especially **Pu mala**, **Mary** and **Mazooi**.*

*I am also thankful to my seniors **Dr. M. P. Ghimire**, **Dr. Sandeep** and **Dr. D. P. Rai** for their continuous support, encouragement and many valuable advices all kind of support and care I got during my work. I also thank **Dr. Jameson Maibam**, Manipur for his tips and suggestions for my work.*

*I acknowledge gratefully the warm and motherly hospitality and encouragement extended by **Mrs. Kamala Thapa**. She has always been a guide and source of inspirations, above all provided a homely atmosphere that has never let me feel the distance of my home. Thanks to **Pranay Da**, **Sunita Di**, **Raju Da and Purnima Bhauju** for their warm hospitality and help. For an enormous help and friendship, I owe an enormous thanks to all my friends, **Hari**, **Sanjay** and **Himangsu**. I had a lot of fun in the Hostel, with my hostel mates and **Engineering guys**, thank you guys. Your presence made me easier and comfortable in the hostel. All the research colleagues **Bena**, **Rebecca**, **Nirmala Devi**, **Mala** and many individuals have helped me to make years in the department into an interesting and enjoyable period of my life. I am also grateful to **Dr. Naddi Shankara (JNU) and Umesh Gomes (IIT, Kharagpur)** for their support, advises and encouragement.*

*I also thank **Nabin Uncle** and **his family**, **Sharda di, Sri. D. B. Cheetri** and **his family** for giving me support and care during my stay in Mizoram. I should not forget to thank my friends from Darjeeling especially **Dhanoj**, **Nagendra**, **Anup**, **Bibek** and **Dipendra** with whom I came to Mizoram University and **Sheila**, **Tshering** and **Nima**, they have been encouraging and supporting from my college time. My special thanks go to my friend and brother **Jolen Da** and **Anand Da** with **Saroja Di**. I have no words to express*

*my gratitude to **Sri Pema Lama**, for his valuable contribution because of which now I am here. I thank **Srijana** and **Varsha**, warm smiling and caring people, they were always there whenever I was in need.*

*Most importantly, none of these would have been possible without the love and support of my family. My **grandparents** are the one who lay down the foundation stone of my education. **My mother**, I always miss you, she was the source of all inspiration in my life. My father **Sri Aem Shankar**, **D.P uncle**, **Pramila aunt**, **Hem uncle**, **Sudhana aunt**, **Lama uncle** and **aunt** have been a constant source of love, concern, support and strength all these years and I express my cordial gratitude to them. They are the main force for whoever I am and it will continue everlasting. My sisters **Roma**, **Hrisika**, **Prativa**, **Prahelika (Funtoos)** and **Buttus**, my brother **Pratik** and **brother in law** have been always behind me to support at various levels with lovely smile, they are the ones who are always pushing me to go one step further ahead. I am also thankful to my close relatives, who understand me and have been encouraging me for an early completion of my work.*

*Finally, I would like to thank everybody, I failed to mention their names one by one but their constant support and encouragement helped me a lot for completion of my work. Once again I thank **God** for all the blessings bestowed upon me and giving all these wonderful people in my life and the opportunity to step forward in the excellent world of science.*

(Amit Shankar)

CONTENTS

List of Figures

List of Tables

Chapter 1

Introduction

1

Introduction

1.1 Skutterudite

The skutterudite compounds named after Skutterud region in Norway, exhibit a wealth of topical behaviours, they are the source and motivation of increasing interest and efforts to study and understand the underlying physics. All these materials "skutterudites" are derived from the archetypal mineral skutterudite $CoAs_3$, which was mined as the source of cobalt (Sales *et al.*, 2003) and was first identified by Oftedal in 1928. Binary skutterudites have cubic structure with general chemical formula of MX_3, where M is a transition metal (Co, Rh or Ir), while X is a pnictogen (P, As or Sb) (Sales *et al*., 1997). With Fe group transition metal (Fe, Os and Ru) as one of the members, no binary skutterudite can be synthesized under equilibrium condition. In the Fe group metal-skutterudite, the d^5-configuration of M^{3+} becomes stable after adding cationic atom, and this structural motif creates electron deficiency with different electronic and magnetic behaviour as reported by Uher (2001), Sales *et al*. (2003) and Leithe-Jasper *et al.* (2003). In order to stabilize such binary compounds of Fe, Os and Ru, it is necessary to add electropositive element as a filler atom, which leads to the total chemical formula $R_yM_4X_{12}$ (filled skutterudite) (Sales *et al.,* 1997). Here R can be rare earth elements (Morelli *et al.*, 1997; Nolas *et al.*, 2000) or alkaline earth elements (Chen *et al.,* 2001; Morelli *et al.*, 1997; Nolas *et al.*, 2000; Zhao *et al.*, 2006) or alkali elements (Pei *et al.*, 2006; Leithe-Jasper *et al.*, 2003). The degree of filling (y) can take its value upto 1,

however the real limit of y depends strongly upon the filler atom R and the host atom M_4X_{12}. Many workers have introduced rare-earth elements into this void and the different interesting results have been obtained for both *n*-type (Lamberton *et al.*, 2002) and *p*-type materials (Sales *et al.*, 1996). The filling of the voids with heavy atoms leads to the reduction of the thermal conductivity as shown by Nolas *et al*. (1999) and Uher (2003), and the substitution of the transition metal or pnictogen can control the electronic property, which enhances the thermoelectric property of the material (Lamberton *et al.*, 2002). The various combinations of guest and transition metal atom can tune the electron count, which give rise to various interesting electronic and magnetic properties of skutterudite. This method of combination of guest atom and transition metal may lead to interesting electronic and magnetic properties which may enhance the thermoelectric properties in case of of filled skutterudites (Nolas *et al.*, 1999; Uher, 2003). The modification of the crystal with other atoms does not affect the crystal structure. The freedom of the composition of the skutterudite structure without disturbing the crystal structure and the electronic properties of binary skutterutdite makes the system challenging for study with the aim for improved thermoelectric efficiency.

Filled skutterudite RM_4X_{12} (y = 1) crystallizes in unique body centred cubic structure of space group $Im\bar{3}$, where one R atom takes the atomic position of 2a (0, 0, 0) and one metal atom M located at 8c (0.25, 0.25, 0.25), while the X atom is located at the position of 24g (0, 0.35, 0.16). The positions of the remaining atoms in the unit cell are determined by symmetry operations associated with $Im\bar{3}$ space group. Fig. 1.1 shows the crystal structure of binary skutterudite and rare earth filled skutterudites. In filled skutterudite, R ions are loosely bounded in their M-X cage and the movement of the

(a)

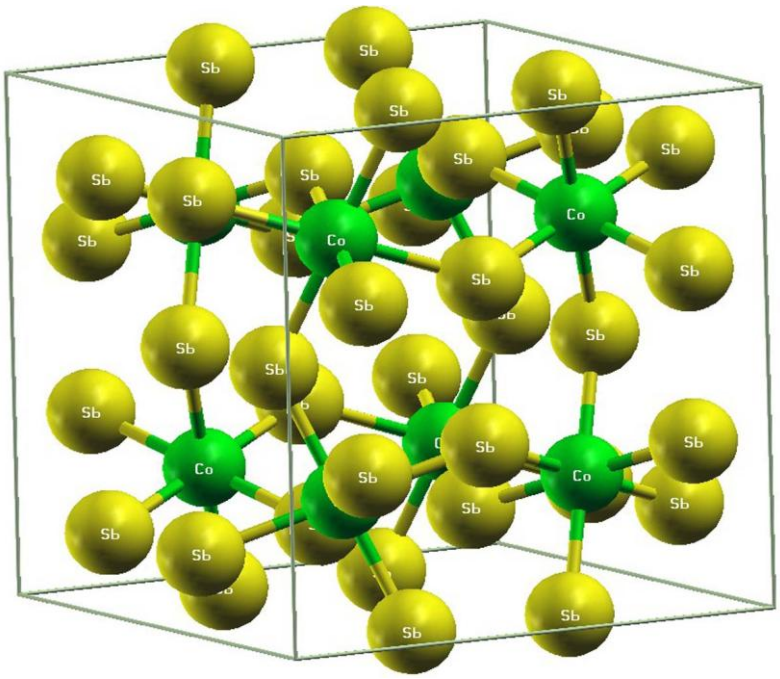

(b)

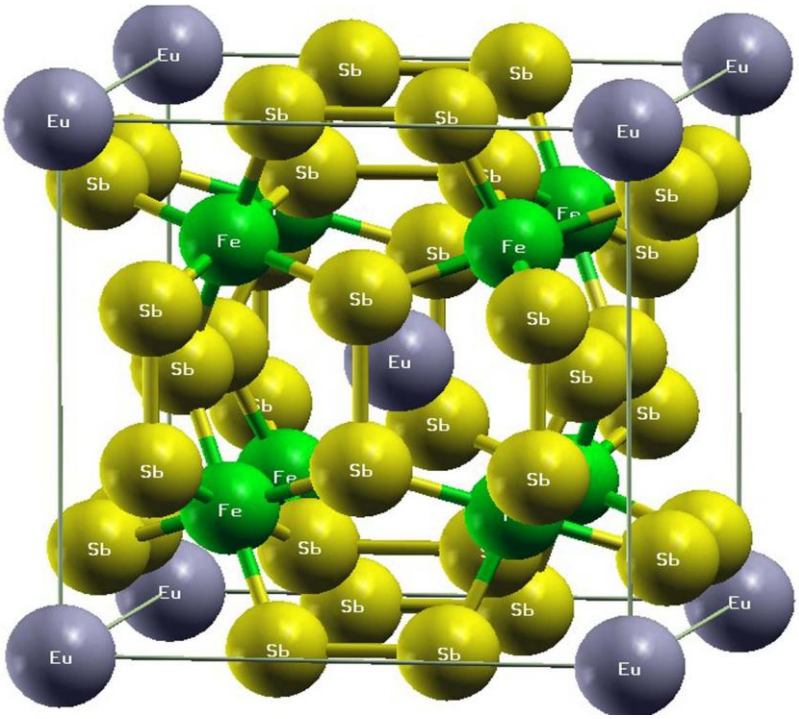

Fig. 1.1: Unit cell crystal structure of (a) binary skutterudite ($CoSb_3$) and (b) filled skutterudite ($EuFe_4Sb_{12}$).

rare-earth atom within these cages dampens the lattice vibration. Each unit cell of a crystal is composed of eight similar cubes, each cube with M atom at the centre and is surrounded by six nearly square four membered rings of X atoms (Kjekhus and Pedersen, 1961). Six different X rings give octahedral structure of M, with each face of a cube sharing quarter of one X ring. The space between octahedral is filled by the R. Each such ring runs parallel to the crystallographic axis and they are oriented mutually orthogonal to each other (Uher, 2001; Leithe-Jasper *et al.*, 2004).

These ternary metal pnictinides have received a large amount of attention in the last few years due to the anomalous physical property at low temperature and variety of strongly correlated electron ground states (Sales *et al*., 1997; Danebrock *et al.*, 1996). Several theoretical and experimental results (Sales *et al*., 1997) are available on electron correlation but they are not sufficient to understand the effects of electron-electron correlation on the physical properties of strongly correlated systems, even the role of transition metal and how the hybridization develops in rare earth skutterudites are also not clear. In M-X cage, rare earth atom is surrounded by 12 X atoms, which result in strong hybridization between R and X. This hybridization of *f*-electrons with the conduction electrons in filled skutterudite give rise to many interesting physical phenomena and dual nature (localized and itinerant) of *d* and *f*-electrons of transition and rare-earth electrons. The dual nature of *d* and *f*-electrons of transition and rare earth atoms give rise to various interesting and novel phenomena such as mixed valence behaviour. Danebrock *et al.* (1996) have studied the magnetic properties of filled skutterudite and have discussed the magnetic ordering with ferromagnetism and antiferromagnetism within the framework of rigid band structure. Sekine *et al.* (1997) have studied the low temperature properties of $PrRu_4P_{12}$ and $PrOs_4P_{12}$ by means of

electrical resistivity and magnetic susceptibility measurements. They have reported a metal-insulator transition at around 60K. Takeda and Ishikawa (1999) have studied the temperature dependence of the magnetic susceptibility $\chi(T)$, electrical resistivity $\rho(T)$ and low-temperature specific heat $C(T)$ of $CeRu_4Sb_{12}$. They have mentioned that $CeRu_4Sb_{12}$ is a Kondo compound with non-Fermi liquid behaviors at low temperatures. Maple *et al.* (2002) and Bauer *et al.* (2002) have reported superconductivity in $PrOs_4Sb_{12}$ at T_C = 1.85 K which involves the heavy fermion quasiparticles with an effective mass $m^* \sim 50\ m_e$. Leithe-Jasper *et al.* (2003) have reported the half-metal ferromagnetic behaviour of alkali-metal filled skutterudites. Quantum criticality, spin and charge gap formation, spin and charge density waves (Verma, 1976; Georges *et al.*, 1996; Stewart, 2001; Amato, 1997) have been the main interest for various theoretical and experimental investigations. Among the novel properties mentioned above, the Kondo insulator behaviour observed in *d* and *f*-electron systems is fascinating and has recently attracted considerable interest in theoretical and experimental condensed matter physics (Riseborough, 1992, 2000; Coleman, 2006). The Kondo insulators usually have cubic symmetry and a mixed-valence character for the *f*-elements. The available experimental data suggest that a system with one conduction electron and one spin per unit cell must be an insulator in agreement with the model proposed by Aeppli and Fisk (1992). These materials exhibit a very small gap, called a hybridization gap near the Fermi level, and it is believed that the gap arises in the lattice from the hybridization between the localized electrons (*d* or *f*-electrons) and the conduction electrons (Meisner *et al*., 1985). The strong electron-electron correlation results the enhancement of the low temperature properties such as the electronic specific heat capacity and static susceptibility as revealed by the electronic structure calculation (Takegahara *et al.*,

1993; Matheiss and Hamman, 1993). Also, promising applications as thermoelectric materials considerably boost the popularity of these compounds (Slack and Tsoukala, 1994; Slaes *et al*., 2003). The main theoretical interest in these materials is due to the existence of large many-body renormalizations. The gaps calculated from optical, magnetic, transport and thermodynamics properties are smaller than those obtained by band structure calculations by Takegahara *et al.* (1993), Matheiss and Hamman (1993) and Fu *et al.* (1994).

1.2 Thermoelectricity and Filled Skutterudite

The basic idea of the thermoelectric device is to convert heat coming from the sun or waste heat from various power plants into useful energy that may solve the demand of eco-friendly energy. However, the performance of commonly used thermoelectric material is only 10% of the thermodynamic limit. The lack of high efficiency materials has prevented the large installation of thermoelectric generators and solid state heating and cooling devices as power generation in deep space, remote sensors and thermal management of high power electronics (Rowe *et al.*, 1997). The efficiency of a thermoelectric device is improvised by increasing the dimensionless figure of merit (Z) of the material (Goldsmid, 1986; Mahan and Sofo, 1996), which is given by

$$ZT = \frac{\sigma S^2 T}{K_e + K_l}, \qquad K = K_e + K_l \tag{1.1}$$

where σ is the electrical conductivity, S is the Seebeck coefficient, T is absolute temperature and K is the thermal conductivity, K_e and K_l are the electronic and lattice thermal conductivity respectively. Therefore the improvement of figure of merit of thermoelectric materials has become a significant area of research for many waste heat and energy application. For metals and degenerate semiconductor, Seebeck coefficient

is given by (Cutler *et al.*, 1964),

$$S = \frac{8\pi^2 k_B^2}{3eh^2} m^* T \left(\frac{\pi}{3n}\right)^{2/3} \quad (1.2)$$

where m^* is effective mass, n is charge carrier concentration, k_B is Boltzmann's constant, e is the charge of an electron and h is Planck's constant. Thus, large thermopower $|S|$ corresponds to large effective mass which is equivalent to large density of states or flat bands at the Fermi level. High electrical conductivity requires a large mobility and large carrier (electrons or holes) concentration (n) (Zheng, 2008). Thus, from Eqs. 1.1 and 1.2, it is clear that in order to achieve high Z, the combination of high thermopower and electrical conductivity is required. This can be obtained by combining high electron density of states (high effective masses) with high carrier concentrations, and high mobility (Slack, 1995; Sales, 1998). Mahan and Sofo (1996) have mentioned that the ideal band structure for a thermoelectric material consists of an infinitely heavy, i.e. dispersionless band near the Fermi energy. In addition to low electron thermal conductivity, the lattice thermal conductivity also must be low in order to optimize the electronic transport property, such as in case of amorphous glass (Slack, 1995; Sales, 1998). These criteria lead to the concept of the ideal material with semiconducting electronic structure and atomic structure of a glass "electron crystal phonon-glass (ECPG)" (Slack, 1995; Sales, 1998). The R atoms vibrate locally and incoherently inside the weakly bonded M-X cage. This rattler reduces the heat carrying phonon mean free path with extra phonon scattering, which results in the reduced thermal conductivity (Nolas *et al.*, 1999). The filler atoms also have great influence on the electrical transport and affect parameters such as carrier concentration, carrier mobility, and carrier effective mass. Hence, in order to enhance Z it is essential to control the

carrier concentration through addition of guest atom without disturbing the carrier.

In order to be attractive and for successful applications of thermoelectric materials, its figure of merit must be between 1.5 to 3.0. Caillat and Borshchevsky (1993) have reported that the Jet Propulsion Laboratory (JPL) have identified several promising classes of materials, and in particular semiconductors with the skutterudite crystal structure. The previous studies have suggested that only 10% of the voids can be filled up using Ce as guest atom as shown by Chen *et al.* (1997), and in case of La it was reported to be upto 23%, giving the low ability to produce *n*-type filled skutterudite. Later on it was found out that the inclusion of Yb (Nolas *et al.,* 2000) and Tl (Sales *et al.,* 2000) as guest atom have the ability to produce high thermoelectric performance *n*-type filled skutterudites. The various theoretical (Yang *et al.*, 2007) and experimental (Nolas *et al.*, 2005; Shi, 2008) results prove that the heavy guest atom with small radius is more effective in reducing the thermal conductivity. The atomic radii of rare earth element decreases with the increasing atomic number due to lanthanide contraction, thus the rare earth elements, Gd - Lu is expected to bring much stronger rattling effect as compared to La - Eu. Therefore it is essential to include the rare earth elements from La to Lu in order to lower the thermal conductivity of filled skutterudite.

In the past two decades, a large volume of research reports have been published on the complex thermoelectric materials and filled skutterudite (Snyder and Toberer, 2008). Several experiments, such as Infrared (IR) absorption spectroscopy (Dordevic *et al*., 1999) and Raman spectroscopy (Nolas *et al*., 1996; Li *et al*., 2001) were not able to reveal the vibrational properties of filled skutterudite. Whereas the density functional theory (DFT) based first-principles calculation shows the effect of rattling in a binary

skutterudite showing the rattling is not Raman active (Feldman *et al.,* 2003).

In this thesis, we have studied the energy band structure and response to the incident photon energy along with the structural behaviour of the solids by using the density functional theory (DFT) (Hohenberg and Kohn, 1964; Kohn and Sham, 1965). DFT provides a modern tool to study the ground state properties of atoms, molecules, and solids. It is based on exact theorems of Hohenberg-Kohn and Kohn-Sham. Since, Kohn-Sham density functional theory (DFT) (Hohenberg and Kohn, 1964; Kohn and Sham, 1965) relies upon good approximations to the exchange-correlation energy as a functional of the electronic spin densities and the wave functions used, it is successful to calculate the ground state electronic structure and properties of solids and molecules. Perdew, Burke and Ernzerhof-Generalized Gradient Approximation (PBE-GGA) (Perdew *et al.,* 1996) being one of the most commonly used approximation for the exchange and correlation in the solid state calculations and it represent a well-tempered balance between computational efficiency, numerical accuracy and reliability. In PBE-GGA approximation it takes care of both density as well as its gradient at each point in the space. PBE reduces the chronic over binding of the local spin density approximation (LSDA) (Kohn and Sham, 1965) while LSDA often slightly underestimates equilibrium lattice constants by about 1-2%, PBE usually overestimates them by about the same amount, which results in overcorrection of lattice parameter dependent properties such as bulk moduli, phonon frequencies, magnetism, and ferroelectricity (Wu, 2006). The electronic structure calculations provide a quantitative way to discuss the phase transitions bonding characters, energy dispersions or topology of Fermi surfaces and magnetic properties are natural outputs of such calculations. In the non-relativistic case, the magnetic moment is the difference between the populations of the spin up and spin

down states and the magnetism can be discussed and justified with the model used. The LSDA and GGA are quite successful in understanding itinerant magnetism and structure trends in metals and intermetallic compounds. The effect of pressure on a material also can be analysed, it was found that the critical temperature of superconductivity may be increased under pressure, which might be due to the enhancement of electron phonon coupling under pressure.

Nordstrom *et al.* (1996) have described the semiconducting nature of $CeFe_4P_{12}$ and $CeFe_4Sb_{12}$ with hybridized (Ce-4*f* with Fe-3*d* and *p*-states of pnictogen) band gap and trivalent state of Ce, using density functional theory based electronic structure calculation. Singh and Mazin (1997) have studied the thermoelectric (TE) and transport properties of $La(Fe,Co)_4Sb_{12}$ using first principles electronic structures calculation within the local-density approximation. Their results suggest that the samples with higher La filling and lower hole concentrations may have even better TE properties. Shirotani *et al.* (1997) have prepared the sample of $LaRu_4As_{12}$ and $PrRu_4As_{12}$ and showed their superconducting nature at low temperature around 10.2 K and 2.4 K respectively with the role of arsenic for the enhancement of superconductivity. Nolas *et al*. (1998) have studied the impact of partial void filling of the polycrystalline La filled antimonides and mentioned that a relatively small concentration of La in the voids results in a relatively large decrease in the lattice thermal conductivity. Nanba *et al.* (1999) have measured the temperature dependence of the optical reflection spectra in the case of $CeRu_4P_{12}$ and $PrRu_4P_{12}$ in the energy region 5 meV- 4 eV. $CeRu_4P_{12}$ is a semiconductor, but $PrRu_4P_{12}$ was found to show a metal-insulator transition at around 60 K. Fornari *et al.* (1999) have shown that a gap is opened up upon filling the metallic CoP_3 with La using the electronic structure calculations for CoP_3 and $LaFe_4P_{12}$. Nolas *et*

al. (2000) have presented the evidence of a relatively high dimensionless figure of merit (*ZT*) in a polycrystalline skutterudite partially filled with Yb ions in the voids of $CoSb_3$. The magnetic properties of $GdRu_4P_{12}$ and $TbRu_4P_{12}$ have been studied by means of electrical resistivity, magnetic susceptibility and magnetization measurements by Sekine *et al*. (2000). Their measurements indicate that Gd and Tb ions in the compounds have trivalent state and an antiferromagnetic transition at T_N = 22 K for $GdRu_4P_{12}$ and two successive antiferromagnetic transitions at T_N = 20 K and T_1 = 10 K for $TbRu_4P_{12}$. Sekine *et al.* (2000) have revealed the mixed valance metallic with ferromagnetically ordered nature of $EuRu_4P_{12}$. Diley *et al.* (2000) have shown the hole-doped metallic nature with low carrier density of $YbFe_4Sb_{12}$, where Yb ion vibrates thermally with large amplitude in the weakly bounded oversized atomic ‘‘cage’’. Devos *et al.* (2001) have studied the bonding in skutterudites using the $CoSb_3$ example. They have calculated the theoretical electronic structure and the band structure in both density-functional theory and empirical tight-binding frameworks.

Kanai *et al*. (2002) have studied the electronic structure of $CeRu_4Sb_{12}$ using Ultrahigh-resolution photoemission (UHRPE) spectra, and they have found the density of states (DOS) at low temperatures to have semimettalic nature. Sugawara *et al*. (2002) have performed the de Haas-van Alphen experiment and confirmed the heavy mass in $PrOs_4Sb_{12}$ indicating this compound to be the first member of heavy fermion-superconductor. Cao *et al.* (2003) have carried out the X-ray-absorption fine-structure (XAFS) measurements to study the local electronic structure and the local lattice distortions of Pr and Os atoms in $PrOs_4Sb_{12}$. Their results suggest that the Pr valence is very close to 3^+ while Os is close to metallic in this material. Harima and Takeghara (2003) have investigated the metal insulator transition, heavy fermion behaviour and

superconductivity in $PrRu_4P_{12}$, $PrFe_4P_{12}$ and $PrOs_4P_{12}$ respectively using band structure calculations. The main conduction band consisting of *p*-orbitals of pnictogen surrounding the rare earth ions has a nesting property and strongly hybridizes with one of 4*f*-electron. One of the other conduction bands does not have mixing matrix elements with 4*f*-electron, resulting in the unique band structure in $CeOs_4Sb_{12}$. They also have found that the density of states at Fermi level increases from P to Sb, due to the rising of the relative position of the Fe-*d*(t_2g) bands and the increase in the interatomic distances in $LaFe_4X_{12}$ (X = P, As, Sb). The study of $ThFe_4P_{12}$ by Takeghara and Harima (2003) found that it is a direct band gap semiconductor with band gap of 0.45 eV using FLAPW method. Bauer *et al*. (2004) have investigated the physical properties of single crystals of filled skutterudite compounds EuT_4Sb_{12} (T = Fe, Ru, Os) by means of X-ray diffraction. They have reported that $EuRu_4Sb_{12}$ and $EuOs_4Sb_{12}$ exhibit ferromagnetism with Curie temperatures of T_C = 4 K and 9 K, respectively. Mutou *et al*. (2004) have used a simple tight-binding model for the description of the electronic structure of few Ce-based filled skutterudites and studied the optical conductivity spectrum. Sanada *et al*. (2005) have studied the electronic structure of rare-earth filled skutterudite. They found the anomalous electronic states, where multi *f*-electron ions show strongly correlated electron behaviour. Prytz *et al*. (2006) have used the density functional theory (DFT) and electron energy loss spectroscopy (EELS) to determine the dielectric function of Co-based binary skutterudites. They have found the qualitative agreement between the calculated theoretical and experimental values. Sichelschmidt *et al*. (2006) have presented the optical investigations of the filled skutterudites AFe_4Sb_{12} with divalent cations A = Yb, Ca, Ba. They have reported a very similar pseudogap structure in the optical conductivity developed in the far-infrared spectral region at temperatures

below 90 K for each of these compounds. Recknagel *et al.* (2007) have performed the Spark plasma sintering (SPS) synthesis of $CoSb_3$ and $LaFe_4Sb_{12}$ and studied the microstructure and mechanical properties and calculated the numerical values of Young's moduli of 148 GPa and 141 GPa for $CoSb_3$ and $LaFe_4Sb_{12}$ respectively. Krishnamurthy *et al.* (2007) have used combine X-ray absorption spectroscopy (XAS) and local spin density calculations to show that the filled skutterudite $Eu_{0.95}Fe_4Sb_{12}$ is a ferrimagnet in which the Fe-3*d* moment and the Eu^{2+} 4*f* moments are magnetically ordered with dominant antiferromagnetic coupling.

Nouneha *et al*. (2007) have performed the band energy and thermoelectricity calculation of $LaFe_4Sb_{12}$ and $CeFe_4Sb_{12}$ using tight binding linear muffin-tin orbital (TB-LMTO) and full potential linear augmented plane wave (FP-LAPW) method. They have reported $LaFe_4Sb_{12}$ to be metallic with a band crossing two times the Fermi level and found direct energy gap equal to 0.81 eV, whereas $CeFe_4Sb_{12}$ was found to be a semiconductor with indirect energy gap equal to 0.66 eV. The large thermopower at room temperature originates from the *d*-states of Fe, that hybridize with the *p*-states of Sb and there is no contribution from the Ce states in case of $CeFe_4Sb_{12}$. Khenata *et al.* (2007) have shown the indirect band gap semiconducting nature of $CeFe_4P_{12}$ and $ThFe_4P_{12}$ using full-potential linearized augmented plane-wave plus local orbitals (FP-LAPW+lo) method based elastic, electronic and optical properties calculations.

Adroja *et al*. (2008) have investigated the spin gap formation and its relation to the charge gap, in several Ce, Yb and U based compounds using inelastic neutron scattering techniques. They have found out the magnitude of the spin gap is in agreement with that observed through the optical study. Benalia *et al.* (2008) have investigated the indirect energy band gap semiconducting nature of $CeFe_4P_{12}$ using FP-LMTO method based

electronic structure calculation. Hachemaoui *et al*. (2009) have used full potential-augmented plane wave + linear orbital (FP-APW+lo) method to calculate the electronic structure of $CeFe_4As_{12}$ and $CeFe_4Sb_{12}$. They have found the indirect band gap (0.238 eV and 0.125 eV for $CeFe_4As_{12}$ and $CeFe_4Sb_{12}$ respectively) semiconducting nature of these compounds. The authors have also studied the elastic constants of $LaFe_4A_{12}$ (A = P, As and Sb). They have shown the value of calculated bulk modulus decreases as we move from P to Sb and the elastic constants increases with the increasing pressure. Benalia *et al.* (2009) have reported the indirect band gap semiconducting nature of $CeRu_4P_{12}$ using elastic and electronic structure calculation. Qiu *et al*. (2011) have prepared and systematically investigated the electrical and thermal transport properties of fully filled skutterudite RFe_4Sb_{12} (R = Ca, Sr, Ba, La, Ce, Pr, Nd, Eu, and Yb). They have found out that the lattice constants of RFe_4Sb_{12} increase almost linearly with increasing ionic radii of the fillers (R) with maximum power factor value around 34 $\mu W/cmK^2$ with low K_L due to the "rattling" effect of the fillers for $CeFe_4Sb_{12}$, $PrFe_4Sb_{12}$, and $YbFe_4Sb_{12}$ at 750 K. Xu *et al.* (2011) have done the systematic study of electronic structure and transport properties of $LaFe_4Sb_{12}$ and $CeFe_4Sb_{12}$ using full-potential linearized augmented plane wave method and semi-classical Boltzmann theory. They have found the large density of states near the Fermi level and concluded that $LaFe_4Sb_{12}$ is more suitable thermoelectric candidate compare to $CeFe_4Sb_{12}$. Ameri *et al.* (2013) have reported the $CeOs_4Sb_{12}$ is elastically stable, brittle and metallic at zero pressure and narrow indirect band gap semiconducting under pressure effect using the full-potential linear muffin-tin orbital method.

In this thesis we report the systematic study of structural, electronic, magnetic and optical properties of rare earth filled skutterudites RM_4X_{12} (R = Eu; M = Fe, Ru, Os; X

= P, As, Sb), using self-consistent full-potential linearized augmented plane wave (FP-LAPW) method based on density functional theory (DFT). The electronic property of any system strongly depends on its crystal structure, hence to study the structure of the filled skutterudite crystal, we have obtained the lattice parameters corresponding to its equilibrium energy and elastic constants of the crystal by volume deformations. The elastic constants are calculated by taking the second order derivative of the total energy of the strained crystal. From the independent elastic constants obtained by volume deformation, other parameters such as bulk moduli, young's moduli, Debye temperature etc. are also evaluated. The electronic properties studied in this thesis are concerned with investigation of energy band structures followed by density of states (DOS). The optical property is studied by calculations of the frequency dependent isotropic complex dielectric function, refractive index, reflectivity and energy loss spectra followed by the optical conductivity of the crystal as a function of photon energy of incident radiation. The optical spectra obtained are correlated with the corresponding energy band structures. From the energy bands and DOS evaluated near the Fermi level, the thermoelectric applications of the given filled skutterudites are also investigated.

The chapters in the thesis are organized as follows:

In Chapter 2, we describe the theory and methodology used in our calculation. We will also present an outline of the density functional theory (DFT) within LSDA, GGA and FP-LAPW method.

In Chapter 3, we discuss the structural and elastic property along with sound velocity and Debye temperature in the case of filled skutterudite RM_4X_{12} (R = Eu; M = Fe, Ru, Os; X = P, As, Sb).

The Chapter 4 deals with the electronic band structures, density of states and

magnetic properties of filled skutterudites under consideration.

In Chapter 5, we present the results and discussions related to optical properties of RM_4X_{12} (R = Eu; M = Fe, Ru, Os; X = P, As, Sb).

Chapter 6 contains the concluding part of the thesis where we summarize the studies done on RM_4X_{12} (R = Eu; M = Fe, Ru, Os; X = P, As, Sb) and it is followed by references.

Chapter 2

Theoretical Formalism and Methodology

2

Theoretical Formalism and Methodology

In this chapter, the theory, methods and approximations used in the calculations of elastic constants, DOS, band structures, magnetic moments and optical spectra are discussed.

2.1 Density Functional Theory

Condensed matter physics is related to the study of the physical, electronic and other basic properties of matter. We can examine and describe the nature by various experimental science, but the interaction between the experiment and theory is also necessary, in order to understand and describe the basic property of matter. The properties of matter under normal conditions are governed by the behaviour motion of electron the field of the nuclei of the constituent atoms. Thus the knowledge of the electronic band structure is essential to understand the physical properties of matter. In condensed matter physics, one studies the physical properties of the systems within the framework of already established quantum theory. Many solids, crystals are ordered and can be successfully described mathematically neglecting the defect in the crystal, which plays a major role in describing the property of matter.

In reality the matter is more complex and composed of a collection of interacting atoms, which may also be affected by some external field. Various techniques that have been developed to describe the motion of collection atoms and electrons are based on Density Functional Theory. Density functional theory (DFT) is one the most widely

used technique obtainable on computational condensed matter physics, which was originally invented and developed by Kohn, Hohenberg and Sham (Hohenberg and Kohn, 1964; Kohn and Sham, 1965), provides a modern tool to study the ground state properties of atoms, molecules and solids. The Hohenberg and Kohn theorem reduces the many body problems of N electrons with 3N spatial coordinates by employing the concept of functional of the electron density. The Kohn and Sham theorem defines energy functional of the system and gives evidences to prove that the proper ground state density minimizes this energy functional. In short, these theorems assert that all information available in the wave function is also available in the ground state electron density and this density can be found through energy minimization procedures. The computational challenge of calculating the properties of a complex material is also greatly reduced. Thus, intractable many-body problem of interacting electrons in a static external potential, within the framework of Kohn-Sham DFT (KS-DFT) is reduced to a tractable problem of non-interacting electrons moving in an effective potential. The effective potential contains the external potential and the effects of Coulomb interactions between the electrons, the exchange and correlation interactions. Modeling the latter two interactions becomes the challenge within KS-DFT.

2.2 Details of Theoretical Methodology

According to Born Oppenheimer approximation the nuclei of the many body system in an electronic structure calculation are seen as fixed generating a static external state is represented by a wave function $\Psi(\vec{r}_1,...,\vec{r}_N)$ satisfying the many-electron Schrodinger equation:

$$H\Psi = \left[T + V + U\right]\Psi = \left[\sum_{i}^{N} -\frac{h^2}{2m}\nabla_i^2 + \sum_{i}^{N} V(\vec{r}_i) + \sum_{i}^{N} U(\vec{r}_i, \vec{r}_j)\right]\Psi = E\,\Psi \qquad (2.1)$$

where H is the electronic Hamiltonian, N is the number of electrons, T is the N-electron kinetic energy, V is the N-electron potential energy from the external field, U is the electron-electron interaction energy for the N-electron system. The operators T and U are common for similar systems, so are called Universal operators. V is system dependent, so is non-universal. Now the difference between a single particle problem and the much more complex many particle problem is the interaction term U. DFT provides a way to systematically map the many-body problem with U onto a single particle problem without U. In DFT the particle density $n(\vec{r})$ for a normalized Ψ is given by:

$$n(\vec{r}) = N\int d^3r_1 \int d^3r_2 ... \int d^3r_N \Psi^*(\vec{r}_1, \vec{r}_2, ..., \vec{r}_N)\Psi(\vec{r}_1, \vec{r}_2, ..., \vec{r}_N) \qquad (2.2)$$

In reverse way, this relation states that for a given ground-sate density $n_0(\vec{r})$ it is possible to construct the corresponding ground-state wave-function $\Psi_0(\vec{r}_1, \vec{r}_2, ..., \vec{r}_N)$. In other words $\Psi_0(\vec{r}_1, \vec{r}_2, ..., \vec{r}_N)$ is a functional of $n_0(\vec{r})$ and hence the ground sate expectation values of an observable $\hat{O}$ is also a functional of $n_0(\vec{r})$.

$$O[n_0] = \left\langle \Psi[n_0] \middle| T + V + U \middle| \Psi[n_0] \right\rangle \qquad (2.3)$$

In particular, the ground state energy is a functional of $n_0(\vec{r})$

$$E_0 = E_0[n_0] = \left\langle \Psi[n_0] \middle| T + V + U \middle| \Psi[n_0] \right\rangle \qquad (2.4)$$

$$= \left\langle \Psi[n_0] \middle| T \middle| \Psi[n_0] \right\rangle + \left\langle \Psi[n_0] \middle| V \middle| \Psi[n_0] \right\rangle + \left\langle \Psi[n_0] \middle| U \middle| \Psi[n_0] \right\rangle \qquad (2.5)$$

$$= T[n_0] + V[n_0] + U[n_0] \qquad (2.6)$$

where the contribution of the external $\langle \Psi[n_0] | V | \Psi[n_0] \rangle$ potential can be written in terms of the ground-state density n_0

$$V[n_0] = \int V(\vec{r})\, n_0(\vec{r}) d^3r \tag{2.7}$$

More commonly, the contribution of the external potential $\langle \Psi | V | \Psi \rangle$ can be written clearly in terms of the density *n* as

$$V[n] = \int V(\vec{r})\, n(\vec{r}) d^3r \tag{2.8}$$

A system is defined by a definite non-universal functional V, as $T[n]$ and $U[n]$ are universal. For a given system with *V* as its external potential

$$E[n] = T[n] + U[n] + \int V(\vec{r})\, n(\vec{r})\, d^3r \tag{2.9}$$

In regard to $n(\vec{r})$, taking for granted one has got dependable terms for $T[n]$ and $U[n]$. A successful reduction of the energy functional will produce the ground state density $n_0(\vec{r})$ and thus all other ground state observables.

The second KS-theorem makes it possible to use the variational principle of Rayleigh-Ritz in order to find the ground-state density. Out of the infinite number of possible densities, the one which minimizes *E*[*n*]is the ground-state density corresponding to the external potential $V(\vec{r})$. Of course, this can be done only if an approximation to $\langle \Psi[n] | T + V | \Psi[n] \rangle$ is known. But having found $n(\vec{r})$, all knowledge about the system is within reach. It is useful to stress the meaning of the energy functional $E[n]$ once more. When it is evaluated for the density $n(\vec{r})$ corresponding to the particular $V(\vec{r})$ for this solid, it gives the ground state energy. When it is evaluated for any other density however, the resulting number has no physical meaning (Cottenier,

2002). Taking the energy functional without electron-electron interaction energy term

$$E_S[n]=\left\langle \Psi_S\left[n\right]\middle|\widehat{T_S}+V_S\middle|\Psi_S\left[n\right]\right\rangle \tag{2.10}$$

where $\widehat{T_S}$ indicates the non-interacting kinetic energy and $\hat{V}_S$ is an external effectual potential in which the particles are moving. Clearly, in $\hat{V}_S$ if $n_S(\hat{r})=n(\hat{r})$ is selected

$$\hat{V}_S=\hat{V}+\hat{U}+(\hat{T}-\hat{T}_S) \tag{2.11}$$

Consequently, we can solve the Kohn-Sham equations for this assisting non-interacting system,

$$\hat{H}_{KS}\phi_i=E_i\phi_i \tag{2.12}$$

which produces the ϕ_i orbital that reproduces the density $n(\vec{r})$ of the authentic many-body system,

$$n(\vec{r})=n_s(\vec{r})=\sum_i^N\left|\phi_i(\vec{r})\right|^2 \tag{2.13}$$

The effective single-particle potential can be written in more detail as

$$V_S(\vec{r})=V(\vec{r})+\int\frac{e^2n_S(\vec{r}')}{\left|\vec{r}-\vec{r}'\right|}d^3r'+V_{XC}\left[n_S(\vec{r})\right] \tag{2.14}$$

The second term in the above Eq. 2.14 stands for the so-called Hartree expression with the electron-electron Coulomb repulsion, while the last expression V_{XC} is called the exchange correlation potential. Now, the Hartree expression and V_{XC} depend on $n(\vec{r})$ which depends on the ϕ_i, which in turn relies on $\hat{V}_S$. Now the problem is that the Kohn-Sham equation has to be solved in a self-consistent way. One typically begins with a first guess $n(\vec{r})$ then works out the corresponding $\hat{V}_S$ and solves the Kohn-Sham equations for the ϕ_i (Kohn and Sham, 1965). The techniques in DFT are complex and

different and can be understood by considering the following two approaches. Firstly the techniques that apply a local density rough calculation (LDA). The LDA is decided exclusively and based on the qualities of the electron density. The significant supposition of this approximation is that for a molecule with many electrons in a gaseous state, the density is consistent throughout the molecule. This is not the case for molecules where the electron density is decidedly not consistent. This approximation does however work well with electronic band structure of solids and hence illustrates the scope of energies in which electrons are allowed or not allowed. Outside of these applications, however, LDA's are not very acceptable.

Secondly, the technique that unites the electron density calculations with a gradient correction factor. A gradient in mathematics is a function that measures the rate of change of some property. In this case, the gradient seems to explain the non-uniformity of the electron density and as such is known as gradient-corrected.

2.3 Kohn-Sham Equation

Since the total energy of the system is

$$E(n) = T(n) + \int V_{ext}(r) n(r)\, dr + V_H[n] + E_{XC}[n] \tag{2.15}$$

where T is the kinetic energy of the system, V_{ext} is an external potential acting on the system, E_{XC} is the exchange-correlation energy and Hartree energy is given by

$$V_H = \frac{e^2}{2} \int \frac{n(r)\, n(r')}{|r - r'|} dr\, dr' \tag{2.16}$$

The straight forward application of this formula has two barriers: First, the exchange-correlation energy E_{XC} is not known precisely and second, the

kinetic term must be created in terms of the charge density. As was first suggested by Kohn and Sham (1965), the charge density $n(r)$ can be written as the sum of the squares of a set of orthonormal wave functions $\phi_i(r)$:

$$n(r)=\sum_i^N |\phi_i(r)|^2 \tag{2.17}$$

where the single particle wave function $\phi_i(r)$ are the N lowest-energy solutions to the Kohn-Sham equation for N non-interacting electrons moving in an effectual potential $V_{eff}(r)$ given by

$$-\frac{\hbar^2}{2m}\nabla^2\phi_i(r)+V_{eff}(r)\phi_i(r)=\varepsilon_i\phi_i(r) \tag{2.18}$$

where the effectual potential is defined to be

$$V_{eff}(r)=V_{ext}(r)+e^2\int\frac{n(r')}{|r-r'|}dr'+\frac{\delta E_{XC}[n]}{\delta_n} \tag{2.19}$$

This system is then solved iteratively until self-consistency is approached. Note that the eigen values ε_i have no physical meaning but the total sum matches the energy of the entire system E through the equation:

$$E=\sum_i^N \varepsilon_i - V_H[n]+E_{XC}[n]-\int\frac{\delta E_{XC}[n]}{\delta n(r)}n(r)dr \tag{2.20}$$

There are several ways in which Kohn-Sham theory can be applied depending on what is being examined. In solid state calculations, the local density approximations are still commonly used along with plane wave basis sets, as an electron gas approach is more suitable for electrons delocalized through an infinite solid. In molecular calculations, however, more complicated functional are needed and a huge variety of exchange-correlation functional have been developed for chemical applications. Some of these are incompatible with the uniform electron gas approximation; however, they

must reduce to LDA in the electron gas limit. The main difficulty with DFT is that the precise functional for exchange and correlation are not identified except for the free electron gas. However, rough calculations exist which allow the calculation of certain physical parameters rather precisely. In physics the most widely used approximation is the local-density approximation.

2.4 Local Density Approximation (LDA)

The LDA has been the most widely used approximation to the exchange-correlation energy in the density functional theory (DFT), for a long time. It has been proposed by Kohn and Sham (1965). The main idea is to consider general inhomogeneous electronic systems as locally homogeneous and then to use exchange-correlation hole corresponding to the homogeneous electron gas. LDA has been widely applied to portray a variety of close-ranged exchange-correlation interactions for instance, covalent bonding systems. However, LDA has serious limitation that this approximation cannot provide estimation to the long-ranged exchange-correlation interaction as typified by the Van der Waals (VdW) interaction. The VdW interaction is one of the long-ranged electronic interactions which mainly add to the first stage of the material reactions such as the chemical reaction, crystal growth and physical absorption. To assess the VdW interaction, many efforts have been devoted to develop useful calculating recipes for the non-local exchange-correlation term. The Hohenberg-Kohn theorem states that the energy of the ground state of a system of electrons is a functional of the electronic density especially, the exchange and correlation (XC) energy is also a functional of the density (this energy can be seen as the quantum part of the electron-electron interaction). This XC functional is not identified accurately and must be

addressed appropriately with correct approxiamtion. LDA is the simplest approximation for this functional, it is local in the sense that the electron exchange and correlation energy at any point in space is a function of the electron density at that point only. The XC functional is the total of a correlation functional and an exchange functional:

$$E_{XC} = E_X + E_C \tag{2.21}$$

LDA uses the exchange for the uniform electron gas of a density equal to the density at the point where the exchange is to be assessed

$$E_{XC} = \int d^3r\, n(\vec{r}) \left(\frac{-3e^2}{4\pi} \right) \left(3\pi^2 n(\vec{r})^{1/3} \right) \tag{2.22}$$

It is found that all quantities are represented as functional of the electronic charge density. The significant point that makes this system easier to solve is that the efficient possibility is local. Therefore there is no more complication added in solving Schrodinger equation. Of course, this is only true if the exchange-correlation energy can be portrayed as a function of the local charge density. A technique of doing this is known as the local density approximation (LDA). As mentioned above in LDA, the exchange-correlation energy of an electronic system is built by taking for granted that the exchange-correlation energy for each electron at a point $\vec{r}$ in the electron gas is equal to the exchange-correlation energy for each electron in an identical electron gas that has the same electron density at the point $\vec{r}$. It follows therefore

$$E_{XC}\left[n(\vec{r})\right] = \int \varepsilon_{XC}(n(\vec{r}))n(\vec{r})dr \tag{2.23}$$

with

$$\varepsilon_{XC}(n(\vec{r})) = \varepsilon_{XC}^{\text{hom}}(n(\vec{r})) \tag{2.24}$$

where $\varepsilon_{XC}^{\text{hom}}(n(\vec{r}))$ is exchange-correlation energy in identical electron gas. Eq. 2.24 is

the supposition that the exchange-correlation energy is purely local. Several parameterizations for $\varepsilon_{XC}^{\text{hom}}(n(\vec{r}))$ exist, such as parameterization of Perdew and Zunger (1981).

2.5 Generalized Gradient Approximation (GGA)

The exchange-correlation energy has a gradient expansion of the type

$$E_{XC}[n(r)] = \int A_{XC}[n(r)]n(r)^{4/3}dr + \int C_{XC}[n(r)]\left|\nabla n(r)\right|^2 \Big/ n(r)^{4/3}dr + ... \qquad (2.25)$$

which is asymptotically valid for densities that vary slowly in space. The LDA retains only the leading term of the above Eq. 2.25. It is well known that a straightforward evaluation of this expansion is ill-behaved, in this sense that it is not monotonically convergent and it exhibits singularities that cancel out only when an infinite number of terms are re-summed. In fact, the first order correction worsens the results and the second order correction plagued with divergences (Ma and Brueckner, 1968; Fetter and Walecka, 1971). The largest error of this approximation actually arises from the gradient contribution to the correlation term. The early work of Gross and Dreizler (1981) provided a derivation of second order expansion of the exchange density matrix, which was later re-analyzed and extended by Perdew (1985). GGAs are typically based either on theoretical developments that reproduce a number of exact results in some known limits, for example 0 and ∞ density or the correlation potential in the He atom, or are generated by fitting a number of parameters to a molecular database. Normally, these improve over some of the drawbacks of the LDA, although this not always the case. The basic idea of GGAs is to express the exchange-correlation energy in the following form:

$$E_{XC}[n(r)] = \int n(r)\varepsilon_{XC}[n(r)]dr + \int F_{XC}[n(r),\ \nabla n(r)]dr \qquad (2.26)$$

where the function F_{XC} is asked to satisfy a number of formal conditions for the exchange-correlation hole, such as sum rule, long-range decay and so on. This cannot be done by considering directly the bare gradient expansion. What is needed for the functional is a form that mimics a re-summation to infinite order and this is the main idea of the GGA, for which there is not a unique recipe. Naturally, not all the formal properties can be enforced at the same time and differentiates one functional from another. A thorough comparison of different GGAs is done by Filippi *et al.* (1994).

The generalized gradient approximation (GGA) has attracted much attention for its abstract simplicity and moderate computational workloads. At present, two GGA functional, one suggested by Becke and Perdew (BP) and the other suggested more recently by Perdew and Wang (PW), are the most popular ones in the literature (Perdew *et al.,* 1996). Many calculations assessing the accuracy of the GGA have been reported and commonly demonstrate that the GGA substantially corrects the LDA error in the cohesive energies of molecules and solids. Generalized gradient approximations (GGA's) to the exchange-correlation (XC) energy in density-functional theory are at present receiving increasing attention as a straightforward substitute to improve over the local-density approximation (LDA) in *ab initio* total-energy calculations (Kresse and Furthmuller, 1996). The lattice parameters always rise in comparison with the LDA, a closer agreement with experimental data is reported for alkali metals, *3d* and some *4d* metals.

2.6 Local Spin Density Approximation (LSDA)

In magnetic systems or, in other words we can say that the systems where open electronic shells are involved, better approximations to the exchange-correlation

functional can be obtained by introducing the two spin densities such as $n\uparrow(\rho(r))$ and $n\downarrow(\rho(r))$ in LDA to obtained LSDA. The $E_{xc}[n^{\sigma}(r)]$ energy is a functional of both the spin-up and down spin densities. With such distinction, the Kohn-Sham equation can be written as:

$$\left[-\frac{1}{2}\nabla^2 + V_{KS}^{\sigma}\right]\phi_i^{\sigma}(r) = \varepsilon_i^{\sigma}\phi_i^{\sigma}(r) \tag{2.27}$$

where V_{KS}^{σ} and $n^{\sigma}(r)$ are the spin extension of the previous quantities and

$$V_{KS}^{\sigma}(r) = v(r) + e^2\int\frac{\rho(r')}{|r-r'|}dr' + \frac{\delta E_{xc}[n\uparrow, n\downarrow]}{\delta\rho^{\sigma}(r)}$$

$$v(r) = \frac{\delta E_{xc}[n\uparrow, n\downarrow]}{\delta\rho^{\sigma}(r)}, \rho^{\sigma}(r) = \sum|\phi_i^{\sigma}|^2, \rho(r = \sum_{\sigma}\rho^{\sigma}(r) \tag{2.28}$$

The imbalance between $n\uparrow$ and $n\downarrow$ producing the magnetization M = $n\uparrow$ - $n\downarrow$, is given by the exchange-correlation potential $U_{\sigma\ xc}$ (r) which accounts for the different populations $n\uparrow$ and $n\downarrow$ by the derivative. In the local spin density approximation (LSDA), the exchange and correlation contributions are separated as:

$$\begin{aligned} E_X^{LSDA}[\rho(r)] &= \sum_{\sigma}\int\varepsilon_{XC}^{\hom}(\rho^{\sigma}(r))\,\rho^{\sigma}(r)\,dr \\ E_C^{LSDA}[\rho(r),\xi(r)] &= \int\left[\varepsilon_C^{U}(\rho(r)) + f(\xi(r))(\varepsilon_C^{P}(\rho(r)) - \varepsilon_C^{U}(\rho(r)))\right]\rho(r)dr \end{aligned} \tag{2.29}$$

where $\xi(r) = |n\uparrow(\rho(r)) - n\downarrow(\rho(r))| / n\uparrow(\rho(r)) + n\downarrow(\rho(r))$ is the normalized magnetization, $f(\xi(r))$ is a smoothing function, ε_C^{P} and ε_C^{U} are proper functional representing the correlation energies for the spin-polarized and unpolarized systems, respectively.

2.7 The Full-Potential Linearized Augmented-Plane Wave (FP-LAPW) Method

The full-potential linearized augmented-plane wave (FP-LAPW) technique is one of the most precise methods of study of the electronic structures, magnetic and optical properties of crystals and surfaces. The application of atomic forces has greatly maximized its applicability, but it is still commonly supposed that FP-LAPW computations need considerable higher computational effort in comparison with the pseudopotential plane wave (PPW) based techniques. FP-LAPW has recently showed important progress which is evident by use of researchers to work out several properties in magnetism and nuclear quantities, for example, isomer shifts, hyperfine fields, electric field gradients, and core level shifts. Nevertheless, because the computational expense and memory requirements are still fairly high, FP-LAPW implementations are suitable to fairly complicated systems. One successful implementation of the FP-LAPW technique is the program package WIEN2k, a code enhanced by Blaha, Schwarz and coworkers (Blaha *et al.*, 2012). It has been successfully implemented to a various scope of difficulties such as electric field gradients and systems such as high-temperature superconductors, minerals, surfaces of transition metals, or anti- ferromagnetic oxides and even molecules (Ernst *et al.,* 2005). So far the main disadvantage of the FP-LAPW-technique in comparison with the pseudopotential plane-wave (PPW) method has been its higher computational expense. This may be largely because of an inconsistency in optimization efforts spent on both techniques and so we have investigated the FP-LAPW technique from a computational arithmetical viewpoint. Lately, the development of the Augmented Plane Wave (APW) techniques from Slater's APW to LAPW and the new APW+lo was portrayed by Schwarz and Blaha (2003).

FP-LAPW is the one of the most precise technique for performing electronic

structure calculation of a crystals and it is based on DFT. The valence states are treated relativistically incorporated with either scalar relativistic or with including spin-orbit coupling. Core states are treated fully relativistically. The FP-LAPW technique, which is like most energy-band techniques is a process for solving the Kohn-Sham equations for the ground state density, total energy and (Kohn-Sham) eigen values (energy bands) of a many-electron system by presenting a basis set which is particularly modified to the problem. This alteration is achieved by partitioning the unit cell (Fig. 2.1) into (I) non-overlapping atomic circles (centered at the atomic sites) and (II) an interstitial region, that's to say, a region between two spaces. In the two sorts of regions, diverse basis sets are used:

i) Inside atomic sphere **t** of radius $\mathbf{R_t}$ a linear combination of radial functions times spherical harmonics $Y_{lm}(r)$ is used:

$$\phi_{kn} = \sum_{lm} \left[A_{lm} u_l \left(\vec{r}, E_l \right) + B_{lm} \dot{u}_l (\vec{r}, E_l) \right] Y_{lm}(\vec{r}) \tag{2.30}$$

where $u_l(r, E_l)$ is the (at the origin) normal way out of the radial Schrodinger equation for energy E_1 and the spherical part of the potential inside sphere, $\dot{u}_l(r, E_l)$ is the energy derived of u_l taken at the similar energy. A linear mixture of these two functions comprise the linearization of the radial function; the coefficients A_{lm} and B_{lm} are functions of k_n decided by requiring that this root function $\dot{u}_l$ goes with the equivalent basis function of the interstitial region; u_l and are achieved by numerical integration of the radial Schrodinger equation on a radial mesh inside the sphere.

(ii) In the interstitial zone a plane wave extension is applied

$$\phi_{kn} = \frac{1}{\sqrt{w}} e^{ik_n r} \tag{2.31}$$

where $k_n = k + K_n$; K_n are the reciprocal lattice vectors and k is the wave vector inside the first Brillouin zone. Each plane wave is increased by an atomic-like function in every atomic sphere.

The solutions to the Kohn-Sham equations are extended in this joint basis set of LAPW's according to the linear dissimilarity technique

$$\psi_k = \sum_n C_n \phi k_n \tag{2.32}$$

and the coefficients C_n are decided by the Rayleigh-Ritz variation rule. The union of this basis set is controlled by a disconnected parameter R_{MT} x K_{max} = 6 - 9, where R_{MT} is the smallest atomic sphere radius in the unit cell and K_{max} is the magnitude of the largest K vector. Additional (K_n independent) basis functions can be added to improve upon the linearization and to make possible a reliable treatment of semi core and valence states in one energy window additional basis functions can be added. They are called "local orbitals" and consist of a linear combination of two radial functions at two dissimilar energies and one energy derivative:

$$\phi_{lm}^{LO} = \left[A_{lm} u_l(\vec{r}, E_{1.l}) + B_{lm} \dot{u}_l(\vec{r}, E_{1.l}) + C_{lm} u_l(\vec{r}, E_{2.l})\right] Y_{l,}(\hat{r}) \tag{2.33}$$

The coefficients A_{lm}, B_{lm}, and C_{lm}, are decided by the necessities that ϕ_{lm}^{LO} should be regularized and has zero value and slope at the sphere border. The general form of potentials in the core region (I) and interstitial region (II) using FP-LAPW technique can be written as

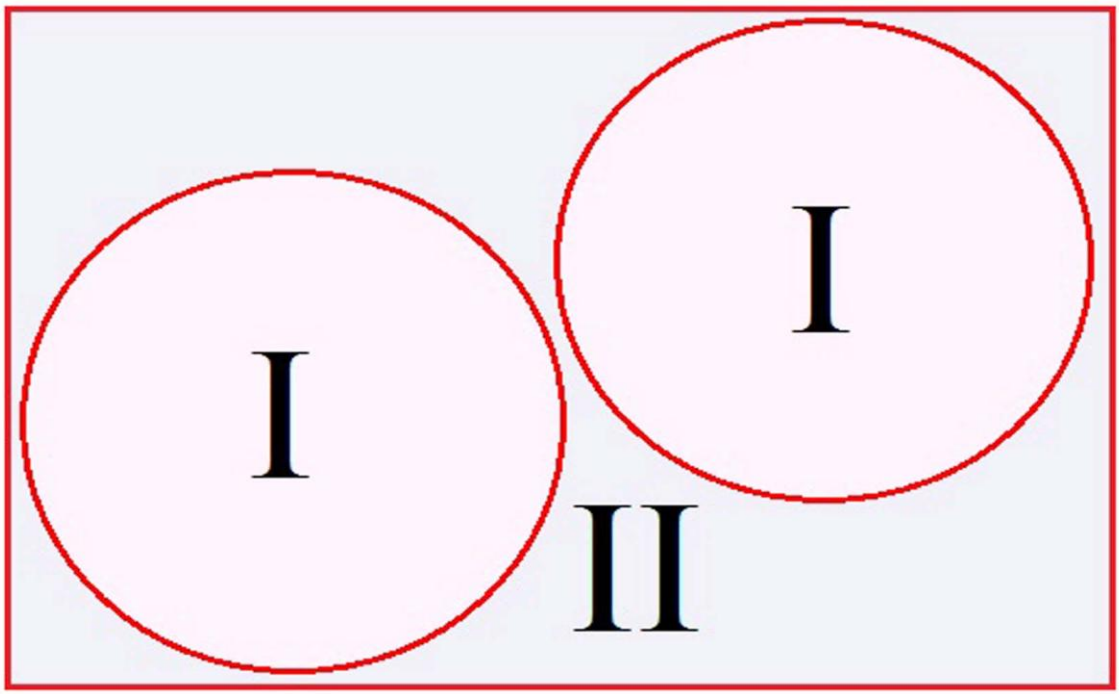

Fig. 2.1: Partitioning of the unit cell into atomic spheres (I) and interstitial region (II).

$$V(\vec{r}) = \begin{cases} \sum_{lm} V_{lm}(\vec{r}) Y_{lm}(\hat{r}) & inside\,sphere \\ \sum_{K} V_K e^{ikr} & outside\,sphere \end{cases} \tag{2.34}$$

2.8 Equation of States

The behaviour of a solid under hydrostatic pressure can be described by using equation of states which is the pressure-volume or energy volume relation. All physical properties are related to the total energy of the crystal. Equilibrium lattice constant, isothermal bulk modulus, its pressure derivative are calculated by fitting the calculated total energy to the Murnaghan's equation of state (Murnaghan, 1944), which is given by

$$E(V) = E_0 + \left[\frac{(V_0/V)^{B_0^{'}}}{B_0^{'} - 1} + 1 \right] - \frac{B_0 V_0}{B_0^{'} - 1} \tag{2.35}$$

Here E_0 is the minimum energy at T = 0K, V_0 is the equilibrium volume corresponding to minimum energy of the crystal. B_0 and $B_0^{'}$ are the bulk modulus and pressure derivative of the bulk modulus at the equilibrium volume respectively.

$$\text{Pressure } (P) = -\frac{dE}{dV} \text{ and Bulk modulus, } (B_0) = -V\frac{dP}{dV} = V\frac{d^2E}{dV^2}$$

2.9 Elastic Constants

Let E_{tot}^0 be the total energy of an initial crystal, and V_0 its volume. By deforming the crystal the energy E_{tot} of the resulting strained state can be expressed as

$$E_{tot} = E_{tot}^0 + P(V - V_0) + \Phi_{elast} \tag{2.36}$$

Here, V is the volume of the strained lattice, Φ_{elast} the elastic energy and the pressure (P) is defined by

$$P = -\left(\frac{\partial E_{tot}^{0}}{\partial V}\right)(V_0) \tag{2.37}$$

To first order, the strained lattice is related to the unstrained lattice by $(1+\bar{\varepsilon})$, where 1 is the identity matrix and $\bar{\varepsilon}$ is the strain tensor. According to Hook's law, the linear elastic constants $C_{i\,jkl}$ are then defined by using the second order development of the elastic energy

$$\Phi_{elast} = \frac{V}{2} C_{ijkl}\varepsilon_{ij}\varepsilon_{kl} \qquad (i, j, k, l = 1, 2, 3)$$

Above equation in Voigt's two-suffix notation is given by

$$\Phi_{elast} = \frac{V}{2} C_{ij}\varepsilon_i\varepsilon_j \tag{2.38}$$

where $(V - V_0)$ term in Eq. 2.36 is linear with respect to the strain i.e.

$$V - V_0 = V_0.Tr(\bar{\varepsilon}) = V_0 \sum_{i=1}^{3} \varepsilon_i$$

Thus, it is possible to derive elastic constants from the second order derivative of E_{tot} as:

$$C_{ij} = \frac{1}{V_0}.\frac{\partial^2 E_{tot}}{\partial\varepsilon_i \partial\varepsilon_j} \tag{2.39}$$

2.10 Optical Properties

Interaction of radiation with matter gives various interesting phenomena such as absorption, transmission, reflection, scattering or emission. The study of these properties provides several informations with regard to the behaviour of matter in various energy ranges (Pines, 1963). The electrons of the matter absorb the energy of the incident light and jumps from occupied valence state to the unoccupied conduction state. This kind of transitions provides the understanding of the location of the initial

and the final energy bands and symmetry of their associated wave functions (Callaway, 1974a). This is infact related to the response function of the system which is strongly dependent on the frequency of the incident radiation and the wave vector which is given by $\varepsilon(\omega, q)$. In the infrared and higher energy radiation (long wavelength limit) the dielectric function is dependent only on frequency compared to wave vector (Callaway, 1974b) and hence the dielectric function can be written as $\varepsilon(\omega, 0)$ which is the combination of real and imaginary parts and is given by

$$\varepsilon(\omega) = \varepsilon_1(\omega) + i\varepsilon_2(\omega), \tag{2.40}$$

where $\varepsilon_1(\omega)$ and $\varepsilon_2(\omega)$ are the real and imaginary parts of dielectric function. When the electromagnetic radiation falls on crystal it interacts with the electrons of the crystal. We assume that the crystal is free of imperfections, the total Hamiltonian of the electromagnetic radiation on perfect crystal is given by

$$H = \frac{1}{2m}\left(\vec{P} + e\vec{A}\right)^2 + V(\vec{r}) \tag{2.41}$$

where $\vec{P}$ is the momentum, $\vec{A}$ and $V(\vec{r})$ are the vector potential and periodic crystal potential respectively.

The first order perturbation operator describing the interaction between the radiation and the electrons is

$$H_o\left(\vec{r}, t\right) = \frac{e}{m}\left(\vec{A}.\vec{p}\right) \tag{2.42}$$

The vector potential for a plane wave can be written as,

$$\vec{A} = \vec{A}_o\hat{e}\exp\left[i\left(\vec{k}.\vec{r} - \omega t\right)\right] + c.c. \tag{2.43}$$

where $\hat{e}$ the unit vector of polarization in the direction of the electric field and *c.c.* is the

complex conjugate. The second term is neglected which is the emission term and only the first term is considered which gives the absorption. The transition probability for an electron going from an occupied valence state $E_v\left(\overrightarrow{k_v}\right)$ to an empty conduction state $E_c\left(\overrightarrow{k_c}\right)$ can be written as,

$$w\left(\omega,t,\overrightarrow{k_v},\overrightarrow{k_c}\right)=\frac{e^2}{m^2\hbar^2}\left|\int_0^t dt'\int_V d\vec{r}\,\psi_c\left(\overrightarrow{k_c},\vec{r},t\right)\vec{A}.\vec{p}\psi_v\left(\overrightarrow{k_v},\vec{r},t\right)\right|^2 \tag{2.44}$$

Here, Bloch type eigen functions ψ_c and ψ_v belongs to E_v and E_c respectively and can be written as

$$\psi_v\left(\overrightarrow{k_v},\vec{r},t\right)=\exp\left[-i\hbar^{-1}E_v\left(\overrightarrow{k_v}\right)t\right]\exp\left(i\overrightarrow{k_v}.\vec{r}\right).u_v\left(\overrightarrow{k_v},\vec{r}\right) \tag{2.45}$$

Here both u_v and u_c are the periodic wave functions with periodicity of the lattice. Combining Eqs. 2.43, 2.44, 2.45, and using

$$\overrightarrow{E}=-\frac{\delta\vec{A}}{\delta t} \tag{2.46}$$

We get

$$w\left(\omega,t,\overrightarrow{k_v},\overrightarrow{k_c}\right)=\frac{e^2E_o^2}{m^2\omega^2}\left|\int_0^t dt'\exp\left[i\hbar^{-1}\left(E_c-E_v-\hbar\omega\right)t'\right].\vec{e}.\overrightarrow{M_{cv}}\right|^2 \tag{2.47}$$

with the matrix element

$$\vec{e}.\overrightarrow{M}_{cv}=\int_v d\vec{r}\exp\left[-i\left(\overrightarrow{k_c}-\vec{k}\right).\vec{r}\right]u_c^*\vec{e}.\vec{\nabla}\exp\left(i\overrightarrow{k_v}.\vec{r}\right)u_v \tag{2.48}$$

here the matrix element will vanish unless $\overrightarrow{k_c}-\vec{k}=\vec{k}_v+\vec{k}_n$,where $\vec{k}_n$ is the reciprocal lattice vector. Since $\vec{k}=\frac{2\pi}{\lambda}$ is very small as compared to the linear dimensions of Brillouin Zone (BZ) it can be neglected. This gives the condition that that only vertical

transitions without a change of the wave vector are allowed and is called direct transitions.

The integration of Eq. 2.47 over *t'* gives

$$w\left(\omega,t,\overrightarrow{k_v},\overrightarrow{k_c}\right)=\frac{e^2E_o^2}{m^2\omega^2}\left|\frac{\exp\left[i\left(E_c-E_v-\hbar\omega\right)t/\hbar\right]-1}{i\left(E_c-E_v-\hbar\omega\right)/\hbar}\vec{e}.\overrightarrow{M}_{cv}\right|^2 \tag{2.49}$$

from which we obtain the transition probability per unit time as

$$\overrightarrow{W}_{cv}=\frac{\hbar e^2E_o^2}{2\pi^2m^2\omega^2}\int d\vec{k}\left|\vec{e}.\overrightarrow{M}_{cv}\right|^2\delta\left(E_c-E_v-\hbar\omega\right) \tag{2.50}$$

The δ function contains the second selection rule and transition probability is different from zero if the initial and final state energy difference is equal to photon energy.

We can now obtain the various optical constants as follows:

The frequency dependent optical conductivity (σ) given by (Reshak, 2007),

$$\sigma\left(\omega\right)=2W_{cv}\hbar\omega/\vec{E}_0^2 \tag{2.51}$$

The imaginary part of dielectric function is

$$\varepsilon_2\left(\omega\right)=\frac{4\hbar^2e^2}{\pi m^2\omega^2}\int d\vec{k}\left|\vec{e}.\overrightarrow{M}_{cv}\right|^2\delta\left(E_c-E_v-\hbar\omega\right) \tag{2.52}$$

$$\varepsilon_2\left(\omega\right)=\frac{4\hbar^2e^2}{\pi m^2\omega^2}\int_c ds\frac{\left|\vec{e}.\overrightarrow{M}_{cv}\right|^2}{\left|\vec{\nabla}_k\left(E_c-E_v\right)\right|_{E_c-E_v=\hbar\omega}} \tag{2.53}$$

The real part of the dielectric function can be calculated using the Kramers-Kronig relations from imaginary part $\varepsilon_2\left(\omega\right)$,

$$\varepsilon_1\left(\omega\right)=1+\frac{2}{\pi}\int_0^\infty\frac{\omega'}{\left(\omega'\right)^2-\omega^2}\varepsilon_2\left(\omega'\right)d\omega' \tag{2.54}$$

The dielectric function is not directly accessible experimentally for the optical measurements, hence they have to be calculated from the other parameters. They are

reflectivity $R(\omega)$, the refractive index $n(\omega)$ and extinction coefficient $k(\omega)$. These experimentally observable quantities are related to real and imaginary parts of the dielectric function as follows:

$$R(\omega)=\frac{(n-1)^2+k^2}{(n+1)^2+k^2} \tag{2.55}$$

$$n(\omega)=\left\{\frac{1}{2}\left[\left(\varepsilon_1^2+\varepsilon_2^2\right)^{\frac{1}{2}}+\varepsilon_1\right]\right\}^{\frac{1}{2}} \tag{2.56}$$

$$k(\omega)=\left\{\frac{1}{2}\left[\left(\varepsilon_1^2+\varepsilon_2^2\right)^{\frac{1}{2}}-\varepsilon_1\right]\right\}^{\frac{1}{2}} \tag{2.57}$$

The electron energy loss spectroscopy (EELS) is a valuable tool for the investigation of various aspects of material (Wooten, 1972). The energy loss function gives the energy loss by a photon moving in a solid. EEL spectrum can be calculated from the relation,

$$\text{EEL}=-\text{Im}\left(\frac{1}{\varepsilon}\right) \tag{2.58}$$

$$\text{or}\quad \text{EEL}=\frac{\varepsilon_2}{\varepsilon_1^2+\varepsilon_2^2} \tag{2.59}$$

The results of optical constants obtained by using Eqs. 2.52 - 2.59 in case of systems under study are given in details in Chapter 5.

2.11 The WIEN2k Code

The calculations in this work are performed using the WIEN2k computer code (Blaha *et al.,* 2012). This code contains several sub-programs, few of which are described briefly below. There are two major parts in the program, the initialization and the selfconsistent field (SCF) cycle. The flow chart of the code is given in Fig. 2.2.

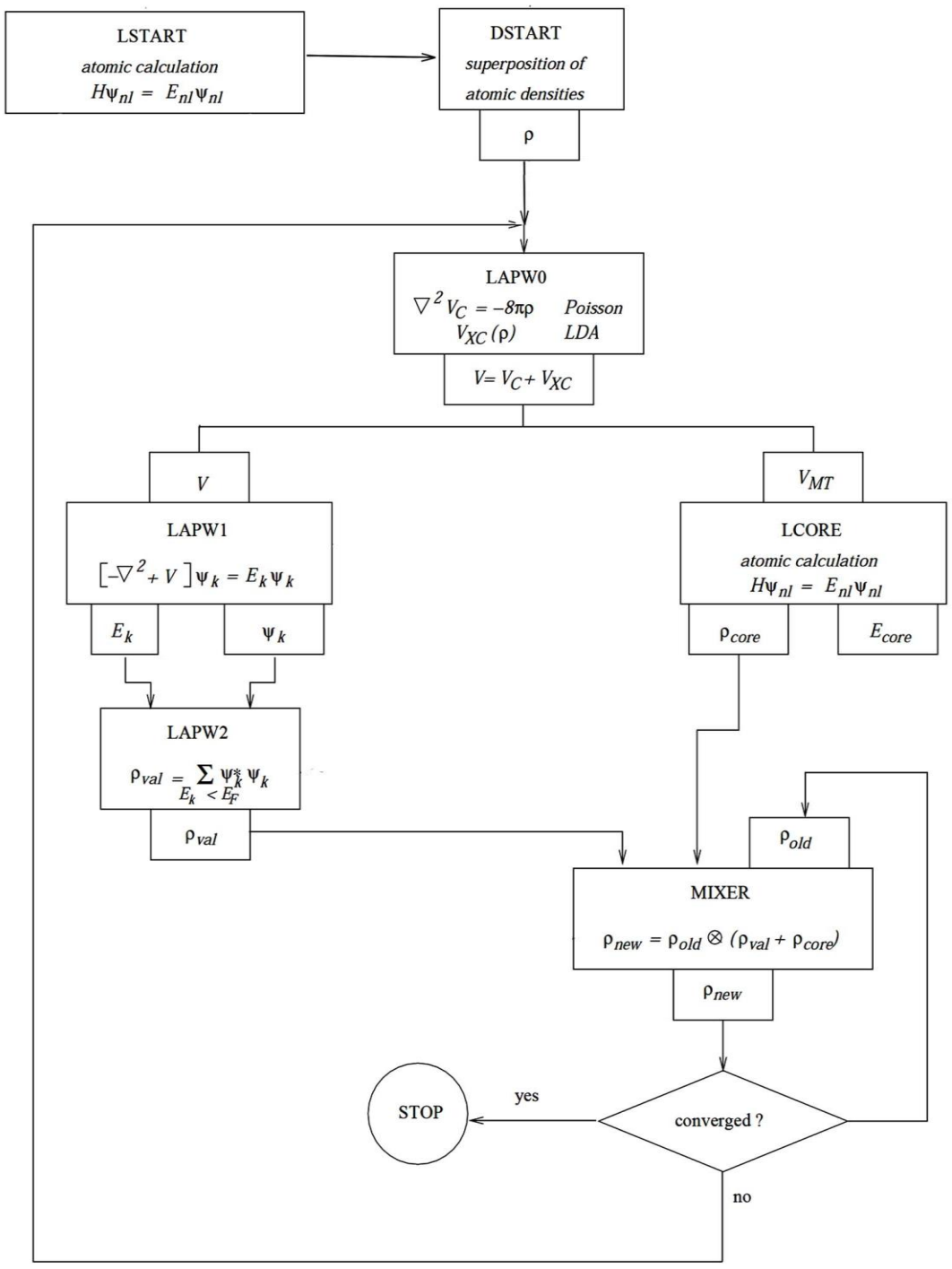

Fig. 2.2: Flow chart of WIEN2k code.

• **Initialization** (Setting up the unit cell and generating the initial density):

In this sub-program, atomic densities are generated and superimposed to obtain a initial crystal density for the SCF calculation. Additionally, the atomic potentials and optionally, atomic valence densities are created. Information about *l, m* values of the lattice harmonics representation and number of Fourier coefficients of the interstitial charge density are inserted as input file in this part.

• **LAPW0** (Construction of the effective potential):

The Poisson equation is solved and the total potential is computed as the sum of the Coulomb and the exchange-correlation potential in the LAPW0 program. The electron (spin) density is used as input and the spherical (l = 0) and the non-spherical parts of the potential are generated. The exchange-correlation potential is computed numerically on a grid. Additionally, the Hellmann-Feynman force contribution to the force is also determined.

• **LAPW1 (**Solving the Kohn-Sham equations of valence electrons):

The Hamiltonian and the overlap matrix are set up in LAPW1. Their diagonalization provides the eigenvalues and eigenvectors. Both the LAPW and the APW+lo methods are supported. For maximum efficiency a mix of both are recommended, i.e. the APW+lo basis functions are used for physically meaningful *l* values, while LAPW basis functions are employed to describe higher *l*-values functions.

• **LAPW2 (**Construction of the new electron density):

The Fermi-energy is computed. The electronic charge densities are expanded according to the representation of Eq. 2.30 for each occupied state and each k-vector.

Afterwards the corresponding (partial) charges inside the atomic spheres are obtained by integration.

• **LCORE (**The treatment of the core electrons):

The potential and the charge density of the core electrons are computed.

• **LMIXER (**Generating the input density for the next iteration):

The electron densities of core, semi-core, and valence states are combined to yield the total new density. Taking only the new densities would, however, lead to instabilities in the iterative SCF process. To have a stable SCF cycle new and old densities need to be mixed, to obtain a new density.

$$n_{new}^{m+1} = (1-\alpha) n_{new}^{m} + \alpha n_{old}^{m} \tag{2.60}$$

here α is a mixing parameter. In the WIEN2k code this is done (mainly) using the Broyden scheme. The total energy and the atomic forces are computed in mixer, as well.

It is well known that for localized electrons LDA and GGA methods are not accurate enough for a proper description of some of the strongly correlated systems. Thus other methods like LDA+U and Orbital polarization are also implemented in this program. In WIEN2k (Blaha *et al*., 2012) the effective Coulomb-exchange interaction (U_{eff} = U −J) is used for the LDA+U calculations (Anisimov *et al.*, 1991, 1997). This particular scheme is used in WIEN2k to include double-counting corrections, however, it neglects multiple terms. It should be mentioned that the +U was used on top of GGA or LSDA parametrization of the exchange-correlation functional. A significant difference was observed using one or the other of the parameterizations.

Chapter 3

Structural and Elastic Properties of Rare-earth Filled Skutterudites

3

Structural and Elastic Properties of Rare earth Filled Skutterudites

3.1. Structural Optimization

All physical and electronic properties of a solid are related to its structure, lattice constants and the total energy of the crystal. In this chapter, the calculations of structural optimization with elastic constants of filled skutterudites EuM_4X_{12} (M = Fe, Ru, Os; X = P, As, Sb) with various combinations of M and X is presented. These calculations are performed with an exchange-correlation functional with Perdew-Burke-Ernnzerhof generalized gradient approximation (PBE-GGA) (Perdew *et al*., 1996) within the frame work of DFT (Hohenberg and Kohn 1964), where full-potential linearized augmented plane wave (FP-LAPW) (Singh, 1994) is adopted for the basis set. The basis functions are expanded into spherical harmonic functions inside the muffin-tin sphere and the Fourier series in the interstitial region. R_{MT} X K_{MAX} calculates the LAPW basis functions for the expansion of the charge density and the potential in the interstitial region and lattice harmonics for the expansion inside the muffin-tin spheres (where R_{MT} is the average radius of the muffin-tin spheres and K_{MAX} is the maximum value of the wave vector $\mathbf{K} = k + \mathbf{G}$). The convergence of basis set was controlled by a cutoff parameter R_{MT} x K_{MAX} = 7. Nonspherical contributions to the charge density and potential within the MT spheres were considered up to l_{max} = 6, while charge density and the potential were expanded as a Fourier series with wave vectors up to G_{max} = 12

$(a.u.)^{-1}$. The dependence of the total energy on the number of *k*-points in the irreducible wedge of the first Brillouin zone has been explored within the linearized tetrahedron scheme (Bloch *et al.,* 1994). The cutoff energy which defines the separation of valence and core states was chosen as -6.0 Ry. Core states will be treated in a fully relativistic manner and the valence states are treated semi-relativistically. Self-consistency is achieved by setting the convergence of both the total energy and the eigen values to be smaller than 10^{-4} Ry. The Muffin Tin sphere radii (R_{MT}) used for each atom in the calculations are given in Table 3.1.

The lattice constants that minimizes the total energy is the equilibrium lattice constant of a crystal. The structural relaxation was performed by volume optimization method based on Murnaghan's equation of states (Murnaghan, 1944). The sample plots of variation of volume of the crystal corresponding to equilibrium energy are given in Fig. 3.1. The lattice constant thus obtained from relaxed structure with minimum ground state energy is the theoretical equilibrium lattice constant. In order to investigate the synthesizability of the related compounds, the enthalpy (H) can be calculated by using the following relation,

$$H = E_0 + PV_0 \tag{3.1}$$

where, P is the bulk pressure, V_O is bulk volume corresponds to minimum energy (E_o) of the system. The negative values of formation enthalpy indicate the stability of the compounds against decomposition into stable solid structures (Hao *et al.,* 2010). The calculated lattice constants corresponding to equilibrium energy and enthalpies are given in Table 3.2.

Table 3.1: Muffin Tin sphere radii (R_{MT}) for each atom.

Compounds	Muffin Tin Radius (R_{MT}) (a. u.)		
	Eu	**M**	**X**
$EuFe_4P_{12}$	2.5	2.27	2.01
$EuFe_4As_{12}$	3.2	2.45	2.17
$EuFe_4Sb_{12}$	4.2	2.5	2.26
$EuRu_4P_{12}$	2.5	2.27	2.01
$EuRu_4As_{12}$	3.2	2.5	2.22
$EuRu_4Sb_{12}$	2.5	2.5	2.25
$EuOs_4P_{12}$	2.5	2.5	1.86
$EuOs_4As_{12}$	3.2	2.49	2.21
$EuOs_4Sb_{12}$	2.5	2.5	2.5

Table 3.2: The calculated lattice constant, equilibrium energy and enthalpy of EuM_4X_{12} (M = Fe, Ru, Os; X = P, As, Sb).

Compound	Lattice constant (*a*) Å			Equilibrium energy (Ry)	Enthalpy (Ry)
	Previous result	**Calculated result**	**Δ(*a*)**		
$EuFe_4P_{12}$	7.805 *	7.989	0.184	-40039.915	-31436.670
$EuFe_4As_{12}$	8.337[†]	8.663	0.326	-86192.893	-28663.578
$EuFe_4Sb_{12}$	9.165*	9.037	-0.128	-187484.231	-63518.187
$EuRu_4P_{12}$	8.040*	8.026	-0.014	-66141.687	-4682.261
$EuRu_4As_{12}$	8.512[†]	8.854	0.342	-112257.753	-37492.073
$EuRu_4Sb_{12}$	9.282*	8.983	-0.299	-213680.610	-117429.678
$EuOs_4P_{12}$	8.079[§]	8.214	0.135	-168171.197	-155400.631
$EuOs_4As_{12}$	8.550[†]	8.812	0.262	-214227.906	-123223.107
$EuOs_4Sb_{12}$	9.318*	10.134	0.816	-315373.749	-297815.588

*(Sales *et al.*, 2003), [†] (Sekine *et al.*, 2009), [§] (Bushow, 2009)

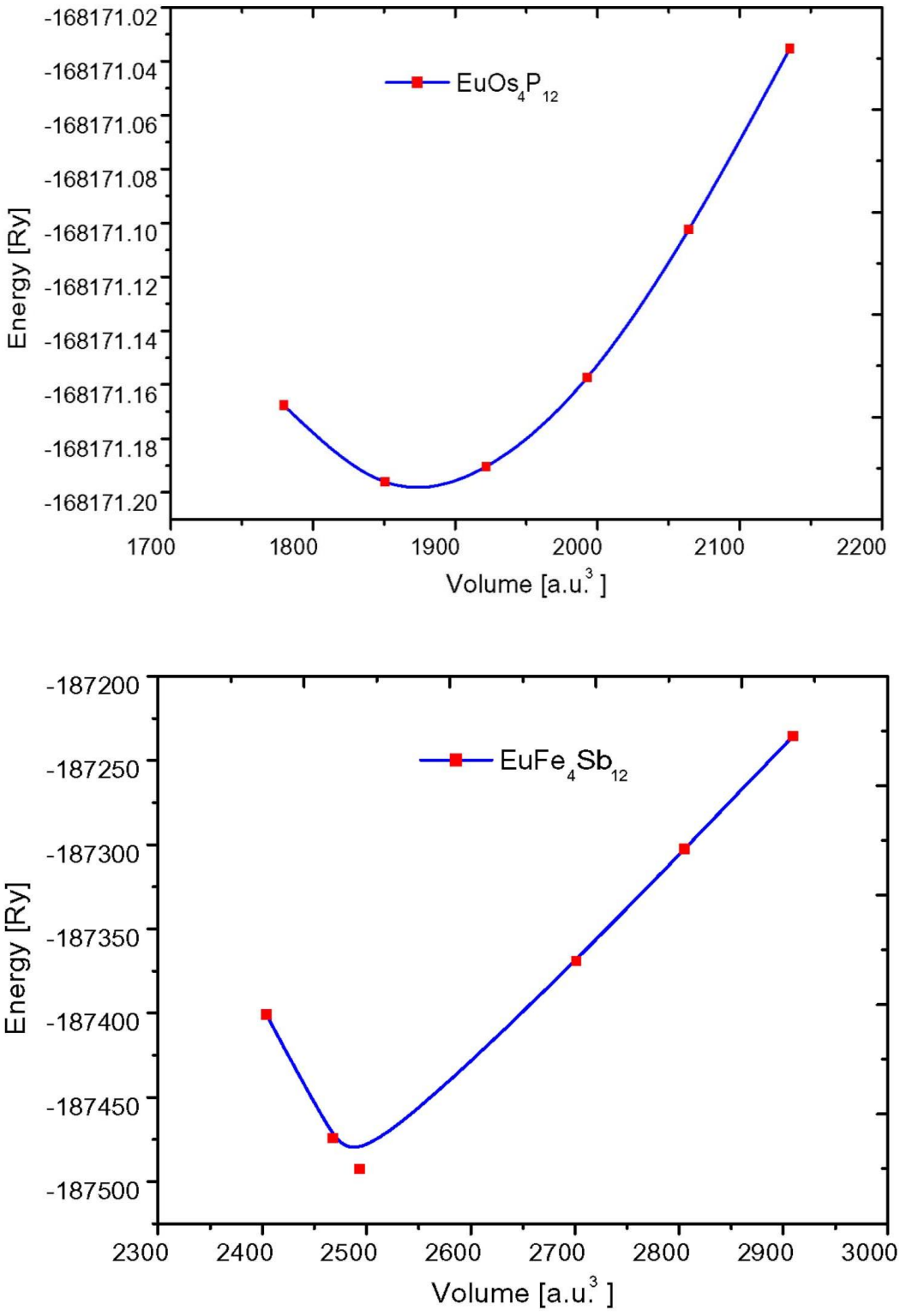

Fig. 3.1: Volume optimization plot for $EuOs_4P_{12}$ and $EuFe_4Sb_{12}$.

3.2. Elastic Properties

The elastic constants of a solid provide a link between the mechanical and dynamical behaviours (Khenata *et al.*, 2007) of crystal and give important information (Mattesini, 2009) with regards to the nature of the forces operating in solids. They are closely related to various fundamental solid state phenomena such as equation of state, inter-atomic bonding and phonon spectra, thermodynamically with specific heat, Debye temperature, thermal expansion and Gruneizen parameter (Benalia *et al*., 2009). To understand the mechanical properties (Benalia *et al*., 2009) and its practical applications elastic constants are the key, such as thermoelastic stress, internal strain, load deflection, sound velocities and fracture toughness of a solid. The elastic parameters of EuM_4X_{12} (M = Fe, Ru, Os; X = P, As, Sb) are calculated using the package called "Elastic" (Jamal, 2012) within WIEN2k code (Blaha *et al.*, 2012). Here, the elastic constants are calculated by using tetrahedral and rhombohedral distortion to cubic $Im\bar{3}$ structure and 'volume conserving' technique (Brich, 1938). For the cubic crystal, due to its higher symmetry, they have three independent elastic constants, such as C_{11} (relates the compression stress and strain along [100] direction), C_{12} (relates the longitudinal stress in one direction to the strain in another direction) and C_{44} (relates the shear stress and strain in the same direction). The system is fully relaxed after each distortion in order to reach the equilibrium state with approximately zero force on the atoms (Wang, 1993). This optimization process is important for rhombohedral case, in which inaccurate results can be obtained for C_{44} without ionic relaxation. After elastic deformation at ambient condition the elastic constants of a cubic crystal follows some of the stability criteria (Wang, 1993), such as,

$$C_{11} + 2C_{12} > 0,\ C_{44} > 0 \text{ and } C_{11} - C_{12} > 0. \quad (3.1)$$

Isotropic shear modulus (C') and bulk modulus (B) are a measure of the hardness of a solid and can be used to describe the mechanical properties such as hardness, brittleness or ductility of the material (Khenata *et al.*, 2007). Bulk modulus has a strong correlation with the binding energy or cohesive energy of a crystal (Benalia *et al.*, 2009). It measures the resistance of a material to a uniform hydrostatic pressure and describes the average atomic bond strength. Since, shear modulus is a measure of resistance to reversible deformations upon shear stress (Shein and Ivanovskii, 2008), it predicts the hardness as similar to bulk modulus. Bulk modulus (B) and C' is given by

$$B = \frac{1}{3}\left(C_{11} + 2C_{12}\right) \quad (3.2)$$

$$C' = \frac{1}{2}\left(C_{11} - C_{12}\right) \quad (3.3)$$

C' is the shear modulus. Young's modulus (which is the ratio of linear stress and strain), is used to provide the measure of the stiffness of the solid. Higher the value of Young's modulus, the stiffer is the material. The Young's modulus can be calculated by using the equation

$$Y = \frac{9BG}{3B + G} \quad (3.4)$$

The independent elastic constants are calculated for single crystal, whereas the filled skutterudite compounds are polycrystalline. Hence it is important to evaluate the elastic constants for polycrystalline by applying Voigt-Reuss-Hill approximation (Hill, 1952; Voigt 1928) in our calculation. In this approximation, the actual effective modulus for polycrystalline compounds is approximated by arithmetic mean of the two well-known bonds for monocrystals and is given by

$$G = \frac{G_R + G_V}{2} \tag{3.5}$$

were, G is Hill's shear (isotropic shear modulus) (Hill, 1952) and

$$G_R = \frac{5(C_{11} - C_{12})C_{44}}{4C_{44} + 3(C_{11} - C_{12})} \tag{3.6}$$

and $$G_V = \frac{C_{11} - C_{12} + 3C_{44}}{5} \tag{3.7}$$

which are known as Voigt's and Reuss's shear module respectively. Cauchy's pressure and Pugh's relation are the two relations which give us the information of the ductile/brittle nature of the given material. Cauchy's pressure (C_{12} - C_{44}), if the pressure is positive, the material is expected to be ductile or else brittle in nature (Pettifor, 1992). Considering B as the resistance to fracture and G as the resistance to plastic deformation, Pugh's relation states that the critical value which separates brittle and ductile behaviour of the material is 1.75, if B/G > 1.75 (Pugh, 1954), the material is expected to be ductile in nature or else brittle. Poisson's ratio (v) gives the idea of the stability of a material against shear. It takes the value from -1 (indicating large volume deformation) to 0.5 (indicating no volume deformation). It also gives the information about the nature of the bonding forces and directionality of the covalent bonds. For covalent materials v = 0.1 and for ionic material, its typical value is v = 0.25 (Bannikov *et al.*, 2007), and it is calculated by using

$$v = \frac{3B - Y}{6B} \tag{3.8}$$

Debye temperature (θ_D) is a fundamental parameter related to thermal properties such as specific heat and melting temperature and gives information about lattice vibrations of a solid (Rajagopalan, 2013). The knowledge of such properties is essential

for developing and manufacturing electronic devices (Mattesini, 2009). θ_D can be estimated using Eq. 3.9, from the average sound velocity (V_m) calculate using elastic constants data using Eq. 3.10 (Anderson, 1963). A higher value of θ_D implies a higher associated thermal conductivity and is given by

$$\theta_D = \frac{h}{k_B}\left[\frac{3n}{4\pi V_a}\right]^{1/3} V_m \tag{3.9}$$

where $$V_m = \left[\frac{1}{3}\left(\frac{2}{V_t^3}+\frac{1}{V_l^3}\right)\right]^{1/3} \tag{3.10}$$

$$V_l = \left(\frac{3B+4G}{3\rho}\right)^{1/2} \tag{3.11}$$

$$V_t = \left(\frac{G}{\rho}\right)^{1/2} \tag{3.12}$$

In the above equations, V_l and V_t are the longitudinal and transverse component of sound velocity, h is Planck's constant, k_B is Boltzmann's constant, V_a is atomic volume, n is the number of atoms per formula unit and ρ is the density of material. The elastic anisotropy (A) of crystal is highly correlated with the possibility to induce micro-cracks in the materials (Tvergaard and Hutchinsin, 1988). A factor takes the value of 1 for isotropic system, the A values smaller or greater than 1 measures the degree of elastic anisotropy. It is calculated using relation (Karki *et al.*, 1997).

$$A = \frac{2C_{44}}{(C_{11}-C_{12})} \tag{3.13}$$

The Kleinman parameter (ζ) describes the relative positions of the cation and anion sub-lattices under volume conserving strain distortions, for which positions are fixed by symmetry. ζ = 0 indicates minimized bond bending and ζ = 1 indicates mini-

mized bond stretching. $\zeta = 0$ is calculated by equation

$$\zeta = \frac{C_{11} + 8C_{12}}{7C_{11} + 2C_{12}} \tag{3.14}$$

Lames coefficients μ and λ are also calculated using the equations

$$\mu = \frac{Y}{2(1+v)} \tag{3.15}$$

$$\lambda = \frac{vY}{(1+v)(1-2v)} \tag{3.16}$$

3.2.1 Results and Discussions

(a) $EuFe_4X_{12}$ (X= P, As, Sb)

$EuFe_4X_{12}$ (X= P, As, Sb) is mechanically stable at normal condition satisfying the stability criteria given by Eq. 3.1. The calculated three independent elastic constants and related parameters are given in Table 3.3 and 3.4. We find that the calculated parameters are qualitatively in similar range of isostructural La-filled skutterudites as reported by Hachemaoui *et al.* (2010). The negative value of Cauchy's pressure (-62.64 GPa and -31.66 GPa for $EuFe_4P_{12}$ and $EuFe_4As_{12}$ respectively) gives the brittle nature of these compounds whereas positive value (16.68 GPa) for $EuFe_4Sb_{12}$ suggests this to be ductile in nature. For the analysis of the result obtained from Cauchy's pressure we used Pugh's relation, B/G ratios for $EuFe_4P_{12}$ and $EuFe_4As_{12}$ (1.07 and 1.16 < 1.75) show these compound to be brittle in nature and for $EuFe_4Sb_{12}$ (2.82 > 1.75) shows this to be ductile in nature and they support the result obtained from the values of Cauchy's pressure. Brittle materials cannot dissipate the thermal stress efficiently via plastic deformation and hence they are subjected to limited thermal shocks as they are very sensitive to thermal shocks and their strength drops impressively. The calculated value of Y for $EuFe_4P_{12}$ is 245.09 GPa > 200 GPa, this compound is stiffer than the steel (Y= 200 GPa) whereas for $EuFe_4As_{12}$ and $EuFe_4Sb_{12}$, Y value less than 200 GPa (142.88 and 106.94 GPa). The calculated values of Poisson's ratio 0.15 and 0.17 for $EuFe_4P_{12}$ and $EuFe_4As_{12}$ respectively, indicate very less volume deformation with covalent contribution in the intra-atomic bonding whereas for $EuFe_4Sb_{12}$ (ν = 0.34), ionic contribution is expected in the bonding. The Debye temperature is also calculated using the mean of transverse and longitudinal sound velocity as given in Table 3.5. Higher the mean sound velocity larger will be the Debye temperature. The calculated value of

θ_D for $EuFe_4P_{12}$ is 782.51 K, which is in between that of $LaFe_4As_{12}$ (619 K) and $LaFe_4P_{12}$ (849 K) (Hachemaoui *et al*., 2010), which implies its thermal conductivity to be in between $LaFe_4As_{12}$ and $LaFe_4P_{12}$ and the thermal conductivities of $EuFe_4As_{12}$ (θ_D = 473.54 K) and $EuFe_4Sb_{12}$ (θ_D = 331.69 K) are comparable to $LaFe_4Sb_{12}$and $CeRu_4P_{12}$ as reported by Hachemaoui *et al.* (2010) and Benalia *et al*. (2009). Since the calculated parameters are derived from elastic constants C_{ij} (i, j = 1, 2, 4) and they also dependent on the calculated bulk modulus values, hence they follow the same pattern as our calculated elastic parameters. The obtianed values of *A*, show certain amount of elastic anisotropy, which might lead to a probability to develop microcracks during the growing process of the material. Lames coefficients, which relates the components of elastic stress at some point of a solid isotropic deformable body to the components of strain at that point. The Lames coefficients obtained in our calculations are given in Table 3.5. The bond length between the two atoms inside the primitive cell under a strain is undetermined and an internal strain can develop. The Kleinman parameter quantifies the internal strain with bond bending and bond stretching. From the values if Kleinman parameters obtained in Table 3.5, one can conclude that the bond stretching is present in the crystal.

Table 3.3: The calculated elastic constants, bulk modulus, Young's modulus and shear modulus of $EuFe_4X_{12}$ (X = P, As, Sb).

Compound	C_{11} **(GPa)**	C_{12} **(GPa)**	C_{44} **(GPa)**	B **(GPa)**	Y **(GPa)**	C' **(GPa)**
$EuFe_4P_{12}$	243.75	52.12	114.76	115.96	245.10	95.82
$EuFe_4As_{12}$	165.34	24.11	55.77	71.18	142.88	70.62
$EuFe_4Sb_{12}$	274.56	31.16	14.48	112.29	106.94	121.70

Table 3.4: The calculated Poisson's ratio, Hill's isotropic shear modulus, Anisotropy factor and B/G ratio of $EuFe_4X_{12}$ (X = P, As, Sb).

Compound	v	Gv **(GPa)**	G_R **(GPa)**	G **(GPa)**	A	B/G	**Nature**
$EuFe_4P_{12}$	0.15	107.18	106.35	106.77	1.20	1.07	Brittle
$EuFe_4As_{12}$	0.17	61.71	60.89	61.29	0.79	1.16	Brittle
$EuFe_4Sb_{12}$	0.34	57.37	22.36	39.87	0.12	2.82	Ductile

Table 3.5: The calculated transverse, longitudinal and average sound velocity, Debye temperature, Kleinman parameter and Lames coefficients of $EuFe_4X_{12}$ (X = P, As, Sb).

Compound	V_t **(m/s)**	V_l **(m/s)**	V_m **(m/s)**	θ_D **(K)**	ζ	μ **(GPa)**	λ **(GPa)**
$EuFe_4P_{12}$	4684.83	7287.55	5144.40	782.51	0.36	106.77	44.82
$EuFe_4As_{12}$	3068.89	4847.13	3375.85	473.54	0.30	61.29	30.32
$EuFe_4Sb_{12}$	2196.39	4474.49	2466.55	331.69	0.26	39.86	85.72

(b) $EuRu_4X_{12}$ (X= P, As, Sb)

At normal condition, $EuRu_4X_{12}$ (X = P, As, Sb) follows the stability criteria given by relation 3.1. The calculated three independent elastic constants and related parameters are given in Table 3.6. The calculated parameters are qualitatively in similar range of isostructural $CeFe_4As_{12}$ as reported by Hachemaoui *et al.* (2009). The calculated negative values of Cauchy's pressure (-24.94 GPa and -187.17 GPa) gives the brittle nature of $EuRu_4P_{12}$ and $EuRu_4As_{12}$, whereas positive value (12.44 GPa) for $EuRu_4Sb_{12}$ suggest this to be ductile in nature. The results of Cauchy's pressure values are also supported by Pugh's relation with B/G ratios 1.48, 0.67 and 1.81 for $EuRu_4P_{12}$, $EuRu_4As_{12}$ and $EuRu_4Sb_{12}$ respectively. The calculated Y values show these compounds are stiffer than steel (Y = 200 GPa). The calculated values of Poisson's ratios for $EuRu_4P_{12}$ and $EuRu_4Sb_{12}$ indicate very low volume deformation with ionic contribution in the intra-atomic bonding whereas for $EuRu_4As_{12}$ it is expected to have large volume deformation with covalent contribution in the intra-atomic bonding. The calculated value of θ_D using mean sound velocity implies that their thermal conductivities are comparable with the value obtained for $LaFe_4X_{12}$ (X = P, As, Sb) (Hachemaoui *et al.*, 2010). The calculated *A* values suggest that $EuRu_4P_{12}$ and $EuRu_4Sb_{12}$ have certain amount of elastic anisotropic, whereas $EuRu_4As_{12}$ is highly elastic anisotropy, which might lead to a probability to develop microcracks during the growing process of the material. The calculated values for Kleinman parameter and Lames coefficients are also given in Table 3.8 and the values of Kleinman parameters suggest these crystals to posses bonding stretching.

Table 3.6: The calculated elastic constants, bulk modulus, Young's modulus and shear modulus of $EuRu_4X_{12}$ (X = P, As, Sb).

Compound	C_{11} **(GPa)**	C_{12} **(GPa)**	C_{44} **(GPa)**	B **(GPa)**	Y **(GPa)**	C' **(GPa)**
$EuRu_4P_{12}$	385.82	109.52	134.46	201.62	332.95	138.15
$EuRu_4As_{12}$	192.08	50.20	237.37	97.49	292.97	70.94
$EuRu_4Sb_{12}$	343.62	100.05	87.61	181.24	253.37	121.79

Table 3.7: The calculated Poisson's ratio, Hill's isotropic shear modulus, Anisotropy factor and B/G ratio of $EuRu_4X_{12}$ (X = P, As, Sb).

Compound	v	Gv **(GPa)**	G_R **(GPa)**	G **(GPa)**	A	B/G	**Nature**
$EuRu_4P_{12}$	0.23	135.94	135.91	135.92	0.97	1.48	Brittle
$EuRu_4As_{12}$	-0.001	170.80	122.46	146.63	3.35	0.67	Brittle
$EuRu_4Sb_{12}$	0.27	101.28	98.69	99.98	0.72	1.81	Ductile

Table 3.8: The calculated transverse, longitudinal and average sound velocity, Debye temperature, Kleinman parameter and Lames coefficients of $EuRu_4X_{12}$ (X = P, As, Sb).

Compound	V_t **(m/s)**	V_l **(m/s)**	V_m **(m/s)**	θ_D **(K)**	ζ	μ **(GPa)**	λ **(GPa)**
$EuRu_4P_{12}$	4756.98	7983.62	5265.91	797.29	0.43	135.92	111.01
$EuRu_4As_{12}$	4577.34	6470.50	4962.69	681.16	0.41	146.63	-0.26
$EuRu_4Sb_{12}$	3283.28	5823.53	3652.44	494.10	0.44	135.92	114.58

(c) $EuOs_4X_{12}$ (X = P, As, Sb)

$EuOs_4X_{12}$ (X = P, As, Sb) is stable at normal condition and the calculated elastic constants and related parameters are given in Table 3.9-3.11. The obtained values are qualitatively in similar range of isostructural $CeOs_4Sb_{12}$ as reported by Ameri *et al.* (2013). The negative values of Cauchy's pressure, -37.89 GPa, -608.97 GPa and 57.33 GPa for $EuOs_4P_{12}$, $EuOs_4Sb_{12}$ and $EuOs_4As_{12}$ respectively and Pugh's relation suggest that $EuOs_4P_{12}$ and $EuOs_4Sb_{12}$ to be brittle in nature whereas $EuOs_4As_{12}$ is ductile. The brittle material cannot dissipate the thermal stress through plastic deformation efficiently, they are very sensitive to thermal shocks and before their strength drops dramatically, hence they are subjected to limited thermal shocks. Among the title materials $EuOs_4P_{12}$ is stiffest of all as suggested by the Y value. The Poisson's ratio values suggest that these compounds have ionic contribution in the intra-atomic bonding except $EuOs_4Sb_{12}$. The calculated value of θ_D implies that the thermal conductivities of $EuOs_4P_{12}$ and $EuOs_4Sb_{12}$ are comparable with the value obtained for $CeFe_4As_{12}$ (Hachemaoui *et al.*, 2009), and for $EuOs_4As_{12}$ is comparable with that of $CeOs_4Sb_{12}$ (Ameri *et al*., 2013) and the mean sound velocity also follows the same trend. The calculated *A* values suggest that $EuOs_4P_{12}$ have certain amount of elastic anisotropy, whereas $EuOs_4As_{12}$ and $EuOs_4Sb_{12}$ is highly elastically anisotropic. The Kleinman parameter and Lames coefficients are also calculated and given in Table 3.11 and the Kleinman parameter obtained suggest these compounds to have bond stretching.

Table 3.9: The calculated elastic constants, bulk modulus, Young's modulus and shear modulus of $EuOs_4X_{12}$ (X = P, As, Sb).

Compound	C_{11} **(GPa)**	C_{12} **(GPa)**	C_{44} **(GPa)**	***B*** **(GPa)**	***Y*** **(GPa)**	***C′*** **(GPa)**
$EuOs_4P_{12}$	334.19	95.80	133.69	175.27	308.22	119.19
$EuOs_4As_{12}$	130.23	94.96	37.63	106.72	76.64	17.64
$EuOs_4Sb_{12}$	62.86	1.32	610.29	21.84	152.21	30.77

Table 3.10: The calculated Poisson's ratio, Hill's isotropic shear modulus, Anisotropy factor and B/G ratio of $EuOs_4X_{12}$ (X = P, As, Sb).

Compound	***v***	***Gv*** **(GPa)**	G_R **(GPa)**	***G*** **(GPa)**	***A***	***B/G***	**Nature**
$EuOs_4P_{12}$	0.21	127.89	127.49	127.69	1.12	1.37	Brittle
$EuOs_4As_{12}$	0.38	29.63	25.89	27.76	2.1	3.84	Ductile
$EuOs_4Sb_{12}$	-0.66	378.48	71.51	224.99	19.83	0.10	Brittle

Table 3.11: The calculated transverse, longitudinal and average sound velocity, Debye temperature, Kleinman parameter and Lames coefficients of $EuOs_4X_{12}$ (X = P, As, Sb).

Compound	V_t **(m/s)**	V_l **(m/s)**	V_m **(m/s)**	θ_D **(K)**	ζ	μ **(GPa)**	λ **(GPa)**
$EuOs_4P_{12}$	4073.39	6700.60	4500.29	665.77	0.43	127.69	90.14
$EuOs_4As_{12}$	1776.91	4043.11	2006.06	276.64	0.81	27.76	88.21
$EuOs_4Sb_{12}$	5451.28	6519.66	5728.98	687.01	0.17	224.99	-128.16

Chapter 4

Electronic and Magnetic Properties of Rare earth Filled Skutterudites

4

Electronic and Magnetic Properties of Rare earth Filled Skutterudites

In ternary skutterudites, from the study of the distribution of density of states (DOS) in the upper valence region and the relative position of the Fermi level with respect to the principal points of the crystalline Brillouin zone (BZ), we can understand the thermoelectric properties of these materials (Nouneh *et al.*, 2007; Nordstrom and Singh, 1996). Nordstrom and Singh (1996) have performed the electronic structure calculations of semiconducting $CeFe_4P_{12}$ and $CeFe_4Sb_{12}$ using density functional theory. Singh and Mazin (1997) have reported the efficient thermoelectric properties of $La(Fe,Co)_4Sb_{12}$ using local-density approximation based on electronic structure calculations. From the electronic structure calculations, Fornari *et al.* (1999) have shown the opening of the gap on filling of CoP_3 by La. Takeghara and Harima (2003) found the enhanced DOS at Fermi level with various pnictogen elements from P to Sb in the electronic structure calculation of $LaFe_4X_{12}$ (X = P, As, Sb) using FP-LAPW method. From the electronic structure calculation of $LaFe_4Sb_{12}$ and $CeFe_4Sb_{12}$ using TB-LMTO and FP-LAPW method, Nouneha *et al*. (2007) have reported the metallic and semiconducting nature of $LaFe_4Sb_{12}$ and $CeFe_4Sb_{12}$ respectively. Recently Ameri *et al.* (2013) have reported the narrow bandgap semiconducting nature of $CeOs_4Sb_{12}$ using DFT based electronic structure calculation. From the previous literature, we have observed that the electronic structure calculation for various combinations of rare-earth

and transition metal have been performed but for europium based filled skutterudites the electronic structure calculations are limited. Hence, in this chapter, we present the electronic properties such as DOS, energy band structures and magnetic moments of filled skutterudites EuM_4X_{12} (M = Fe, Ru, Os; X = P, As, Sb) with various combinations of M and X. From this study we can understand how the replacement of the cationic transitional element and anionic pnictogen influence the relative position of Fermi level and DOS in the valence region and magnetic behaviour of filled skutterudite. Wherever possible, the calculated results will be compared with the available experimental results as well as previously calculated theoretical results of same system or isostructural systems. We have used LSDA for exchange and correlation within the framework of DFT (Kohn and Sham, 1965) for our calculation (Shankar *et al*., 2013a, b) and for the basis function full-potential linearized augmented plane wave (FP-LAPW) (Singh, 1994). The basis functions are expanded into spherical harmonic functions inside the muffin-tin sphere and the Fourier series in the interstitial region. R_{MT} x K_{MAX} will calculate the LAPW basis functions for the expansion of the charge density and the potential in the interstitial region and lattice harmonics for the expansion inside the muffin-tin spheres (where R_{MT} is the average radius of the muffin-tin spheres and K_{MAX} is the maximum value of the wave vector $\mathbf{K} = k + \mathbf{G}$). The convergence of basis set was controlled by a cutoff parameter R_{MT} x K_{MAX} = 7. Nonspherical contributions to the charge density and potential within the MT spheres were considered up to l_{max} = 6, while charge density and the potential were expanded as a Fourier series with wave vectors up to G_{max} = 12 $(a.u.)^{-1}$. The dependence of the total energy on the number of *k* points in the irreducible wedge of the first Brillouin zone has been explored within the linearized tetrahedron scheme (Bloch *et al.,* 1994). The cutoff

energy which defines the separation of valence and core states was chosen as -6.0 Ry. Core states will be treated in a fully relativistic manner and the valence states are treated semi-relativistically. Self-consistency is achieved by setting the convergence of both the total energy and the eigen values to be smaller than 10^{-4} Ry. WIEN2k code (Blaha *et al.*, 2012) is employed for the computation of DOS and band structures of filled skutterudites. The theoretically obtained lattice parameters are discussed in Chapter 3 have been used for DOS and energy bands calculations. The muffin-tin radii for the systems under study are same as used for structural and elastic property calculations which are given in Table 3.1 of Chapter 3.

3.1 Results and Discussions

a) EuM_4P_{12} (M = Fe, Ru, Os)

To understand the electronic property of the filled skutterudites we have done the electronic band structure calculations along the high symmetry directions of the Brilllouin zone for both spin channels (spin up and spin down) within the framework of LSDA approach. In our report, we have explored how the replacement of various transition elements (namely Fe, Ru and Os) influences the band structure, DOS and related thermoelectric behaviour. The band structures for $EuFe_4P_{12}$, $EuRu_4P_{12}$ and $EuOs_4P_{12}$ are given in Figs. 4.1, 4.3, 4.5 respectively. The fundamental electronic structures of these compounds are qualitatively similar natured as they have same chemical formula. The overall profile of our calculated band structure is in fairly good agreement with previous FP-LAPW investigated results of La and Ce filled skutterudites (Nouneh *et al.*, 2007; Nordstrom and Singh, 1996; Harima and Takegahara, 2003). Our result is also in close agreement with the result of binary skutterudites (Singh and Pickett, 1994; Sofo and Mahan, 1998; Wojcjechowski *et al.*, 2003; Lefebvre-Devos *et al*., 2001; Jung *et al*., 1990) except for the region close to Fermi level (0 eV in our calculation). In our band structure calculation the replacement of transition metal atoms T (Co, Ir) by M (M = Fe, Ru, Os) and the insertion of Eu atoms in the binary skutterudite vacuum are responsible for the variation in the region close to Fermi level. Following the DOS and band structure plots (Figs. 4.1- 4.6) one can remark that there are three distinct regions separated from each other by small energy gaps.

(i) The core region (below ~ -7.0 eV), primarily formed by *s* and *p*-electrons of P

for both spin channels. From the same figures one can observe that the contributions of P atom in the valence region are negligible for both spin channels.

(ii) The valence region is mainly contributed by 4*f*-state electrons of Eu with very small contribution of 3*d*, 4*d* and 5*d* state electrons of Fe, Ru and Os respectively for spin up channel. For spin down channel the valence region is mainly contributed by transition-*d* state electrons. iii) The conduction region is mainly contributed by Eu-*f* states. From the Figs. (4.1, 4.3, and 4.5) it is distinct that the valence and conduction bands have significantly different band profile, originating from the localized holes and delocalized non-occupied bands. In the spin up channel, as we move close to Fermi level in the valence region the bands are highly populated, whereas there is no such feature in the conduction region. Similarly for spin down channel the bands are highly populated in the middle of the conduction region. Singh and Mazin (1997) have shown that $LaFe_3CoSb_{12}$ possesses an indirect energy gap of 0.6 eV using LAPW approach and was also supported by the theoretical result of Harima (1998), with the highest occupied state formed by bands originated from Sb *p*-states. Our result contradicts the result of Harima (1998), as one can see that in our result Eu *f*-states have the highest contribution with small contribution of M-*d* in the valence band [Figs. 4.2, 4.4, 4.6]. Singh and Mazin (1997) also established that there are also *d*-bands of transition metal below anionic *p*-like valence states and similar type of results are obtained in our case. From the band structure plots (Figs. 4.1, 4.3, 4.5) one can observe that the energy bands are highly populated just below the Fermi level for spin up channel which is mainly contributed by the Eu-4*f* electrons as seen from the partial DOS plots (Figs. 4.2, 4.4, 4.6). Similarly for spin down channel the energy region close to 4.0 eV is highly populated by the bands due to Eu-4*f* states. In the energy band structure, we have found

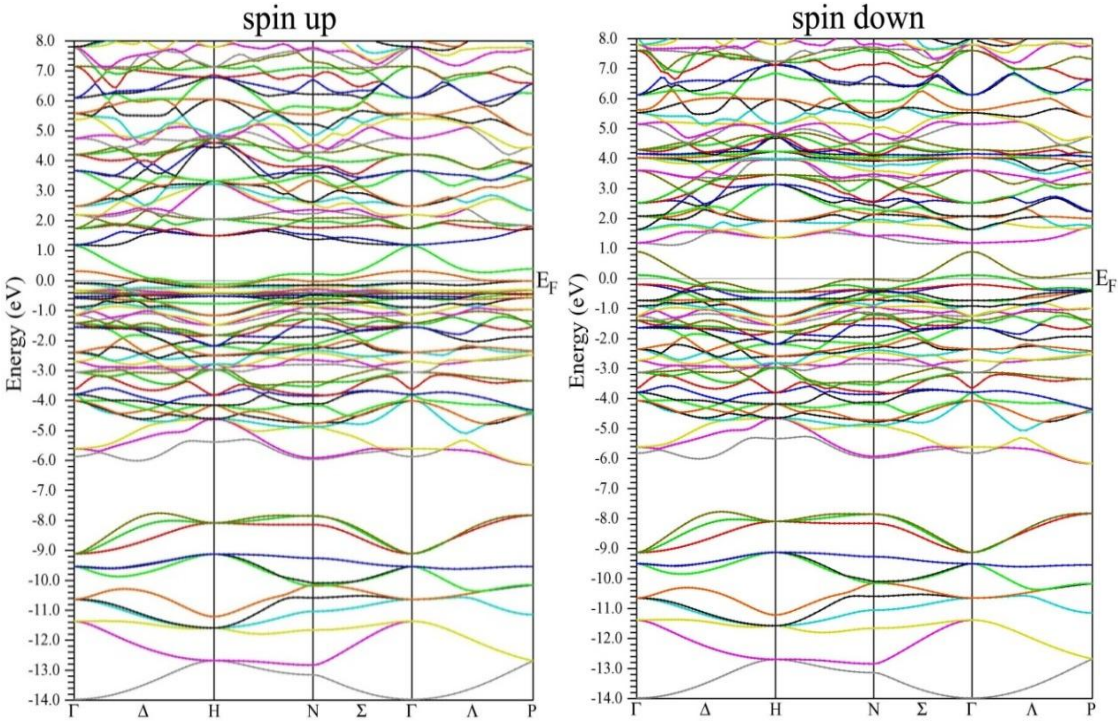

Fig. 4.1: Energy band structure plot of $EuFe_4P_{12}$ for spin up and spin down channels.

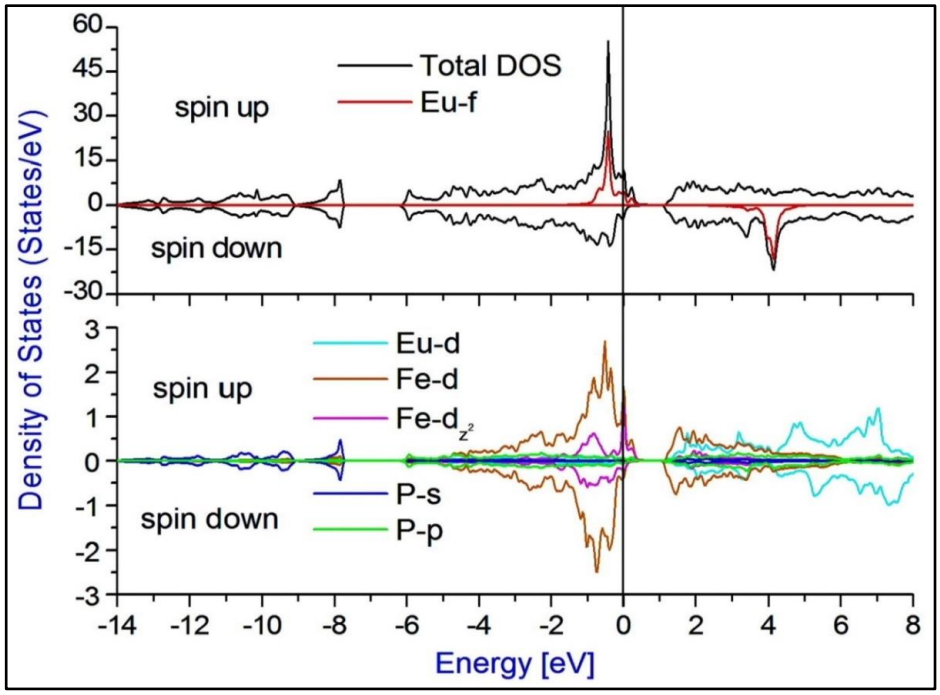

Fig. 4.2: Total and partial DOS of $EuFe_4P_{12}$.

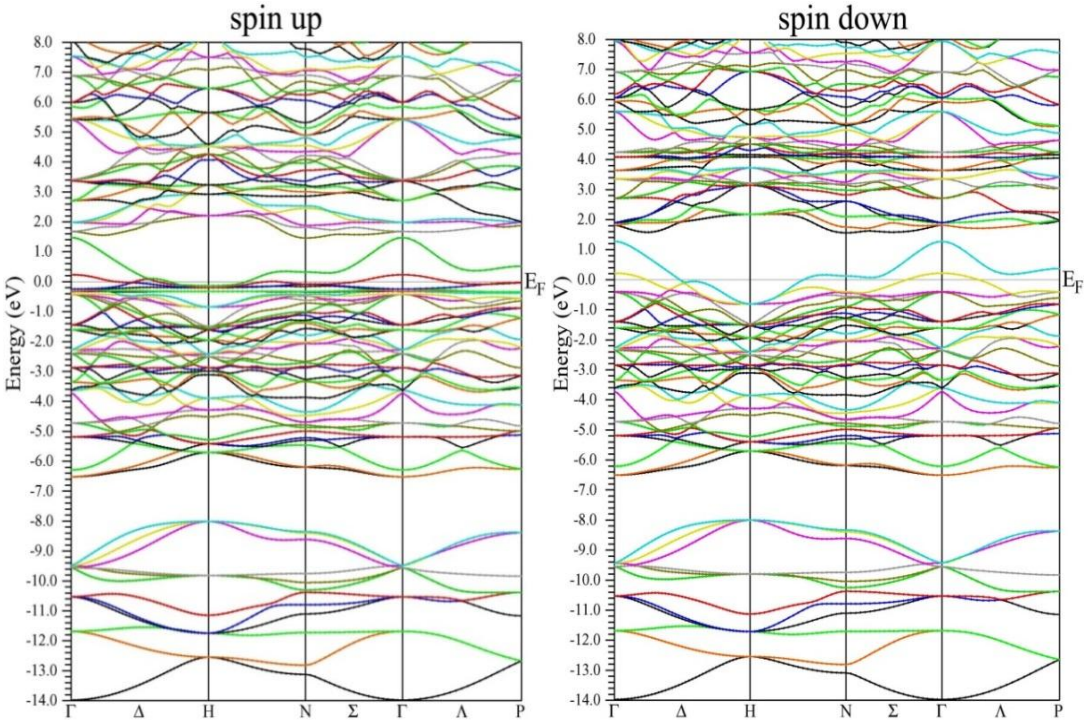

Fig. 4.3: Energy band structure plot of $EuRu_4P_{12}$ for spin up and spin down channels.

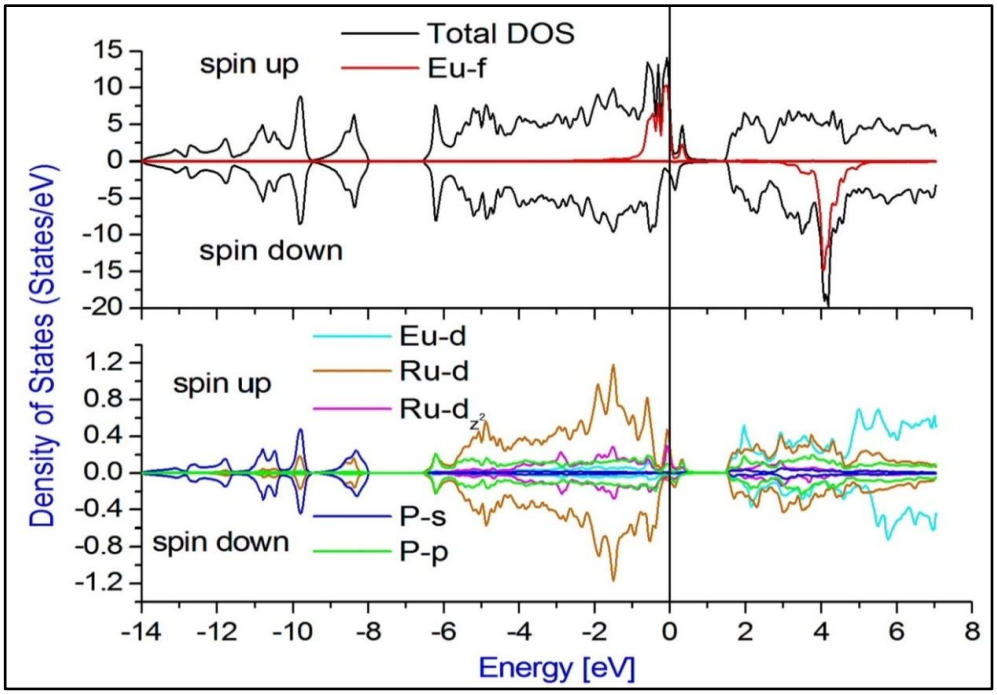

Fig. 4.4: Total and partial DOS of $EuRu_4P_{12}$.

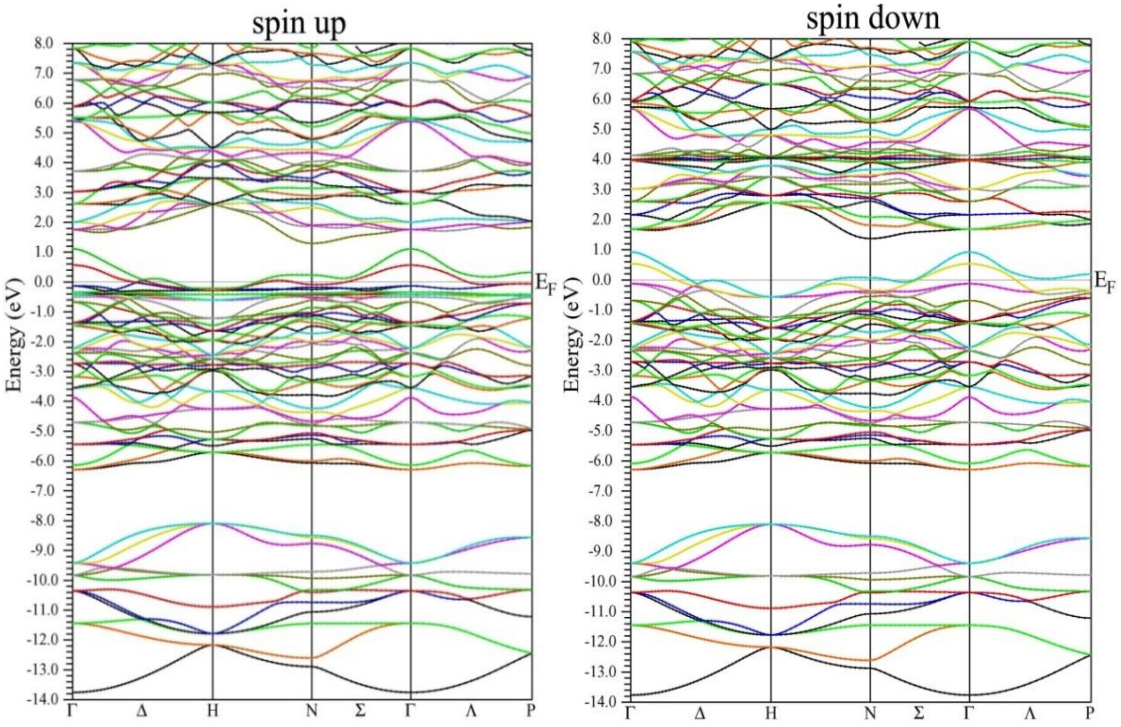

Fig. 4.5: Energy band structure plot of $EuOs_4P_{12}$ for spin up and spin down channels.

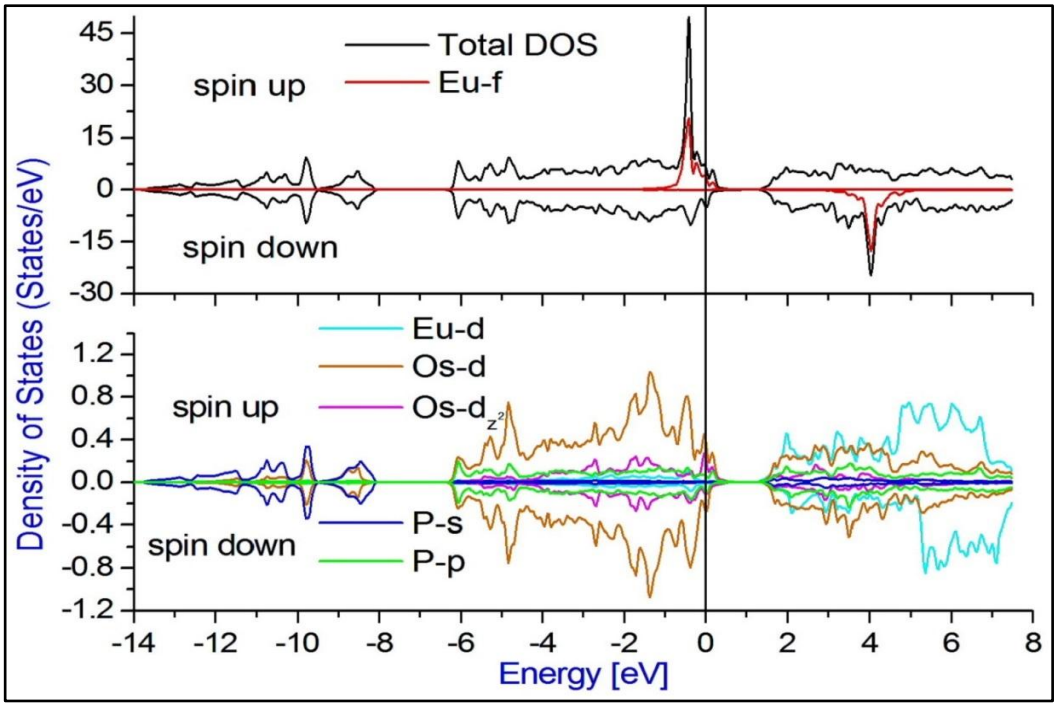

Fig. 4.6: Total and partial DOS of $EuOs_4P_{12}$.

that two bands originating from the bottom of the unoccupied region penetrates the top of the occupied region, and crosses the Fermi level in accordance with previous work for $CeOs_4Sb_{12}$ as obtained by Harima and Takegahara (2003). These bands are due to pnicogen-*p* electrons, which are dominated by *d* and *f*-states of transition elements and europium. Harima *et al.* (2007) have mentioned that the interaction between the rare earth atoms and transition atoms with the band of light holes crossing the Fermi level results in the shift of these bands as well as the increase of the energy gap values compared to binary skutterudites. The Fermi energy level is not inside this gap but within the valence band at an energy corresponding to the filling of this band by holes and the density of state $N(E_F)$ on the Fermi level relatively high in this type of system as reported for analogous $CeOs_4Sb_{12}$ (Harima, 1998; Harima and Takegahara, 2003). Thus these compounds are metals, in agreement with the experiment results of analogous UFe_4P_{12}, $CeFe_4P_{12}$ and $LaFe_4Sb_{12}$ (Meisner *et al*., 1985; Sato *et al*., 2000; Viennois *et al*., 2005). The result also favors a larger electronic specific heat for EuM_4P_{12} similar to $LaFe_4Sb_{12}$ (Vinnois *et al*., 2005; Bauer *et al*., 2001).

Chen *et* a*l.* (2003) have mentioned that the efficient thermoelectric materials are semiconductor or semimetal with optimal charge carrier concentration of around 10^{19} cm^{-3}. We have analysed the region close to 0 eV, which is taken as the Fermi level (E_F). The important feature of the DOS plot is the presence of a region above the Fermi level, where the DOS is very small for both spin channels. The presence of such region with a low density of states is typical characteristic of the skutterudites (Nouneh *et al*., 2007; Takegahara and Harima, 2003; Fornari and Singh, 1999). The density of state is very low in this region but not zero and it is referred as the pseudo-gap. We have found indirect energy gap of ~ (0.1- 0.5 eV) as shown in Table 4.1 for Fe – Os as central

transition metal. The indirect gaps are from Γ to a point in Γ- H line for $EuFe_4P_{12}$ and $EuRu_4P_{12}$, and Γ- N along Σ direction of the BZ for $EuOs_4P_{12}$. The band gap values obtained are smaller than the expected for ternary filled skutterudites (Nouneh *et al*., 2007), it is caused by the underestimation of the gap within the framework of LSDA approach. The results of the DOS show negligible changes in the overall band profile but the band gap values increases when under goes from Fe to Os as can be seen form Table 4.1. The top of the valence band (VB) crosses Fermi energy level at least two times (directions $\Gamma - H$ and $H - N - P$), which favours enhanced $N(E_F)$ (density of states at Fermi level) determining the thermoelectricity [Figs. 4.1, 4.3, 4.5]. Similar type of behaviour was observed for $LaFe_4Sb_{12}$ by Harima and Takegahara (2003). To determine $N(E_F)$ for EuM_4P_{12} and for their comparison with the low-temperature electronic specific heat (γ), we have evaluated $N(E_F)$ as shown in Table 4.1. The obtained value of $N(E_F)$ is close to that one obtained by Harima (1998), Harima and Takegahara (2003), Nouneh *et al*. (2007) for isosturctural $LaFe_4Sb_{12}$ and $CeFe_4Sb_{12}$. Singh and co-workers (Singh and Mazin, 1997) have also used such approach of comparison of electronic part of specific heat in case of the filled skutterudites. The γ is maximum for $EuFe_4P_{12}$ compared to other members of the table, the lower values of γ is due to different states present in transition atoms and hence different values of $N(E_F)$.

It can be seen from the band structure plots [Figs. 4.1, 4.3, 4.5], there are many dispersionless bands below the Fermi level E_F, which become closer to E_F from Os to Fe. From the electronic structures plots one can observe that the valence width is maximum for ruthenium-phosphide giving that the wave function is more localized with less covalent and more ionic nature of this compound compared to Fe and Os phosphides. When the valence state becomes localized, the material becomes less

covalent and more ionic, which supports the result obtained from the Poisson ratio values for these compounds (Table 3.7 of Chapter 3). The ionic nature of the compound are in sequence of Ru > Os > Fe. From the band structure plots (Figs. 4.1, 4.3, 4.5) one can see that the valence band crosses the Fermi level and over laps at the *N*-point with a flat conduction band arising from 4*f*-states of Eu, revealing the metallic behavior of the studied compound and high effective masses, which give substantial rise to the large value of thermoelectric Seebeck coefficients (Nouneh *et al*., 2007).

The splitting of the DOS in the spin-up and spin-down channels were observed for Eu-*f* state, which contribute to the magnetic moments of these compounds. In Table 4.2 we have given the total and individual magnetic moments for the compounds under study. From the Table 4.2 one can observe that the replacement of transition metal form Fe to Os, the total magnetic moment of the system increases in the same order. In the total magnetic moment the major contribution is from spin polarization of Eu-*f* state electrons (Table 4.2). In our study the negative sign of transitional elements moment indicates that they are antiferromagnetically (AFM) coupled to Eu but the coupling is very negligible compared to the host atom (Eu) giving the ferromagnetic nature of these compounds. Stoner criteria for ferromagnetism, $I_{ex}N(E_F) > 1$ (Krishnamurthy *et al*., 2007), also satisfies the results obtained, where I_{ex} is the effective exchange interaction given in Table 4.2. Jeitschko and Braun (1977) have reported $EuFe_4P_{12}$ and $EuRu_4P_{12}$ to be ferromagnetic with T_C = 100 K and 18 K respectively. Grandjean *et al*. (1984) have also reported the ferromagnetic with T_C = 99 K for EuFe4P_{12}. The results of Grandjean *et al*. (1984) and Sekine *et al.* (2000) supports the results of Jeitschko and Braun (1977) for $EuRu_4P_{12}$. Kihou *et al.* (2004) have investigated the $EuOs_4P_{12}$ to be ferromagnetic metal with T_C = 15 K. Europium is trivalent with Eu-f^7 and have completely unfilled

spin down states. Hence it is expected to have the magnetic moment value close to $7\mu_B$ but our calculation gives slightly lower value than expected. From Table 4.2, it is seen that our calculated values are slightly lower than the experimental values. The choice of LSDA method and neglecting the electron-electron correlation (Coulomb interaction U) in our calculation may be responsible for the lower magnetic moments. The LSDA method has a tendency to underestimate the intra-atomic correlation between the *f*-electrons and hence overestimate the hybridization (Kanai *et al*., 2002) between the states of Eu-*f* and M-*d* which leads to a less prominent splitting of the *f* and *d*-states giving rise to lower magnetic moments for europium and transition atoms.

Table 4.1: Calculated energy gaps, DOS at E_F and electronic specific heat of EuM_4P_{12} (M = Fe, Ru, Os).

Compound	**E_g (eV) for spin**		**$N(E_F)$ (States/eV)**	**γ (mJ/mol-K^2)**
	up	**down**		
$EuFe_4P_{12}$	----	0.2	19.32	45.88
$EuRu_4P_{12}$	----	0.3	8.92	21.18
$EuOs_4P_{12}$	0.16	0.45	10.94	25.99

Table 4.2: Total and individual magnetic moments and effective exchange interaction of EuM_4P_{12} (M = Fe, Ru, Os).

Compound	**Magnetic moment (μ_B)**					**Effective exchange interaction (I_{ex}) (eV)**
	Eu	**M**	**P**	**Total**	**Previous result**	
$EuFe_4P_{12}$	6.51	-0.18	-0.014	5.62	6.20*	4.65
$EuRu_4P_{12}$	6.56	-0.02	-0.001	5.98	6.30*	4.25
$EuOs_4P_{12}$	6.54	-0.05	-0.017	6.13	7.81**	4.47

* (Sales *et al.*, 2003), ** (Buschow, 2009)

b) EuM_4As_{12} (M = Fe, Ru, Os)

The calculated band structures for EuM_4As_{12} (M = P, Ru, Os) are given in Figs 4.7, 4.9, 4.11 respectively for Fe, Ru and Os as the central transition atom. The DOS and band structure plots show similar profile with the plots of EuM_4P_{12} (M = Fe, Ru, Os). Similar to the results of EuM_4P_{12} (M = Fe, Ru, Os), the core region (below -8.0 eV) are primarily formed by *s* and *p*-state electrons of arsenic with negligible contribution in the valence region. The valence region is mainly contributed by europium with very small contribution from transition metal for spin up channel, whereas spin down channel has transition *d*-state contribution, Singh and Mazin (1997) have also obtained similar type of result. From the band structure plots (Figs. 4.7, 4.9, 4.11) one can observe that the energy bands are highly populated just below the Fermi level for spin up channel which is mainly contributed by the Eu-4*f* electrons as seen from the partial DOS plots (Figs. 4.8, 4.10, 4.12). Similarly for spin down channel the energy region close to 4.0 eV is highly populated by the bands due to Eu 4*f*-states. We have also found that two bands originating from the bottom of the conduction region penetrates the top of the valence region, cross the Fermi level. The analysis of DOS in the region close to E_F gives an interesting result that the region above E_F, there exist a very small DOS but not zero. The presence of such region with a low density of states is typical characteristic of the skutterudites as mentioned by Nouneh *et al*. (2007), Takegahara and Harima (2003), Fornari and Singh (1999), and often it is referred as the pseudogap. For $EuOs_4As_{12}$, we have indirect energy gap of ~ 0.1 eV from Γ to *N* along Σ direction for spin up channel. The Fermi energy level is not inside this gap but within the valence band (VB) and this VB crosses Fermi energy level at least two times ($\Gamma - H$ and $H - N - P$) [Figs. 4.7, 4.9, 4.11] and $N(E_F)$ is relatively high in this type of system

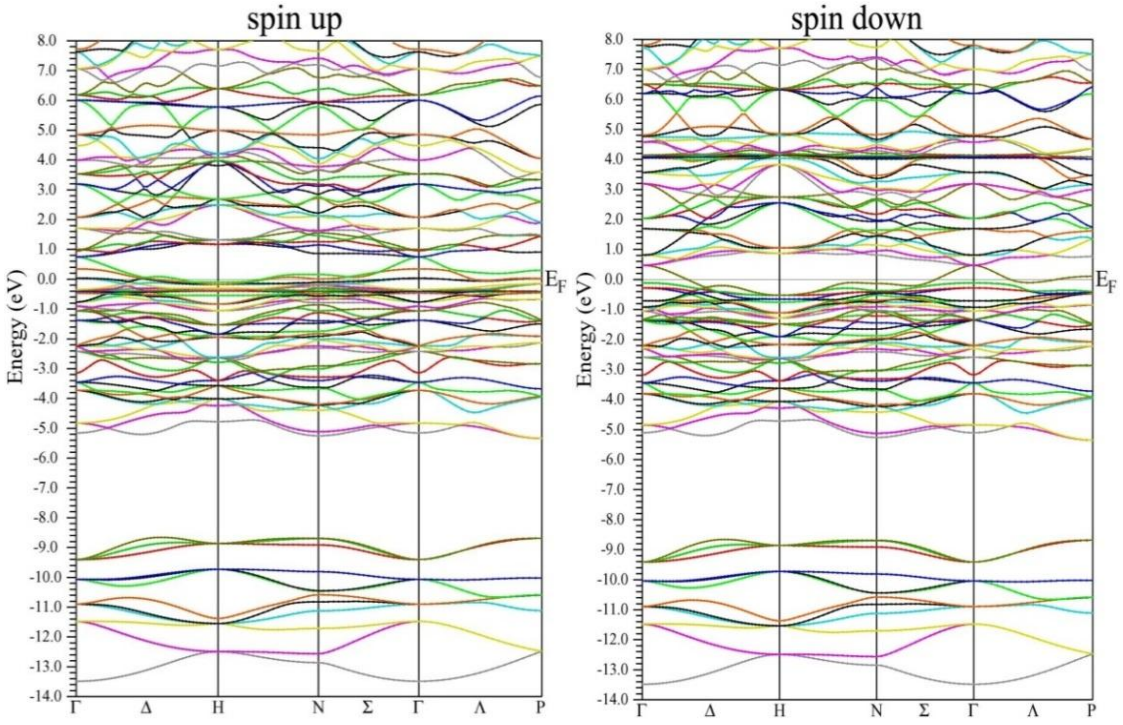

Fig. 4.7: Energy band structure plot of $EuFe_4As_{12}$ for spin up and spin down channels.

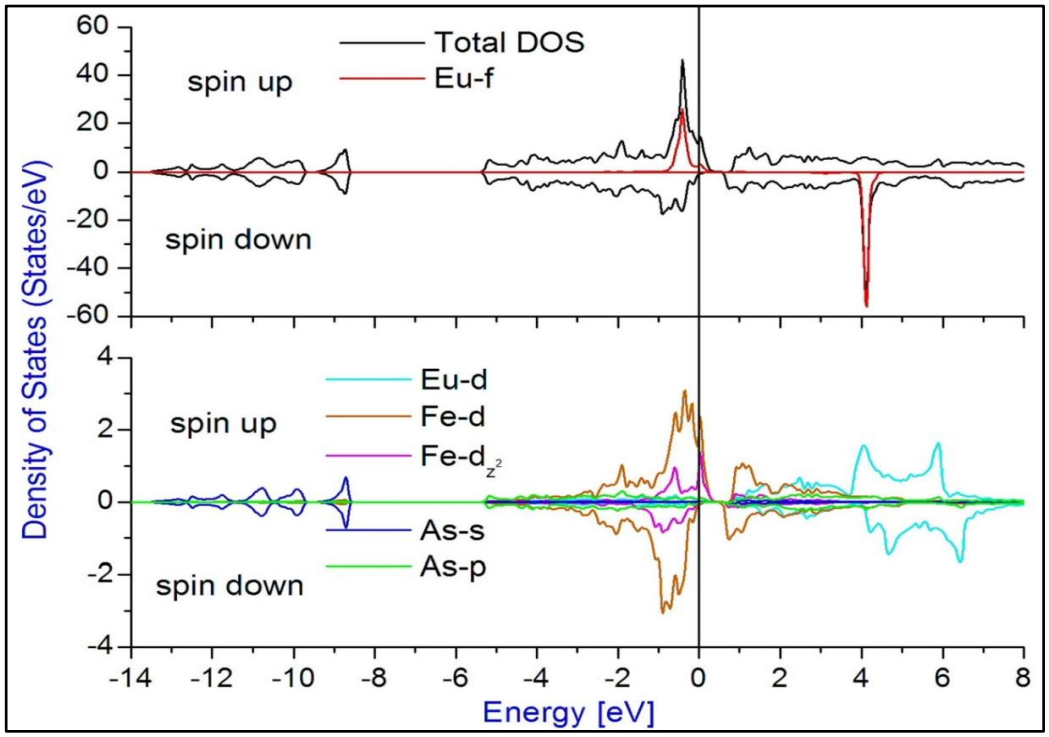

Fig. 4.8: Total and partial DOS of $EuFe_4As_{12}$.

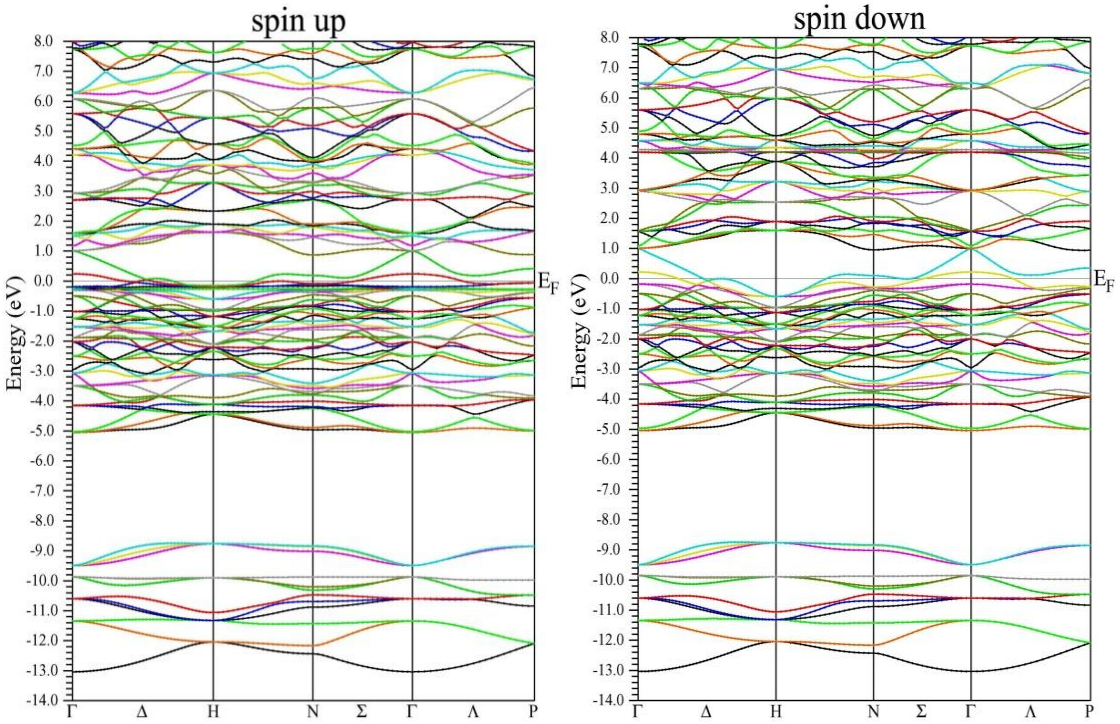

Fig. 4.9: Energy band structure plot of $EuRu_4As_{12}$ for spin up and spin down channels.

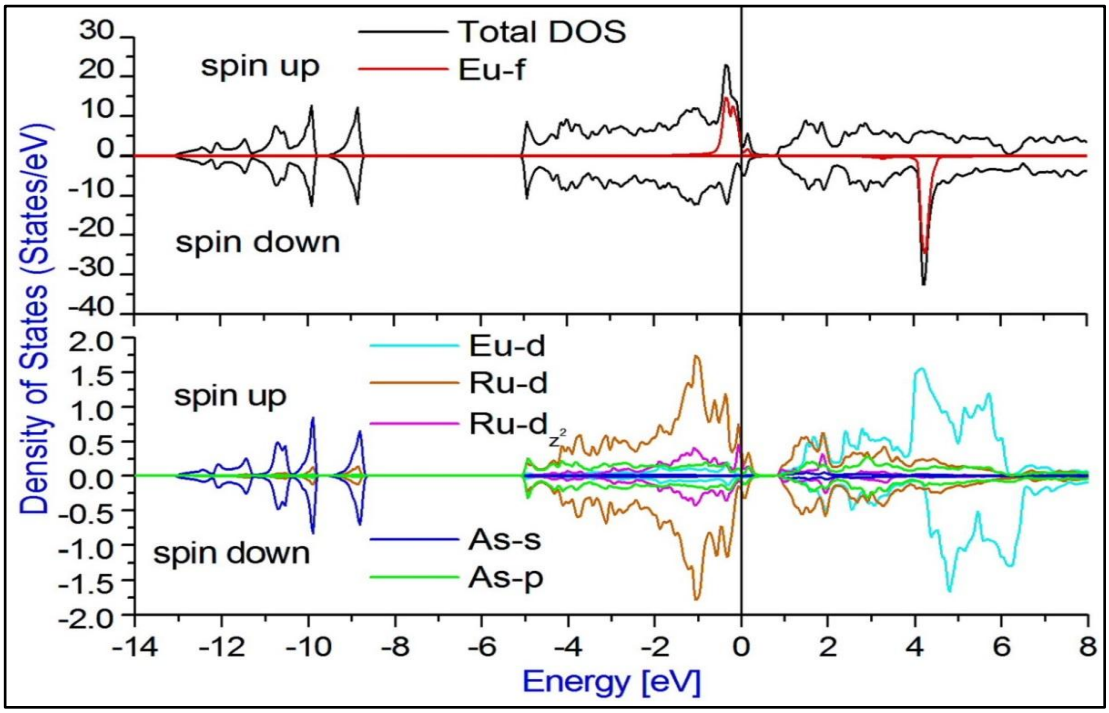

Fig. 4.10: Total and partial DOS of $EuRu_4As_{12}$.

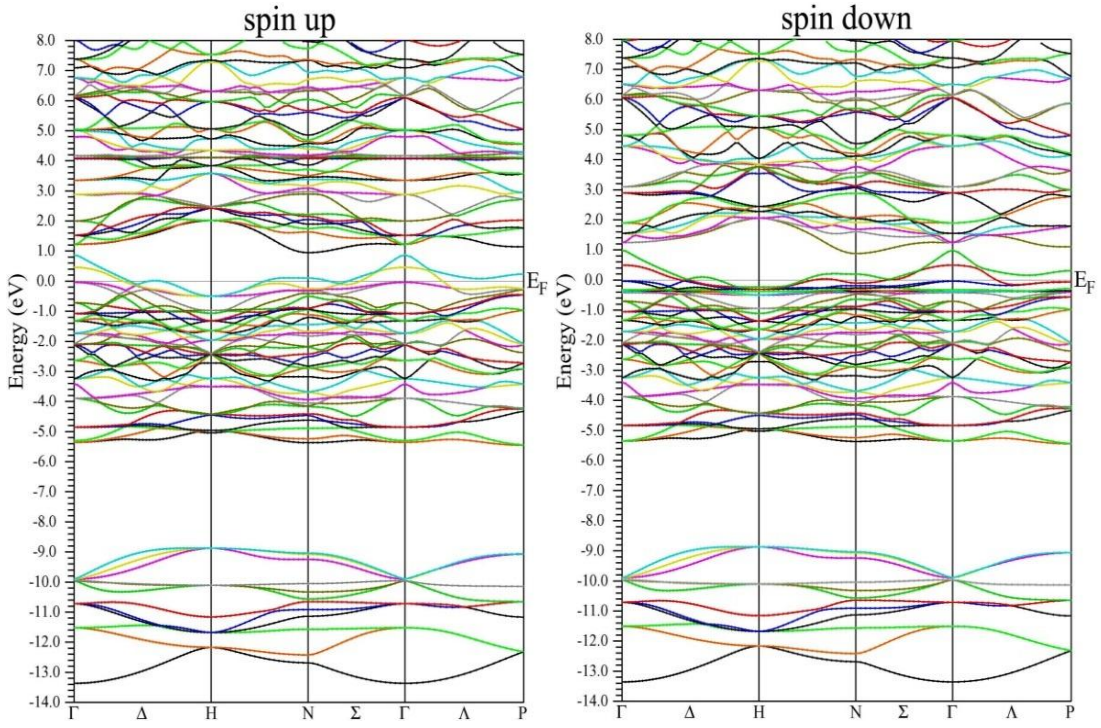

Fig. 4.11: Energy band structure plot of $EuOs_4As_{12}$ for spin up and spin down channels.

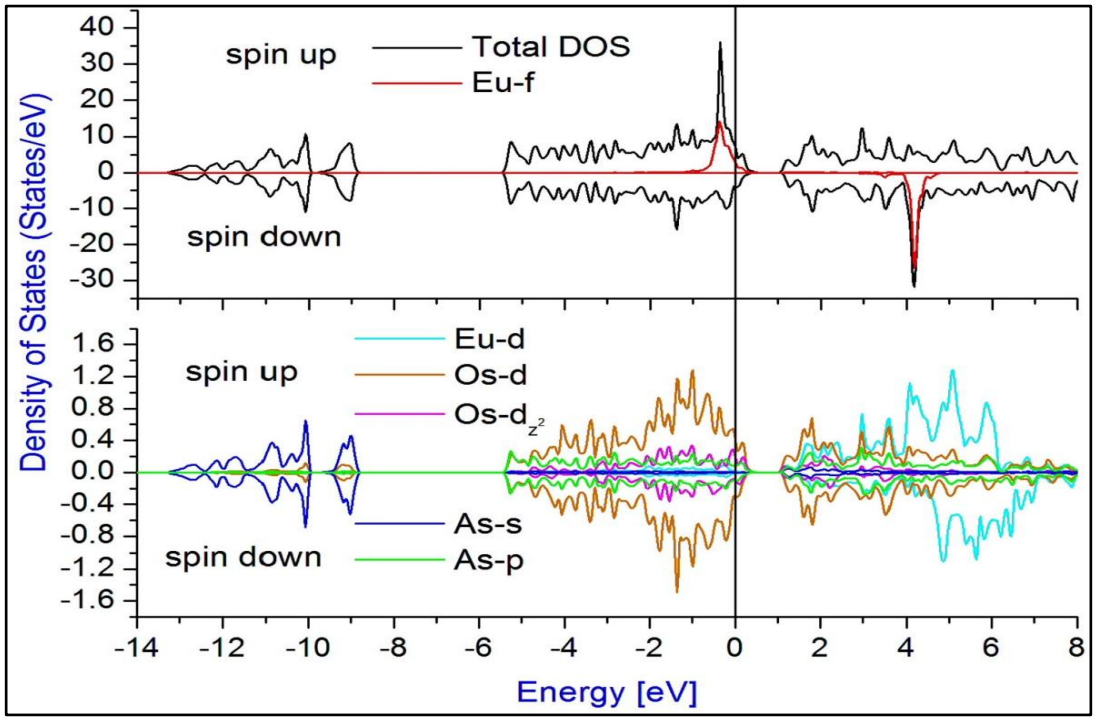

Fig. 4.12: Total and partial DOS of $EuOs_4As_{12}$.

similar to EuM_4P_{12} (M = Fe, Ru, Os). Thus these compounds are also metals. The results also favor a larger electronic specific heat for EuM_4As_{12} similar to $LaFe_4Sb_{12}$ (Vinnois *et al*., 2005; Bauer *et al*., 2001). To determine the density of states at Fermi energy $N(E_F)$ for EuM_4P_{12} and for their comparison with the low-temperature specific heat, we have evaluated $N(E_F)$ as shown in Table 4.3. The value of $N(E_F)$ which we obtain is close to that obtained by Harima (1998), Harima and Takegahara (2003) and Nouneh *et al*. (2007) for isosturctural $LaFe_4Sb_{12}$ and $CeFe_4Sb_{12}$. From the electronic structure plots one can observe that the valence width is maximum for Os-arsenide, which gives the material to be less covalent and more ionic nature of this compound, which supports the result obtained from the Poisson's ratio value for these compounds (Table 3.10 of Chapter 3). From the band structure plots (Figs. 4.1, 4.3, 4.5) one can see that the valence band crosses the Fermi level and overlaps at the *N* point with a flat conduction band arising from 4*f*-states of Eu, revealing the metallic behavior of the compounds investigated and high effective masses, which give substantial rise to the large value of thermoelectric Seebeck coefficients.

The splitting of the DOS in the spin-up and spin-down channels were observed for Eu-*f* state which contributes to the magnetic moments of these compounds. In Table 4.4, we have given the total and individual magnetic moments for the compounds under study. Though the transition metals are antiferromagnetically coupled to europium moments, since the coupling is negligible, it gives the overall ferromagnetic behavior of the compounds and the result is also supported by Stoner criteria. Previously, Sekine *et al.* (2009) have also reported the ferromagnetic transition of $EuFe_4As_{12}$ and $EuOs_4As_{12}$ at T_c = 152 K and 25 K respectively.

Table 4.3: Calculated energy gaps, DOS at E_F and electronic specific heat of EuM_4As_{12} (M = Fe, Ru, Os).

Compound	**E_g (eV) for spin**		**$N(E_F)$ (States/eV)**	**γ (mJ/mol-K^2)**
	up	**down**		
$EuFe_4As_{12}$	-----	-----	9.04	21.48
$EuRu_4As_{12}$	----	-----	8.72	20.70
$EuOs_4As_{12}$	0.1	----	11.15	26.48

Table 4.4: Total and individual magnetic moments and effective exchange interaction of EuM_4As_{12} (M = Fe, Ru, Os).

Compound	**Magnetic moment (μ_B)**					**Effective exchange interaction (I_{ex}) (eV)**
	Eu	**M**	**As**	**Total**	**Previous result**	
$EuFe_4As_{12}$	6.80	-0.45	0.003	5.18	6.93*	4.60
$EuRu_4As_{12}$	6.79	-0.02	-0.002	6.75	8.31*	4.47
$EuOs_4As_{12}$	6.69	-0.05	-0.009	6.48	7.29*	4.58

*(Sekine *et al.*, 2009)

C) EuM_4Sb_{12} (M = Fe, Ru, Os)

The energy band structures and DOS for EuM_4Sb_{12} (M = Fe, Ru, Os) are given in Figs. 4.13 - 4.17 for Fe, Ru and Os respectively as the central transition element. The similar chemical formula of these compounds results similar profile of the DOS and band structure plots. From the band structure plots (Figs. 4.13, 4.15, 4.17) one can conclude that the energy bands are highly populated just below the Fermi level in the valence region for spin up channel. Similar to the report of Singh and Mazin (1997) and Harima (1998), we have also observed the contribution from *d*-bands of transition metal below anionic *p*-like valence states. In our calculation, the region above E_F there exist a very small DOS but not zero. The presence of such region with a low density of states is termed as pseudogap and is typical characteristic of the skutterudites (Nouneh *et al*., 2007; Takegahara and Harima, 2003; Fornari and Singh, 1999). The two bands originating from the bottom of the unoccupied region penetrates the top of the occupied region, cross the Fermi energy level at least two times (directions $\Gamma - H$ and $H - N - P$) in accordance with previous work for analogous system (Harima and Takegahara, 2003). Hence the Fermi energy level is not in between the conduction and valence band but within the valence band and $N(E_F)$ is relatively high with high effective masses, which give substantial rise to the large value of thermoelectric Seebeck coefficients in this type of system as reported for anoalogous $CeOs_4Sb_{12}$ (Harima, 1998; Harima and Takegahara, 2003). Thus these compounds are also metals and similar type of result was obtained by Meisner *et al*. (1985), Sato *et al*. (2000) for metallic $LaFe_4P_{12}$ and $CeFe_4P_{12}$. The results also favor a larger electronic specific heat for EuM_4Sb_{12} as given in Table 4.5 similar to $LaFe_4Sb_{12}$ (Viennois *et al*., 2005; Bauer *et al.*, 2001). The value of $N(E_F)$ are given in Table 4.5.

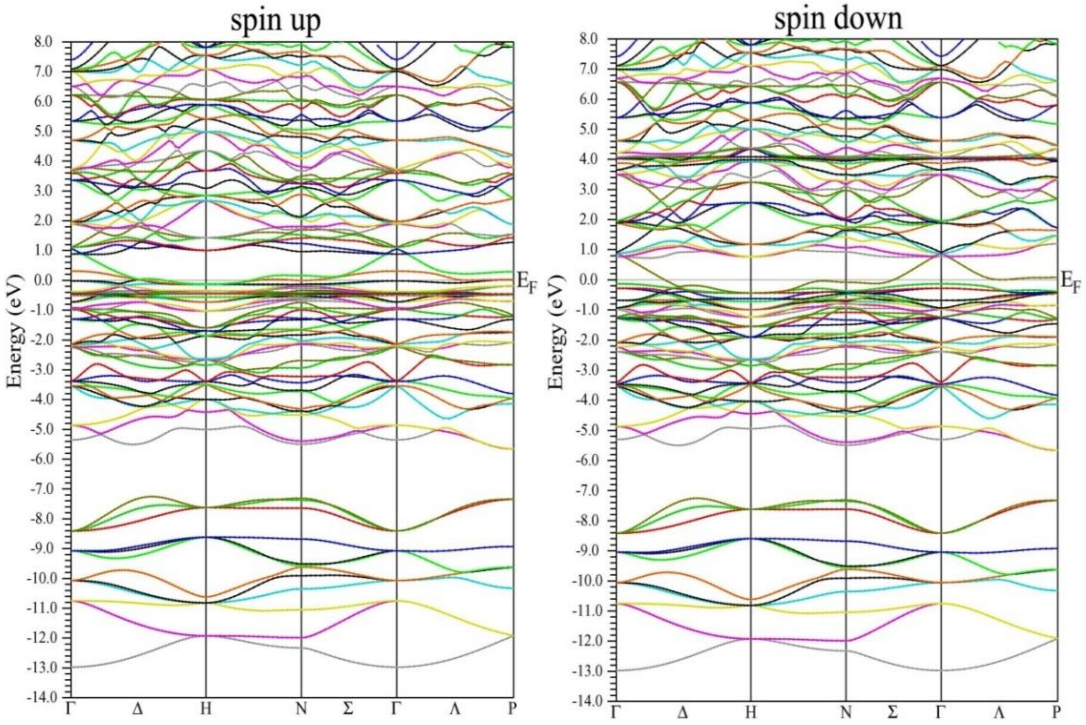

Fig. 4.13: Energy band structure plot of $EuFe_4Sb_{12}$ for spin up and spin down channels.

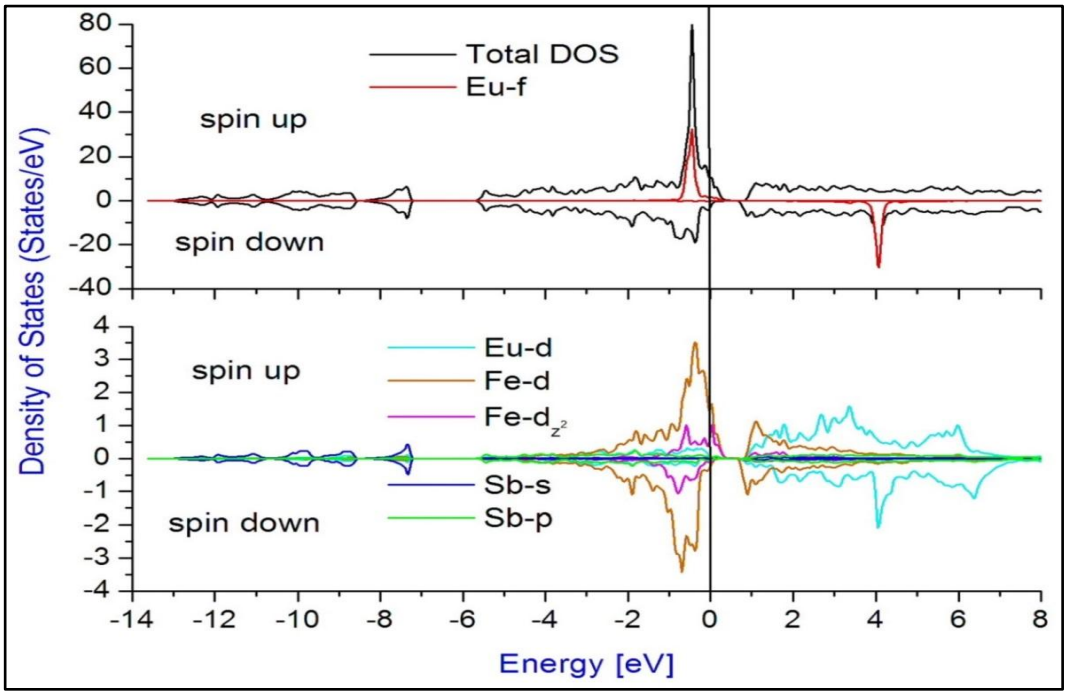

Fig. 4.14: Total and partial DOS of $EuFe_4Sb_{12}$.

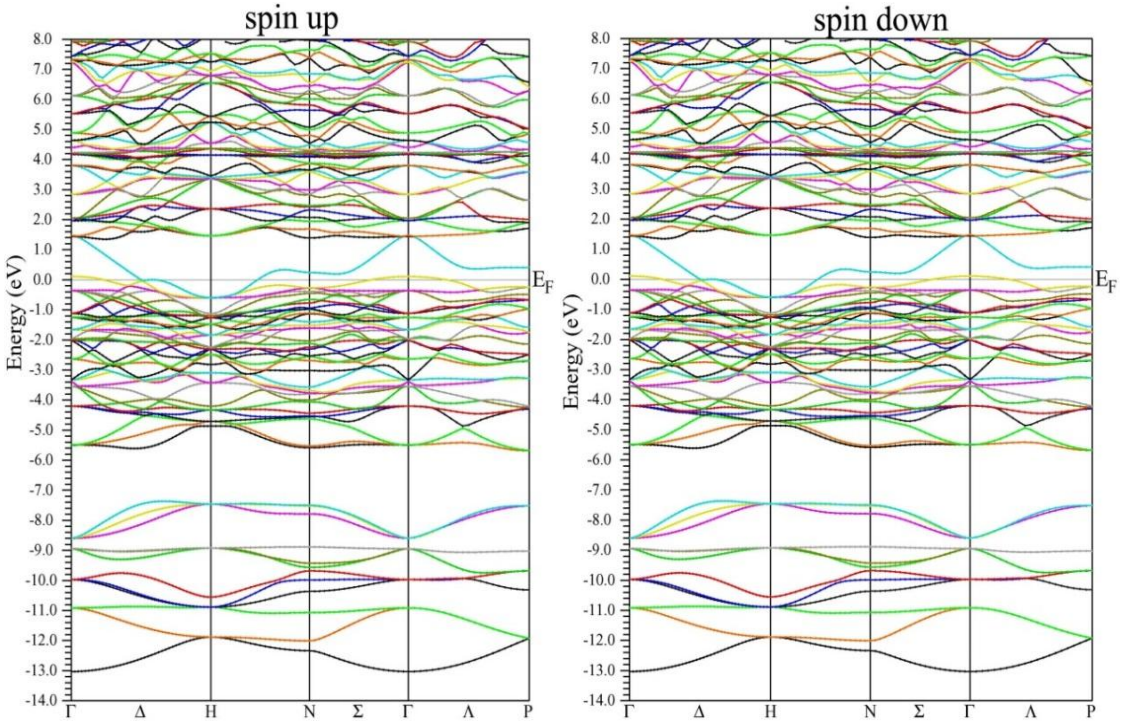

Fig. 4.15: Energy band structure plot of $EuRu_4Sb_{12}$ for spin up and spin down channels.

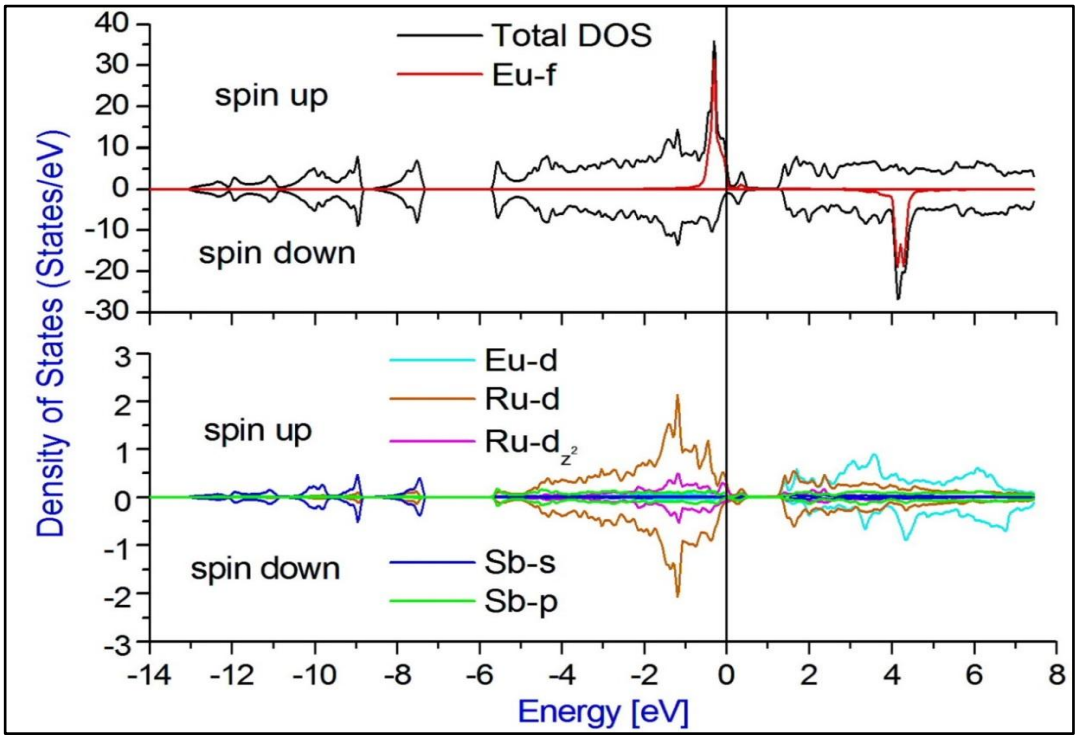

Fig. 4.16: Total and partial DOS of $EuRu_4Sb_{12}$.

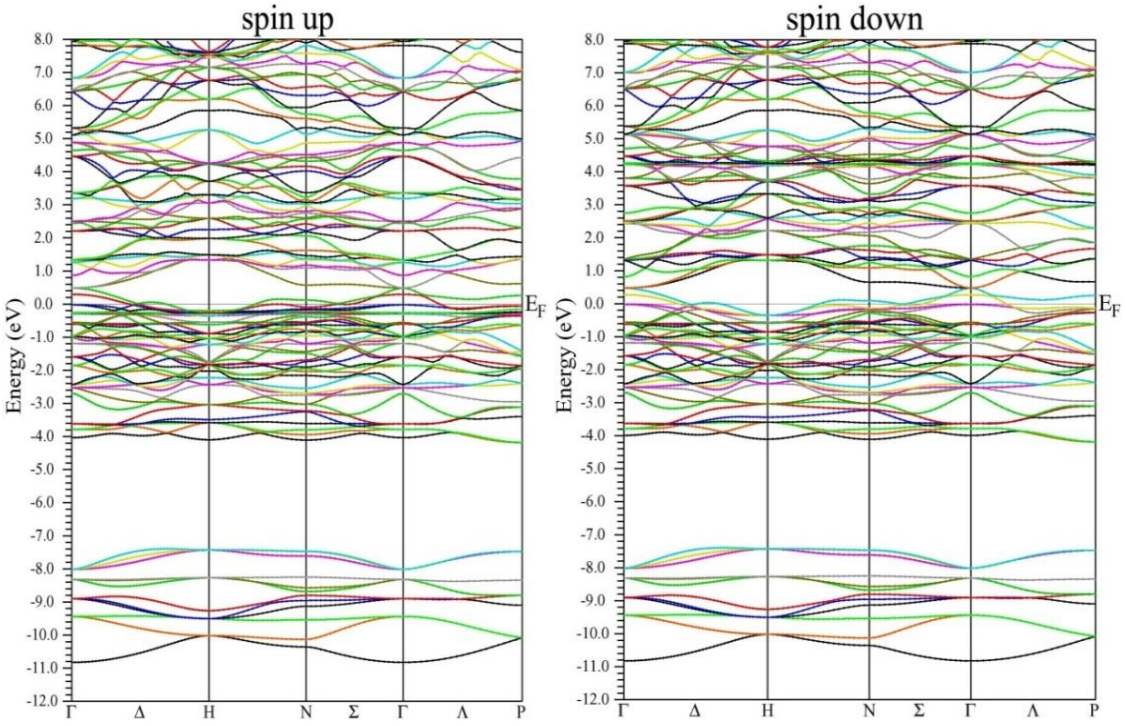

Fig. 4.17: Energy band structure plot of $EuOs_4Sb_{12}$ for spin up and spin down channels.

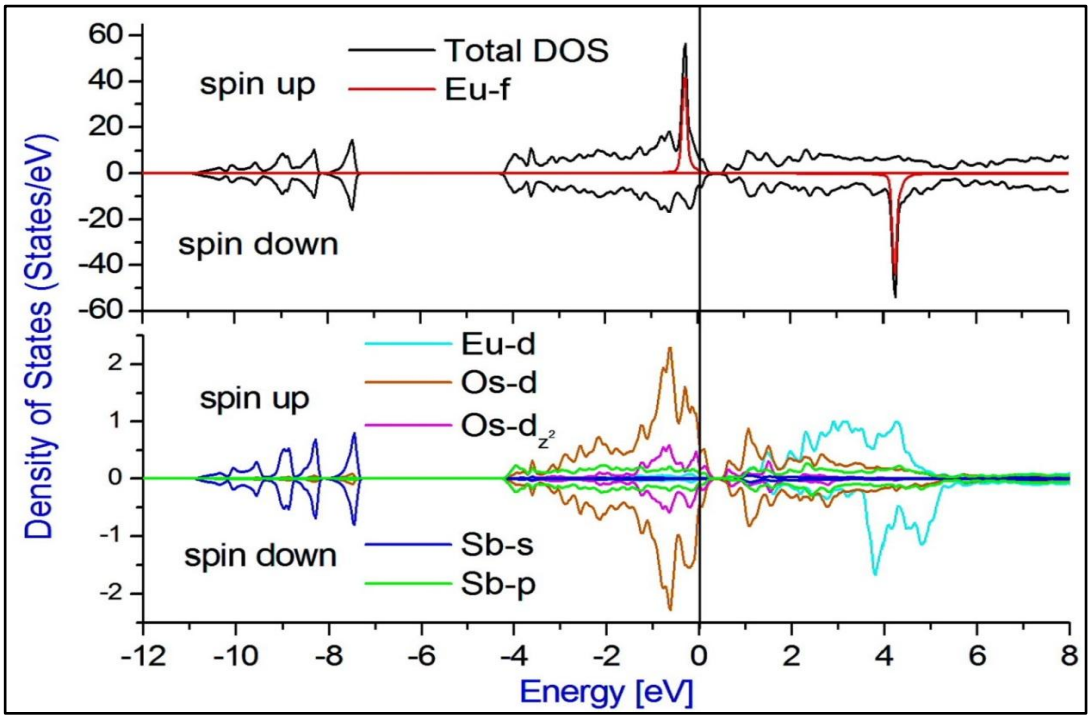

Fig. 4.18: Total and partial DOS of $EuOs_4Sb_{12}$.

From the DOS plots (Figs. 4.14, 4.16, 4.18) it is observable that there is splitting of the total DOS in the spin up and spin down channel and it is responsible for the magnetic behavior of the system under consideration. The calculated total and individual magnetic moments for the europium, transition elements and pnictogens are given in Table 4.5. From the Table 4.5 and DOS plots (Figs. 4.14, 4.16, 4.18) it is clear that the Eu have the highest contribution in the total magnetic moments of these filled skutterudites. Krishnamurthy *et al.* (2007) and have reported the ferrimagnetic behavior of $EuFe_4Sb_{12}$, whereas, Evers *et al.* (1995), Bauer *et al.* (2004), Danebrock *et al.* (1996) have reported the $EuFe_4Sb_{12}$ is a ferromagnetic metal with T_C = 88 K. Similarly, Bauer *et al*. (2004), Takeda and Ishikawa (2000), Braun and Jeitschko (1980) have reported the $EuRu_4Sb_{12}$ to be ferromagnetic metal with T_C = 4 K. $EuOs_4Sb_{12}$ is a ferromagnetic metal with T_C = 9 K as reported by Bauer *et al.* (2004). Our calculation also supports the previous results of ferromagnetic behaviour of compounds mentioned in the table 4.5 satisfying Stoner criteria as well.

Table 4.5: Calculated DOS at E_F, electronic specific heat, magnetic moments and effective exchange interaction of EuM_4Sb_{12} (M = Fe, Ru, Os).

Compound	**N(E_F) (States/eV)**	**γ (mJ/mol-K^2)**	**Magnetic moment (μ_B)**					**Effective exchange interaction (I_{ex}) (eV)**
			Eu	**M**	**Sb**	**Total**	**Previous result**	
$EuFe_4Sb_{12}$	10.46	24.83	6.93	-0.40	0.001	5.35	8.40*	4.7
$EuRu_4Sb_{12}$	5.83	13.84	6.69	-0.01	-0.001	6.80	8.00*	4.39
$EuOs_4Sb_{12}$	11.41	27.09	6.79	-0.01	-0.003	6.82	7.30*	4.42

* (Bauer *et al*., 2004)

Chapter 5

Optical Properties of Rare earth Filled Skutterudites

5

Optical Properties of Rare earth Filled Skutterudites

The study of the optical properties of a compound in the spectral range of infrared to ultraviolet and above the band gap plays an important role to understand the nature of the material and also to understand about its applications in optoelectronics devices (Mutou and Saso, 2009). We have calculated the optical properties of the compounds under study as a function of incident photon energy. Since filled skutterudites have cubic symmetry, to characterize completely the optical properties of the system, we need to calculate only one component of the imaginary part of the frequency dependent dielectric function $\varepsilon_2(\omega)$ (Shankar *et al*., 2013b) as it is related to the absorption of the incident photon by medium. A description of the formalism for calculations of optical properties is already discussed in Chapter 2. For optical calculations a dense mesh of uniformly distributed *k*- points is used and no scissor shift was performed to adjust the theoretical bandgap with experimental values as implemented in WIEN2k code (Blaha *et al.*, 2012) due to the non-availability of experimental bandgap value. Hachemaoui *et al.* (2009), Mutou and Saso (2009) have reported the optical spectra for some of filled skutterudites using FP-APW+lo and tight binding model respectively, but to our knowledge, no experimental or theoretical results for the optical spectra are available for the compounds under study. This therefore implies that the present results can be considered as a predictive study, with the model used.

5.1 Results and Discussion

a) EuM_4P_{12} (M = Fe, Ru, Os)

Our theoretically calculated absorptive (ε_2) and dispersive (ε_1) parts of the electronic dielectric function spectrums are shown in Figs. 5.1 - 5.3 for EuM_4P_{12} (M = Fe, Ru, Os) respectively, for photon energy radiation 0 - 12.0 eV. The optical transitions from the valence region to the conduction region of the energy bands give the various peaks in the optical spectra. The nearly same band structure plots of the compounds under study give similar profile in the optical spectra of these materials. Each peak in ε_1 and ε_2 in the optical response plots can be determined by the electric-dipole transitions between the occupied and unoccupied states of the band structure plots. In our calculations we have considered only the direct inter-band transition and neglect the indirect transition, because it gives very small contribution to dielectric function. As it can be seen from the Figs. 5.1 - 5.3, that they have some common features, with first peak for real (ε_1) part is close to Fermi level. Thus the first critical point (absorption edge) is embedded within the zero energy. We note that the peak heights are reduced as we move from Fe to Ru and then it increases with moving from Ru to Os. One can observe from the $\varepsilon_2(\omega)$ spectra, there is sharp peak below 1 eV, which comes close to Fermi level in increasing order of the atomic radii of transition elements. From the same plot it is also clear that the peak height decreases with the increasing value of the corresponding energy value of the peak and can be explained as $1/\omega^2$ behaviour of $\varepsilon_2(\omega)$. From the optical spectra one can conclude that the peaks in $\varepsilon_2(\omega)$ in infrared regions are due to the transitions from band just below the Fermi level to the bands just

above the Fermi level (preferably in *N* and Γ symmetry points). Similarly the peaks in the visible region are due to transition due to middle of the occupied states to the unoccupied states. The static dielectric constant is an important quantity, it is ε_1 at the zero frequency limits $\varepsilon_1(0)$, where there is no contribution from the lattice vibration and its values are given in Table 5.1. It is noted from the table that $\varepsilon_1(0)$ is band gap dependent and follows an inverse square relation between $\varepsilon_1(0)$ and E_g given by Penn model (Penn, 1962) $\varepsilon_1(0) \approx 1 + \left(\hbar\omega_p / E_g \right)^2$, where ω_p is plasmon energy. The $\varepsilon_1(\omega)$ spectrum lower than 1 shows metallic behavior at certain energy range with high value of reflectiveness for the incident electromagnetic radiation. So, these compounds can be used as a protection from electromagnetic radiations in this specific energy limits. The negative values of $\varepsilon_1(\omega)$ correspond to the local maxima of reflectivity in this energy range as shown in Figs. 5.4 - 5.6 with a further increase in energy, $\varepsilon_1(\omega)$ increases and shows a steady behavior at high energy limits.

The refractive index is one of important characteristic for optical design and applications. High refractive materials are used in ophthalmic lenses, filters and optical adhesives, antireflection coating and advanced optoelectronic devises. We have also calculated the frequency dependent refractive indices for the given materials and the plots are given in Figs. 5.4 - 5.6 respectively for Fe, Ru and Os as the central transitional element. Since the materials under study, at low energy have high refractive index so these materials can be used in the above mentioned fields. At zero frequency limits, the static refractive indices are given in Table 5.1. The table also reveals that at zero frequency limits, the refractive indices decreases in similar pattern as $\varepsilon_1(0)$. The

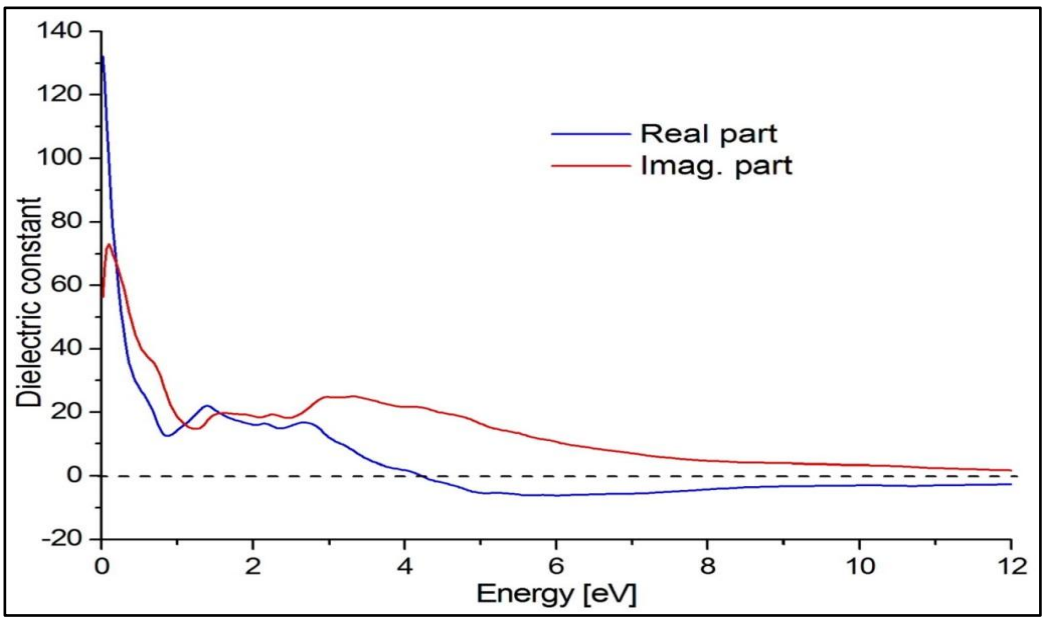

Fig. 5.1: Calculated real and imaginary parts of the dielectric functions of $EuFe_4P_{12}$.

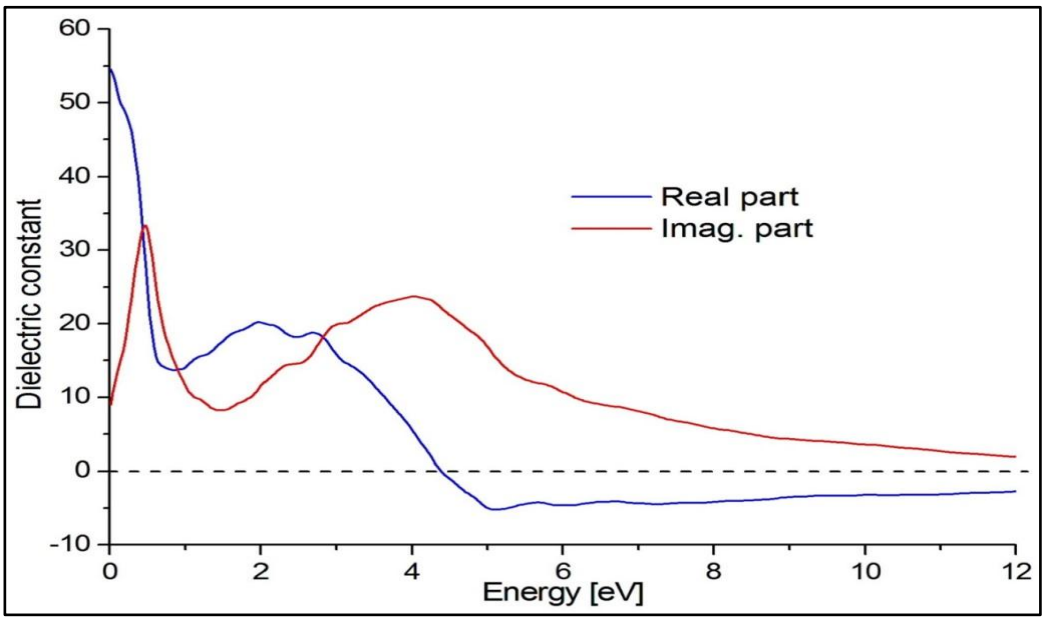

Fig. 5.2: Calculated real and imaginary parts of the dielectric functions of $EuRu_4P_{12}$.

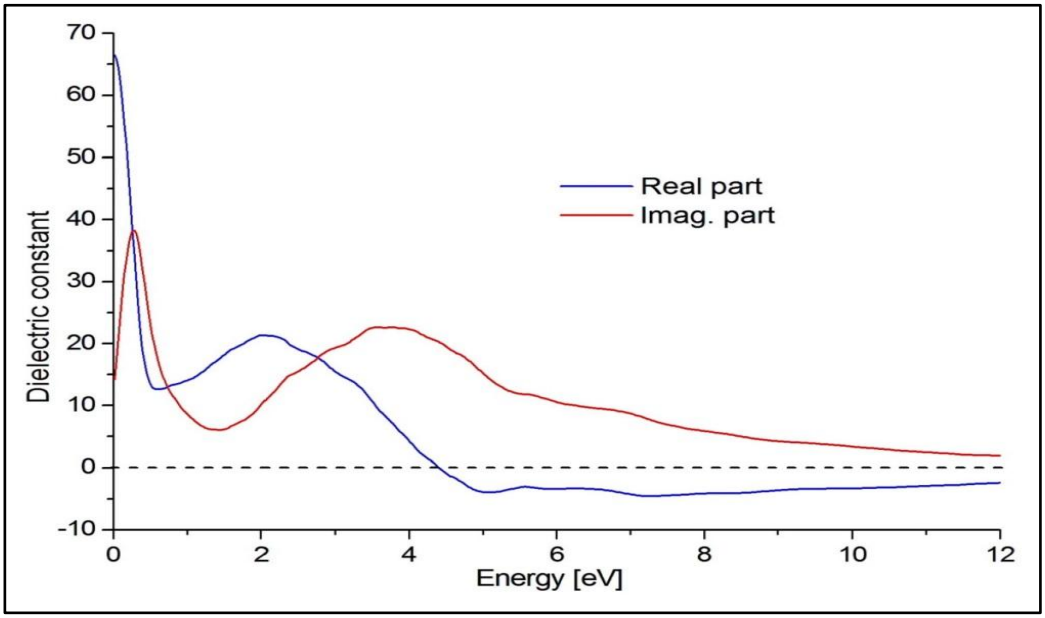

Fig. 5.3: Calculated real and imaginary parts of the dielectric functions of $EuOs_4P_{12}$.

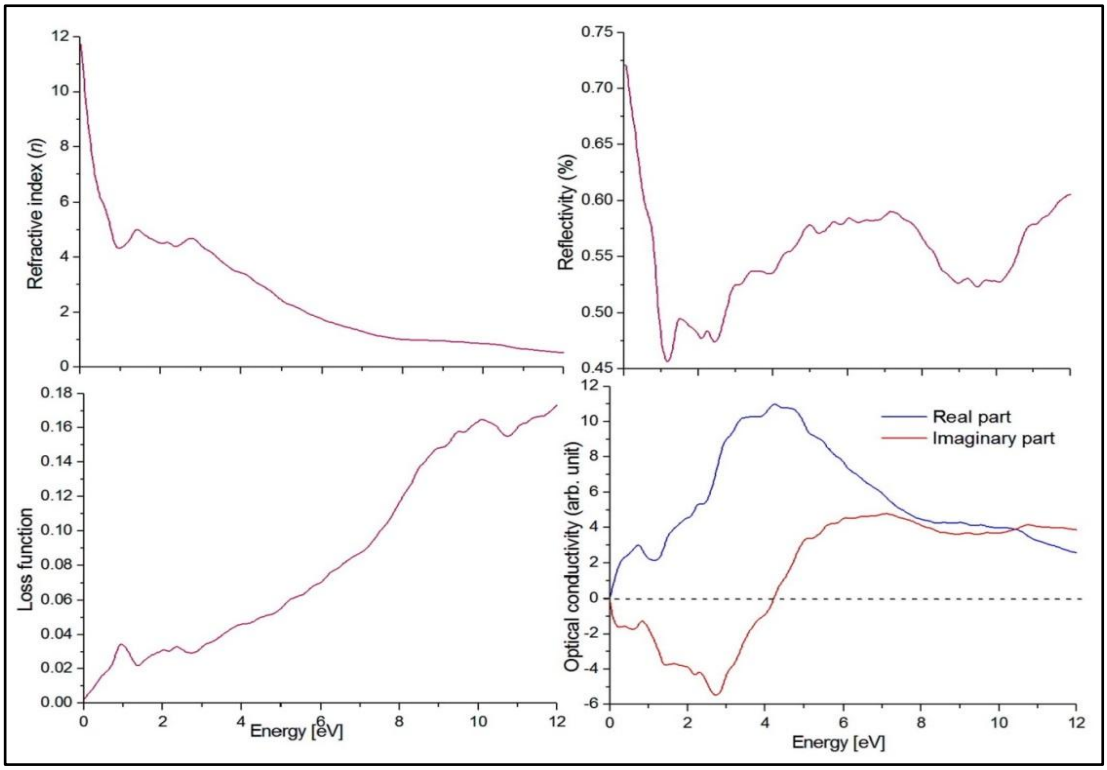

Fig. 5.4: Calculated electron refractive index, reflectivity, loss spectra, real and imaginary part of the optical conductivity of $EuFe_4P_{12}$.

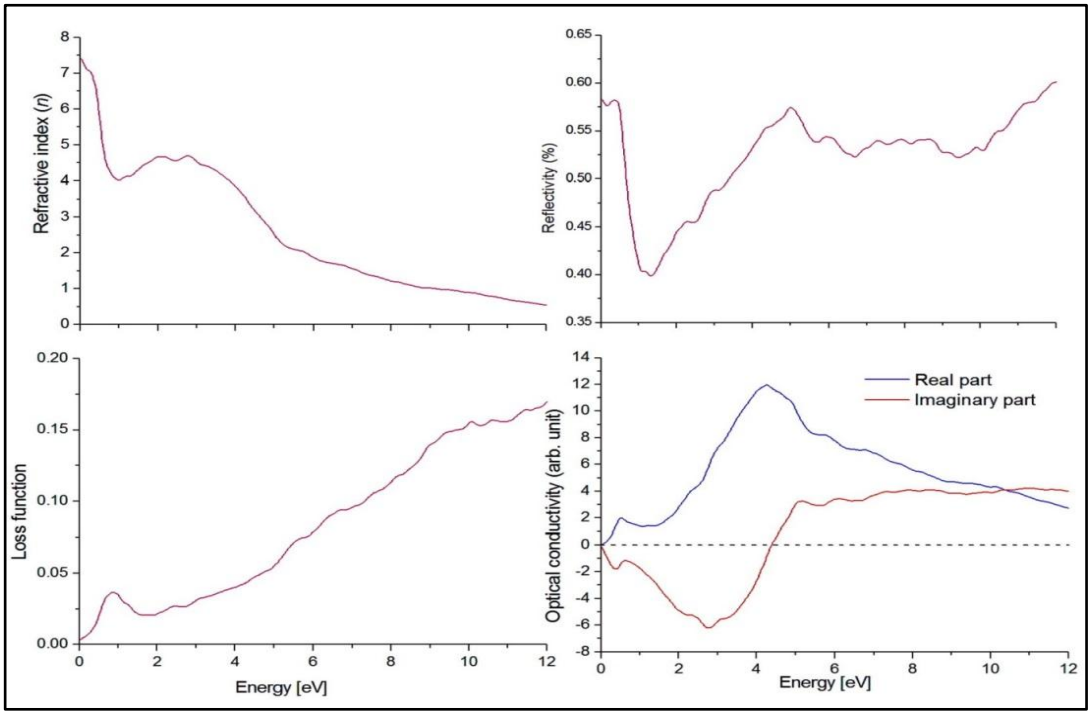

Fig. 5.5: Calculated electron refractive index, reflectivity, loss spectra, real and imaginary part of the optical conductivity of $EuRu_4P_{12}$.

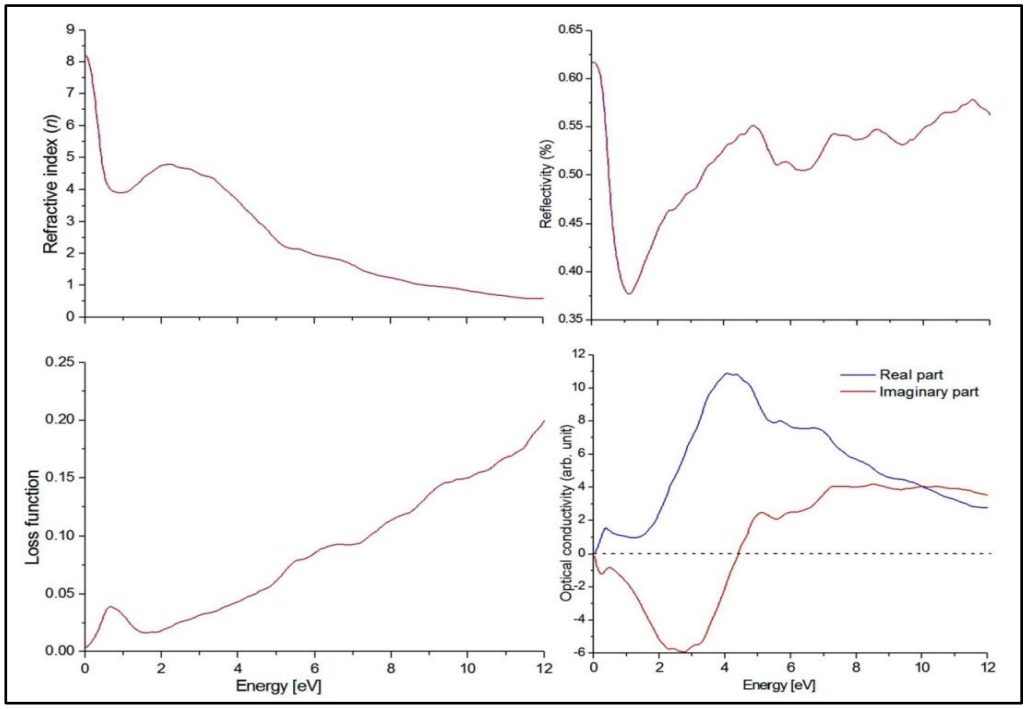

Fig. 5.6: Calculated electron refractive index, reflectivity, loss spectra, real and imaginary part of the optical conductivity of $EuOs_4P_{12}$.

refractive index plots decreases from 2 eV energy range with increase of energy, this decrease in refractive indices at higher energies are due to the fact that direct de-excitation of the electron is not possible and hence energy is dissipated at higher energies. It is found that at certain frequency, refractive index falls below unity. This shows that where $n(\omega)$ is lesser than unity, the material no longer acts as a transparent material with superluminal behavior. The refractive index less than unity shows that the phase velocity greater than light velocity, which is in disagreement to relativity. This suggests that in a dispersive medium signal transmitted as wave packet propagating at the group velocity. At higher frequency range the refractive index tends to zero showing the material absorbs high energy photons.

The normal incident reflectivity spectra for EuM_4P_{12} are shown in Figs. 5.4- 5.6. An abrupt reduction in reflectivity spectra or absorption at low energy occurs due to d- f transition of rare earth. The strong maxima are present close to 0 eV and abrupt reduction to 1 eV confirming the occurrence of collective plasmon resonance exciton with the strong minima near 1 eV [Figs. 5.4 - 5.6]. The local maxima of reflectivity occurs in the energy range of 5 eV as shown in Figs. 5.4- 5.6, which attribute to the negative values of $\varepsilon_1(\omega)$ (Figs. 5.1- 5.3).

Electron energy loss spectroscopy (EELS) is a precious tool for the investigation of the different physical aspects of a material (Lougin *et al*., 1996). It provides information about elastically scattered and non-scattered electrons and the number and type of atom being struck by the beam. The electron energy loss spectra for EuM_4P_{12} (M = Fe, Ru, Os) systems under study are given in Figs. 5.4 - 5.6. Inelastic scattering is observed till energy radiation of 5.0 eV and it increases with increasing energy. At zero

energy the energy loss spectra is minimum and no scattering is occurring and since ε_2 is maximum at this energy. With the increase of photon energy radiation, ε_2 decreases gradually and becomes minimum at photon energy ~3 eV and at high photon energy ε_2 is smaller. This has a correlation with the EELS, which increases for a minimum to a maximum with the increase in photon energy.

The optical conductivity is related to the frequency dependent dielectric constant $\varepsilon(\omega)$ by $\varepsilon(\omega)=1+4\pi i\sigma(\omega)/\omega$. In Figs. 5.4 - 5.6, the calculated real and imaginary parts of the optical conductivity for EuM_4P_{12} are shown for the infrared to ultraviolet radiation, the spectra contain a lot of peaks (at 0.4 eV, 4.0 eV, 6.0 eV) which corresponds to electronic transition from the valence band to the conduction band similar to the case of imaginary part of dielectric constant. After a smooth start with zero conductivity, we obtain a sharp increase that reaches a peak at ~ 4.0 eV energy range. It is known that the real part of optical conductivity of a system is directly proportional to the product of energy and the imaginary part of the dielectric function ε_2. As such, the origin of the peak in imaginary part of the dielectric function also explains those of the optical conductivity. The relative amplitudes of the structures scale as $\omega\varepsilon_2$. After 11 eV of energy the spectra becomes almost stable (not shown in figure clearly) for higher energy range indicating that the material does not interact with photons. However, imaginary(σ) decreases with the increase in the photon energy and goes in the negative axis giving a valley for ~ 3.0 eV of energy and then a sharp increase towards zero and crosses the real part at higher energy.

Table 5.1: Calculated energy gaps, static dielectric constant and static refractive index of EuM_4P_{12} (M = Fe, Ru, Os).

Compound	**E_g (eV) for spin**		**$\varepsilon_1(0)$**	***n*(0)**
	up	**down**		
$EuFe_4P_{12}$	----	0.2	132	11.5
$EuRu_4P_{12}$	----	0.3	54	7.4
$EuOs_4P_{12}$	0.16	0.4	62	8.2

b) EuM_4As_{12} (M = Fe, Ru, Os)

The real and imaginary parts of the electronic dielectric function spectrums are shown in Figs. 5.7 - 5.9 for EuM_4As_{12} (M = Fe, Ru, Os respectively), for energy radiation 0 - 12.0 eV. The calculated optical spectra are similar to that of EuM_4P_{12}, as they have similar type of band profile and the similar type of optical transitions are occurring from valence to conduction band. In our title materials the indirect transitions have very negligible contributions, hence only the direct inter-band transitions are considered to calculate the peaks in the dielectric functions. From the Figs. 5.7 – 5.9, it is observable that the real part of the dielectric function $\varepsilon_1(\omega)$ shows a sharp peak close to E_F and the absorption edge (first critical point) is within the zero energy. The static dielectric constants $\varepsilon_1(0)$ are also calculated and its values are summarized in Table 5.2. The $\varepsilon_1(\omega)$ spectrum have a maximum at zero frequency and for ultraviolet radiation it goes to negative values, which suggest that these materials show metallic behavior for ultraviolet radiation. The imaginary part of the dielectric function $\varepsilon_2(\omega)$ shows the highest peak for infrared radiation and the peak height decreases with the increasing value of the corresponding energy.

We have also investigated the frequency dependence of refractive indices and the plots are given in Figs. 5.10 – 5.12, respectively for Fe, Ru and Os as the central transitional element. At zero frequency limits, the static refractive indices are given in Table 5.2. From Figs. 5.10 - 5.12, one can observe that the refractive indices values decrease for the radiation of visible region with increase of energy which is due to the energy dissipation beyond that energy and the electrons are not directly de-excite. It is also found that, for ultraviolet radiation the refractive indices fall below unity, which

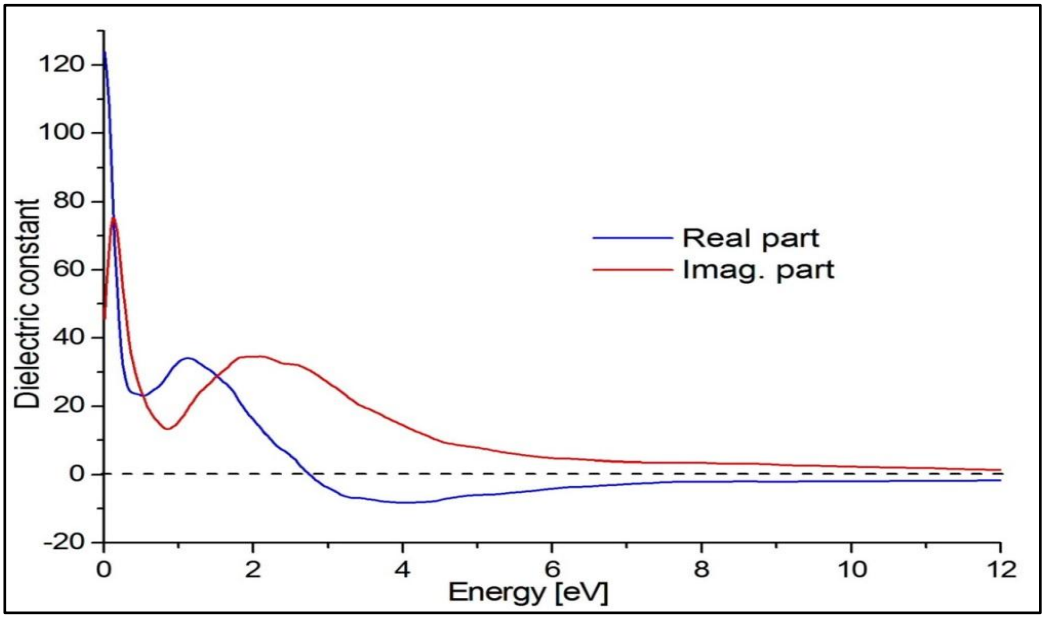

Fig. 5.7: Calculated real and imaginary parts of the dielectric functions of $EuFe_4As_{12}$.

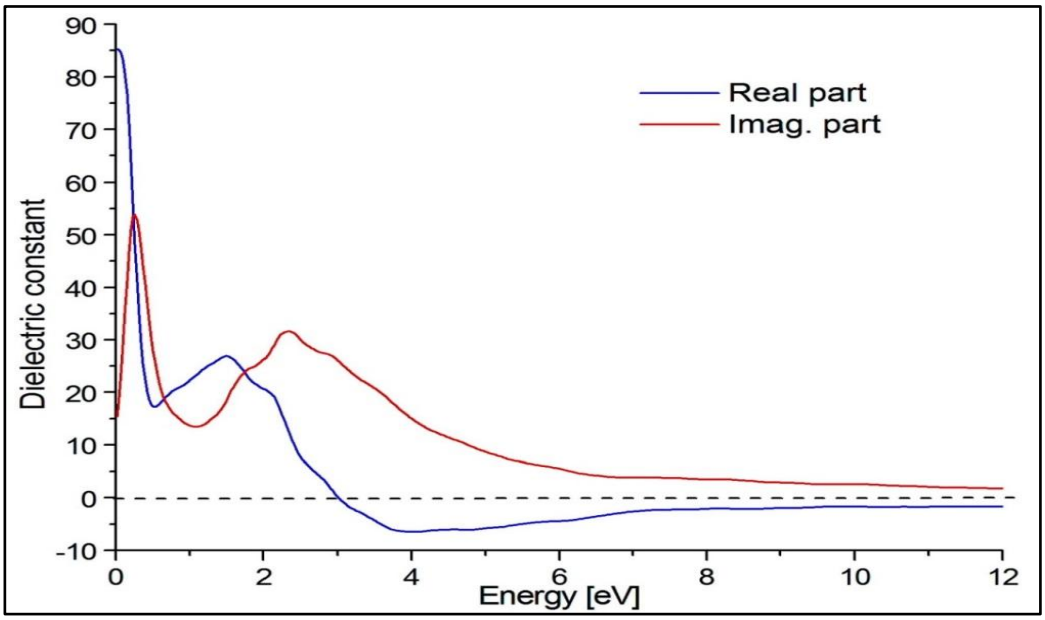

Fig. 5.8: Calculated real and imaginary parts of the dielectric functions of $EuRu_4As_{12}$.

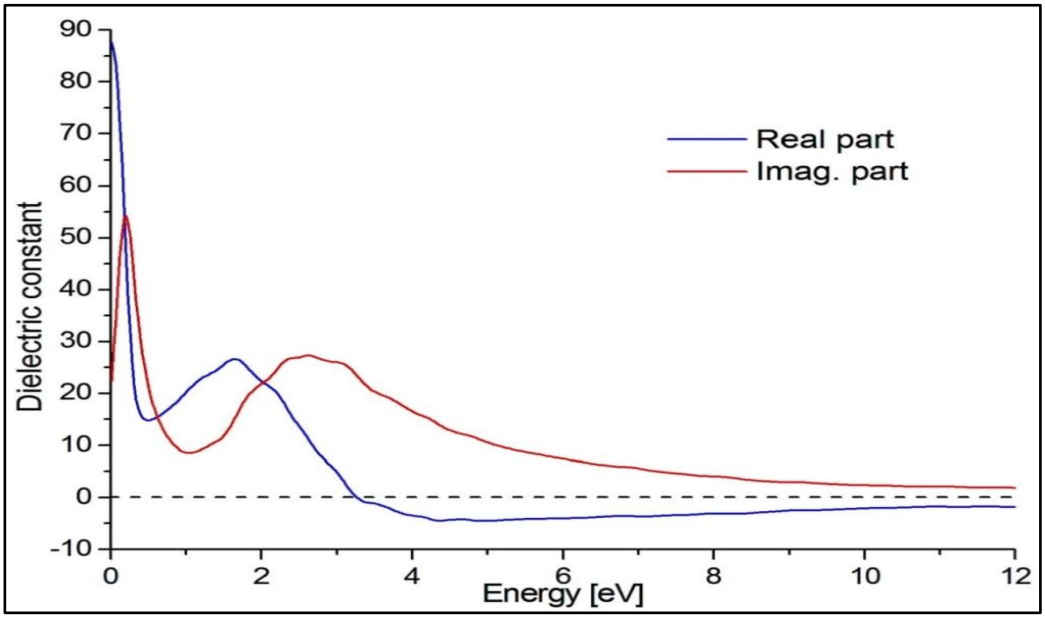

Fig. 5.9: Calculated real and imaginary parts of the dielectric functions of $EuOs_4As_{12}$.

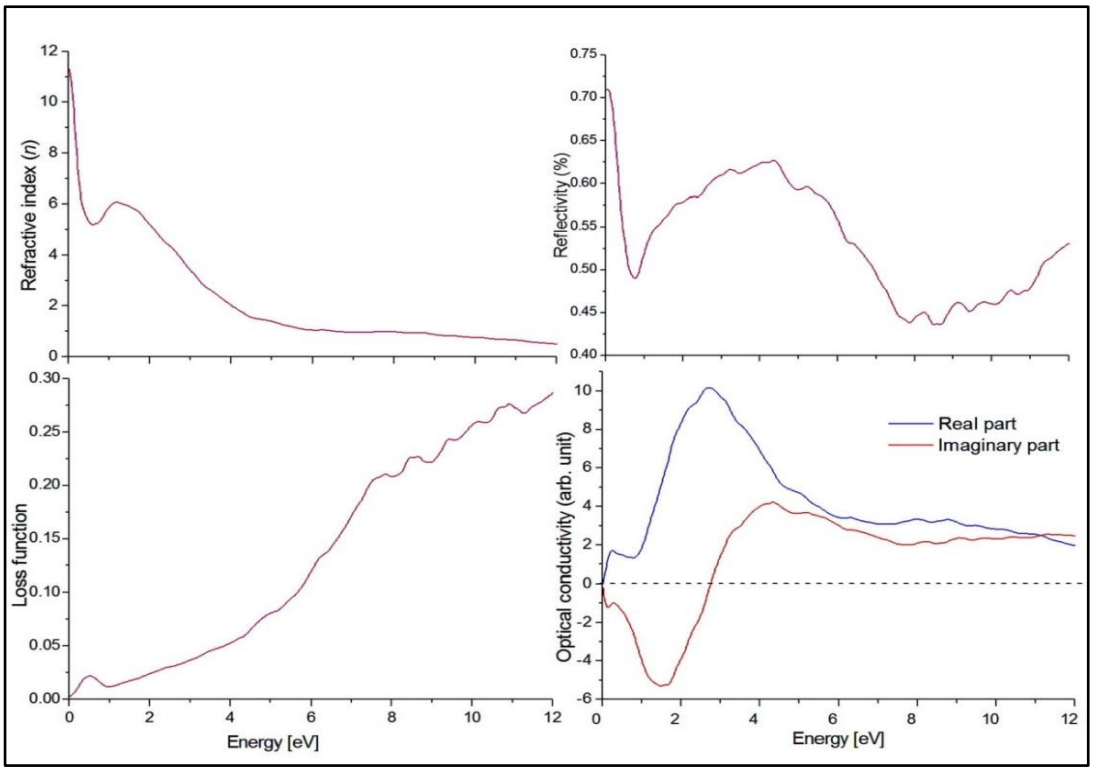

Fig. 5.10: Calculated electron refractive index, reflectivity, loss spectra, real and imaginary part of the optical conductivity of $EuFe_4As_{12}$.

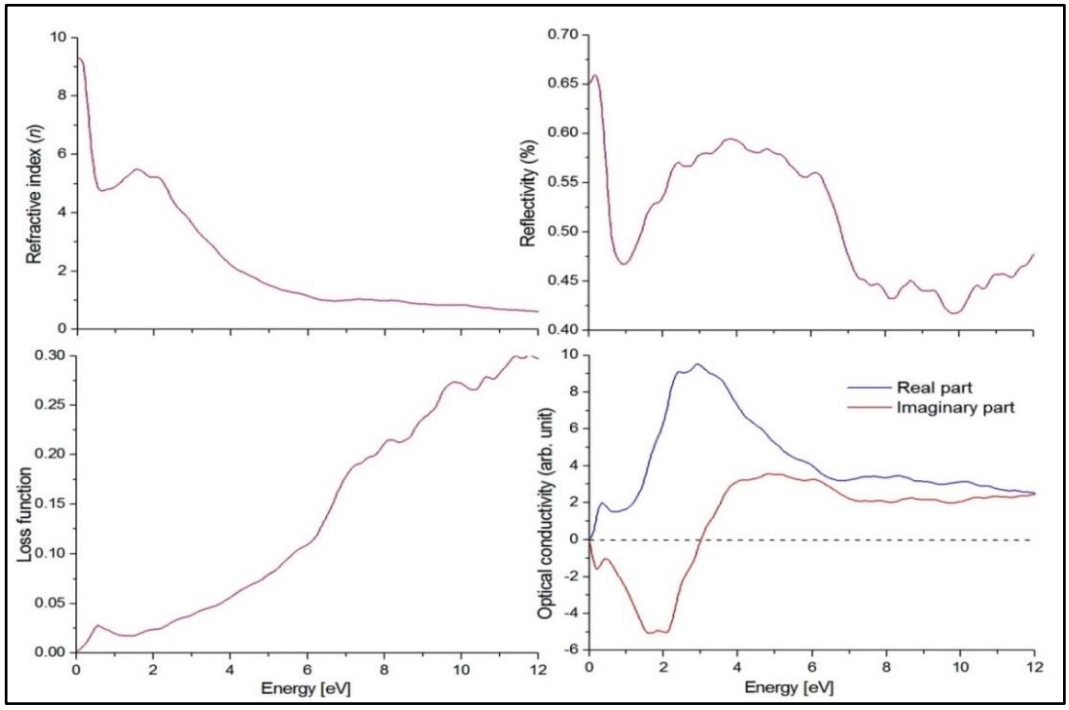

Fig. 5.11: Calculated electron refractive index, reflectivity, loss spectra, real and imaginary part of the optical conductivity of $EuRu_4As_{12}$.

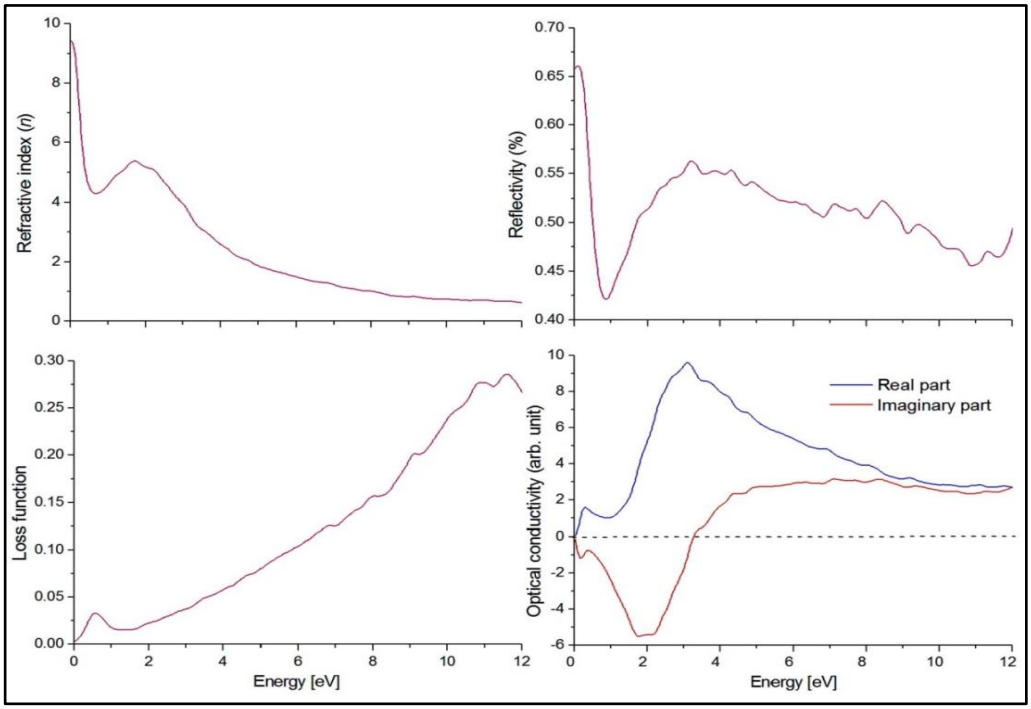

Fig. 5.12: Calculated electron refractive index, reflectivity, loss spectra, real and imaginary part of the optical conductivity of $EuOs_4As_{12}$.

shows that the material no longer acts as a transparent material and the material absorbs the high energy photons and hence the refractive index tends to zero.

The reflectivity spectra for EuM_4P_{12} for energy radiation of 0 - 12 eV are given in Figs. 5.10 – 5.12. At lower energy radiation there exist the transition between *d* to *f*-states of rare earth and hence the reflectivity decreases ~ upto 1 eV. The strong maximum is present close to 0 eV and abrupt reduction to 1 eV confirming the occurrence of collective plasmon resonance exciton with the strong minima near 1 eV.

The electron energy loss spectra are given in Figs. 5.10 – 5.12. Inelastic scattering is observed for visible range of radiation and it increases with increasing energy. At zero energy the energy loss spectra is minimum and hence no scattering is happening, since ε_2 is maximum at this energy. With the increase of photon energy radiation, ε_2 decreases gradually and becomes minimum at photon energy ~2.5 eV and at high photon energy ε_2 is smaller. This has a correlation with the EELS, which increases from a minimum to a maximum with the increase in photon energy.

In Figs. 5.10 – 5.12, the calculated real and imaginary parts of the optical conductivity for EuM_4As_{12} are given for the energy range 0 - 12 eV. The peaks in the spectra correspond to the transitions form valence to conduction band. After a start of a smooth and zero conductivity, we obtain a sharp increase that reaches peak at ~ 4.0 eV energy for real part. The imaginary part decreases from zero energy and gives minimum at energy value ~ 3 eV. For high energy radiation the spectra becomes almost stable indicating that the material does not interact with photons.

Table 5.2: Calculated static dielectric constant and static refractive index of EuM_4As_{12} (M = Fe, Ru, Os).

Compound	$\varepsilon_1(0)$	***n(0)***
$EuFe_4As_{12}$	124	11.2
$EuRu_4As_{12}$	85	9.2
$EuOs_4As_{12}$	87	9.3

c) EuM_4Sb_{12} (M = Fe, Ru, Os)

In Figs. 5.13 – 5.15, we have plotted the real and imaginary parts of the frequency dependent dielectric constants for infrared to ultraviolet radiation for EuM_4Sb_{12} (M = Fe, Ru, Os respectively). $\varepsilon_1(\omega)$ shows a sharp peak close to 0 eV and the first critical points are within 0 eV energy. The calculated values of static dielectric constant $\varepsilon_1(0)$ are summarized in Table 5.3. The energy radiation above 3 eV, it goes to negative value giving the metallic behavior of the material. The imaginary part of the dielectric function $\varepsilon_2(\omega)$ shows the highest peak below 1eV energy and the peak height decreases with the increasing value of the corresponding energy for $EuFe_4Sb_{12}$, $EuRu_4Sb_{12}$ and $EuOs_4Sb_{12}$.

The frequency dependent refractive indices are plotted in Figs. 5.16 – 5.18, for $EuFe_4Sb_{12}$, $EuRu_4Sb_{12}$ and $EuOs_4Sb_{12}$ respectively. The values of static refractive indices are given in Table 5.3. From the refractive index plots of Figs. 5.16 – 5.18, one can observe that the refractive index value decreases from ~2.0 eV energy with increase of energy due to the energy dissipation beyond that energy and the electrons are not directly de-excited. It is also found that beyond 6 eV energy radiations the refractive index falls below unity, which shows that the material no longer acts as a transparent material. With the increase of energy radiation the material absorbs the high energy photons and hence the refractive index tends to zero.

The calculated reflectivity spectra for $EuFe_4Sb_{12}$, $EuRu_4Sb_{12}$ and $EuOs_4Sb_{12}$ are given in Figs. 5.16 – 5.18 respectively. The strong maximum is present close to 0 eV and abrupt reduction to 1 eV confirming the occurrence of collective plasmon resonance exciton with the strong minima near 1 eV.

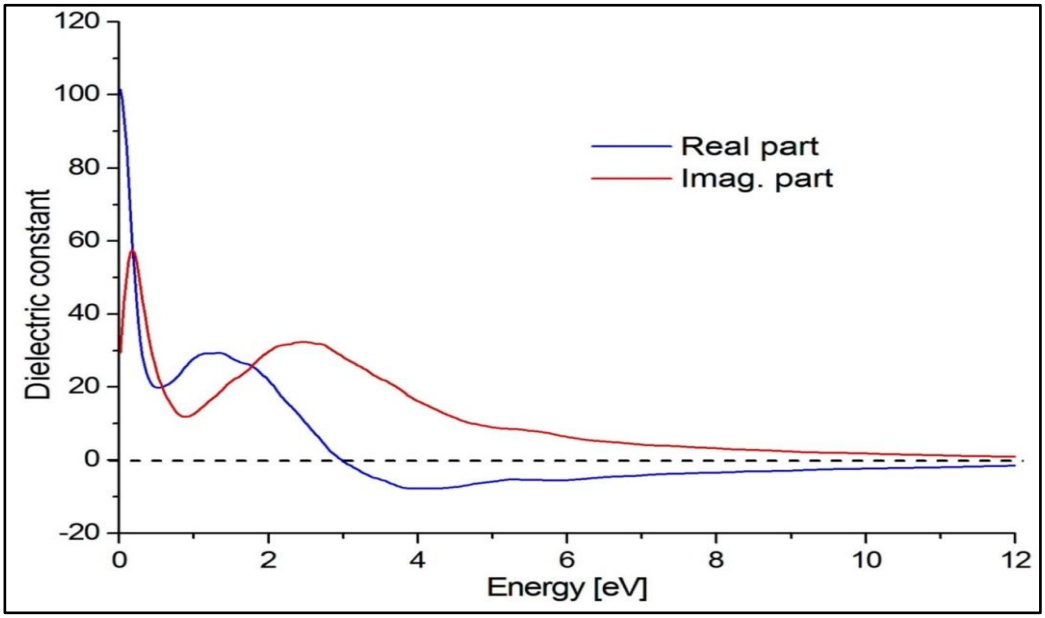

Fig. 5.13: Calculated real and imaginary parts of the dielectric functions of $EuFe_4Sb_{12}$.

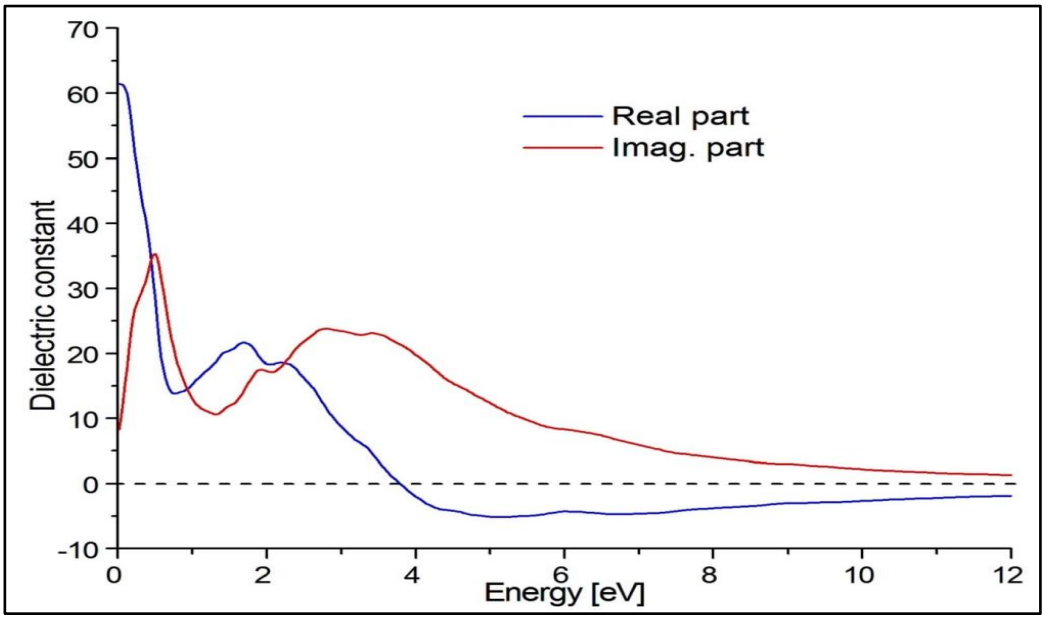

Fig. 5.14: Calculated real and imaginary parts of the dielectric functions of $EuRu_4Sb_{12}$.

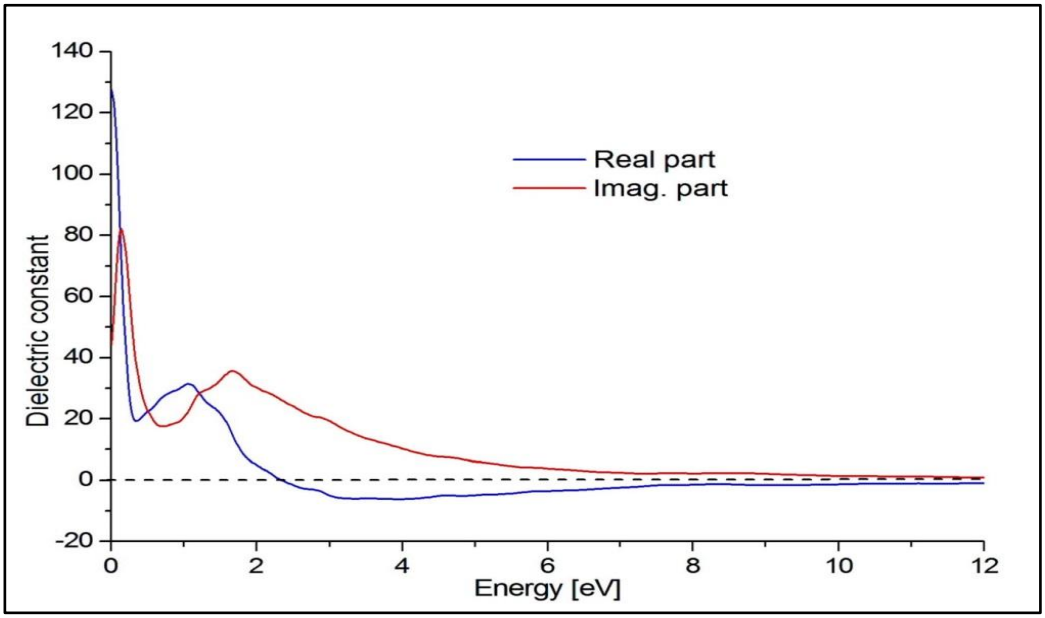

Fig. 5.15: Calculated real and imaginary parts of the dielectric functions of $EuOs_4Sb_{12}$.

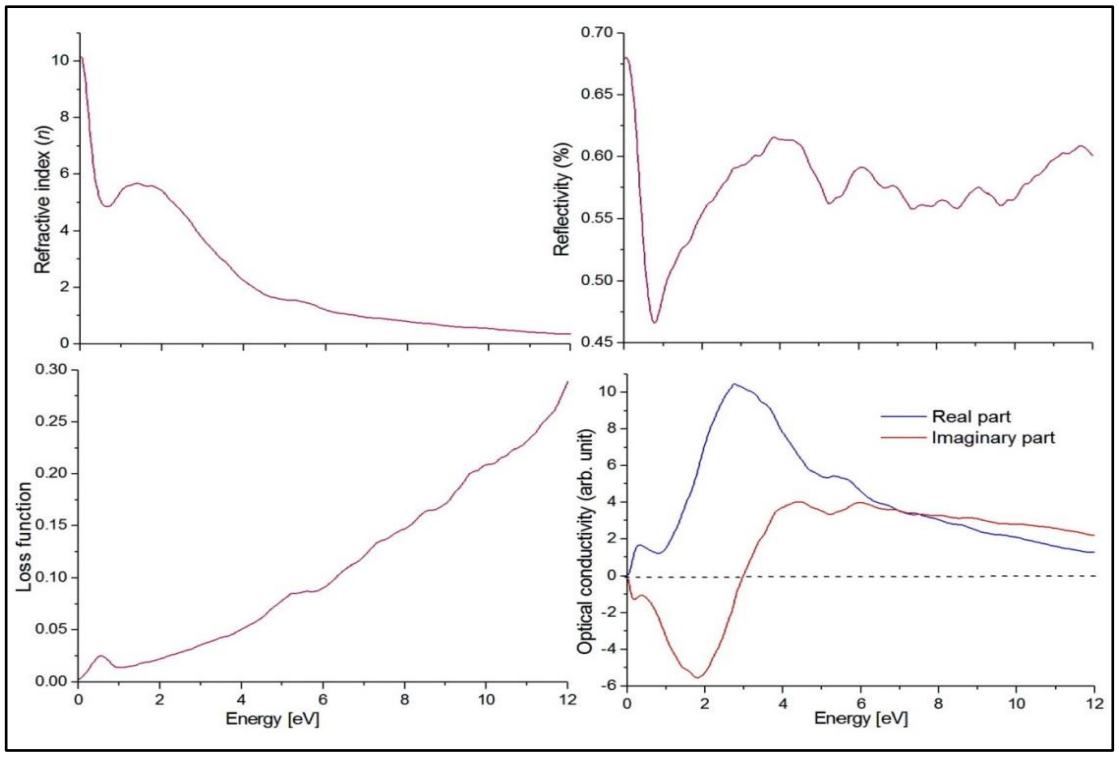

Fig. 5.16: Calculated electron refractive index, reflectivity, loss spectra, real and imaginary part of the optical conductivity of $EuFe_4Sb_{12}$.

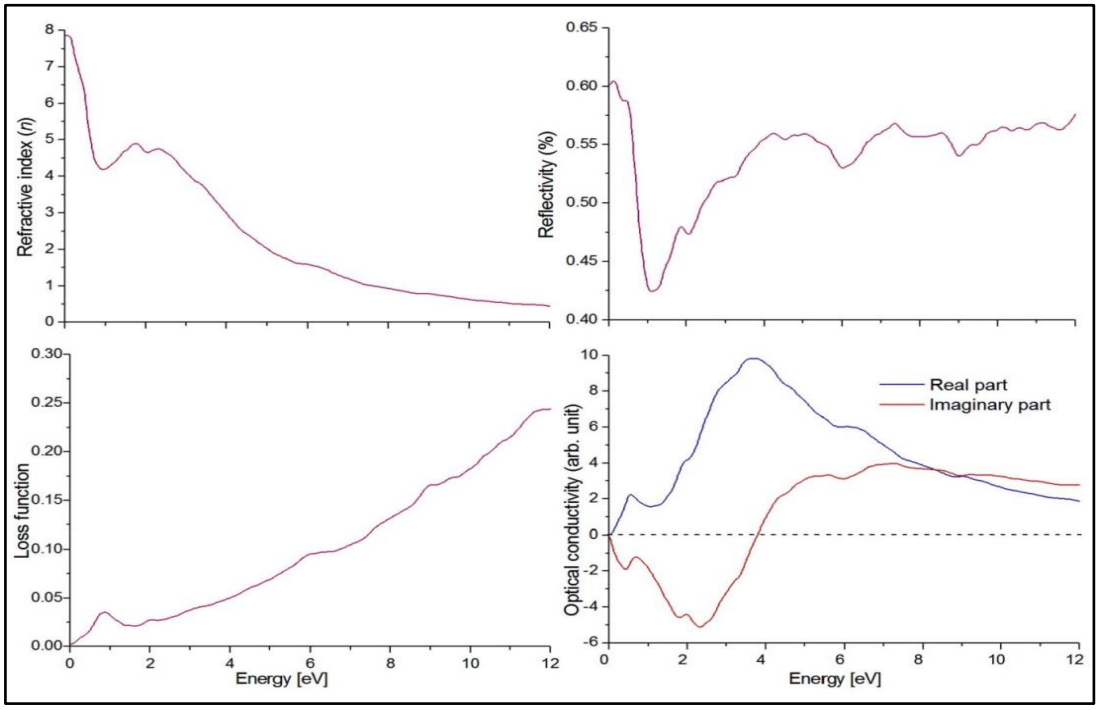

Fig. 5.17: Calculated electron refractive index, reflectivity, loss spectra, real and imaginary part of the optical conductivity of $EuRu_4Sb_{12}$.

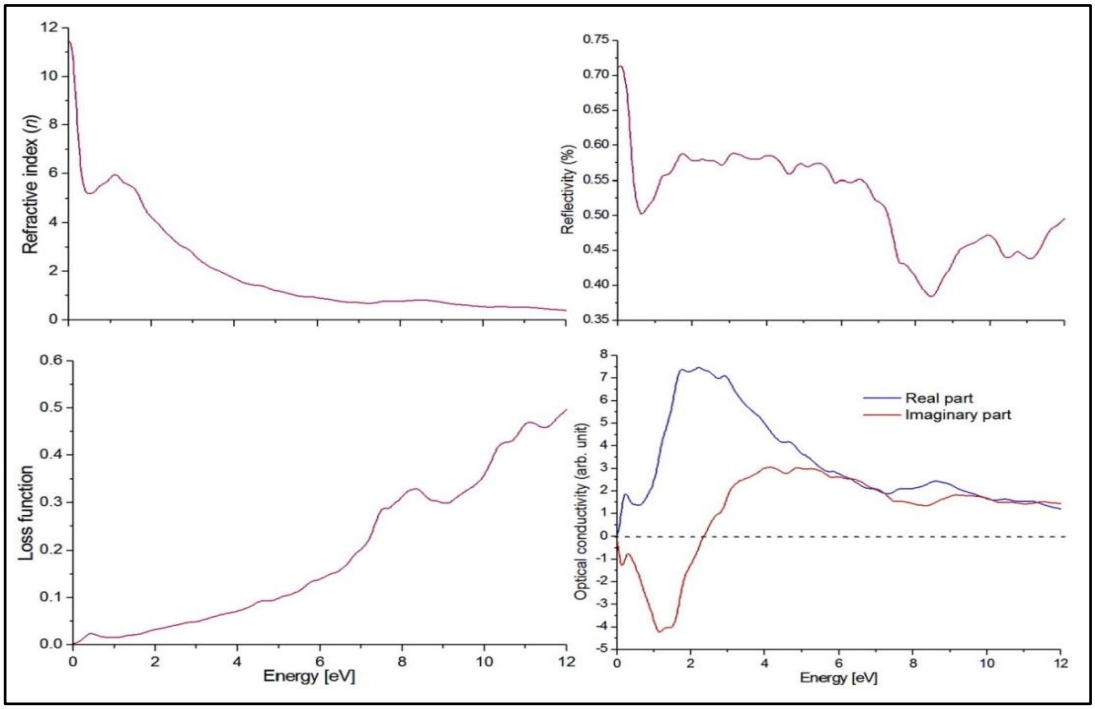

Fig. 5.18: Calculated electron refractive index, reflectivity, loss spectra, real and imaginary part of the optical conductivity of $EuOs_4Sb_{12}$.

The electron energy loss spectra for $EuFe_4Sb_{12}$, $EuRu_4Sb_{12}$ and $EuOs_4Sb_{12}$ are given in Figs. 5.16 – 5.18. Inelastic scattering is observed from energy ~ 1.8 eV and it increases with increasing energy. At zero energy the energy loss spectra is minimum, since ε_2 is maximum at this energy. However, the real and imaginary part of dielectric function goes on decreasing with energy, the energy loss spectrum increases with the photon energy.

In Figs. 5.16 – 5.18, the calculated real and imaginary parts of the optical conductivity for $EuFe_4Sb_{12}$, $EuRu_4Sb_{12}$ and $EuOs_4Sb_{12}$ are given for the energy range 0-12 eV. The peaks in the spectra correspond to the transitions form valence to conduction band. After a start of a smooth and zero conductivity, we obtain a sharp increase that reaches peak at ~ 4.0 eV energy for real part. And the imaginary part decreases from zero energy and gives minimum at energy value ~ 3 eV. For high energy radiation the spectra becomes almost stable indicating that the material does not interact with photons.

Our study shows that significant changes are not observed in the optical response of the compounds with various combinations of central transition metal.

Table 5.3: Calculated dielectric constant and static refractive index of EuM_4Sb_{12} (M = Fe, Ru, Os).

Compound	**$\varepsilon_1(0)$**	***n(0)***
$EuFe_4Sb_{12}$	101	10.1
$EuRu_4Sb_{12}$	61	7.9
$EuOs_4Sb_{12}$	127	11.2

Chapter 6

Conclusions

6

Conclusions

In this thesis, we have presented a systematic study of ground state properties of rare earth filled skuttterudites RM_4X_{12} (R = Eu; M = Fe, Ru, Os; X = P, As, Sb), which crystallize into unique BCC structure with space group $Im\bar{3}$ (no. 204). The calculations were performed by using FP-LAPW method based on density functional theory (DFT). We have studied the structural properties, electronic band structure, density of states, magnetic moments and optical spectra of the title compounds in its equilibrium position. The optimized lattice parameters agree well with the available experimental results. The slight variation of optimized lattice parameters from the experimental values may be due to the choice of approximations like PBE-GGA. It is known that PBE-GGA often overcorrects the approximation by predicting calculated values around 1% - 2% larger than the experimental ones. Not only the choice of PBE-GGA as exchange-correlation but the exclusion of the effect of thermal expansion and zero-point quantum fluctuation in DFT are also responsible for this change in the obtained values. Hence, to compare the experimental results with our DFT-calculated results, the experimental lattice constant should be extrapolated down to 0 K. The negative enthalpy obtained for the compounds indicate that these compounds have a good alloying ability (Shankar *et al*., 2013).

The three independent elastic constants, such as C_{11} (stiffness against principal strain), C_{12} (relates the longitudinal stress in one direction to the strain in another

direction) and C_{44} (resistance to shape) have been investigated for RM_4X_{12} (R = Eu; M = Fe, Ru, Os; X = P, As, Sb) in their fully relaxed position after the tetrahedral and rhombohedral distortion of the cubic structure. The other elastic constants dependent parameters such as Young's moduli, bulk moduli, Poisson's ratio, Debye temperature, elastic anisotropy, Kleinman parameter and Lames coefficients, which give the mechanical and thermal properties of the solids are also studied for their polycrystalline structure by using Voigt-Reuss-Hill approximation. Unfortunately, for the present crystals there are no theoretical or experimental results to compare with the present values. Hence wherever possible we have compared our results with the available results of analogous compounds. Our theoretically obtained results are in qualitative agreement with the results of analogous $CeFe_4P_{12}$ (Benalia *et al*., 2008), $CeRu_4P_{12}$ (Benalia *et al.,* 2009), $CeOs_4Sb_{12}$ (Ameri *et al*., 2013), $CeFe_4As_{12}$ and $CeFe_4Sb_{12}$ (Hachemaoui *et al.,* 2009), $LaFe_4A_{12}$ (A= P, As, Sb) (Hachemaoui *et al.,* 2010), $CeFe_4P_{12}$ and $ThFe_4P_{12}$, (Khenata *et al*., 2007). From the obtained values of bulk moduli we can conclude that $EuRu_4P_{12}$ and $EuOs_4Sb_{12}$ have the highest and lowest resistance to uniform compression respectively. Similarly, the studies of Young's moduli reveal that $EuRu_4P_{12}$ is the stiffest as compared to the other materials under study. Among the systems under study $EuFe_4P_{12}$, $EuFe_4As_{12}$, $EuRu_4As_{12}$ and $EuOs_4Sb_{12}$ are brittle in nature with covalent contribution in intra-atomic bonding whereas $EuRu_4P_{12}$, $EuOs_4P_{12}$ are brittle but with ionic contribution in the intra-atomic bonding whereas $EuFe_4Sb_{12}$, $EuOs_4As_{12}$ and $EuRu_4Sb_{12}$ are ductile and with ionic contribution in the intra-atomic bonding as revealed form their respective values of Cauchy's pressure, Pugh's relation and Poisson's ratio. From the study of Debye temperature it has been investigated that $EuOs_4As_{12}$ has the lowest thermal conductivity, which makes this compound suitable

for thermoelectric applications (Shankar *et al.*, 2013). Due to the limited number of previous theoretical and experimental results of this type of compounds the accuracy of the calculated results are difficult to predict for the systems under consideration. Hence this calculation is prediction study for the title system and they are able to provide reference data for the experimentalists.

The electronic and magnetic properties of rare earth filled skuttterudites RM_4X_{12} (R = Eu; M = Fe, Ru, Os; X = P, As, Sb) were studied using theoretically optimized lattice parameters within the framework of LSDA approach. From the energy band structure and DOS plots it can be concluded that the fundamental electronic properties of the compounds under study are qualitatively similar with Fermi level at the top of the valence band, and presence of low DOS region above E_F, since they have same type of chemical formula. From the total and partial DOS plots one can conclude that Eu-4*f* states have highest contribution in the valence region with the contribution of *d* states of transitional element as similar to analogous La-filled skutterudites reported by Sing and Mazin (1997). The core region has the highest contribution from the *s* and *p* states of pnictogen, whereas in the conduction region again Eu-*f* has the highest contribution. The two bands, which are mainly contributed by *d* and *f*-states of transitional and rare earth, originating from the bottom of the unoccupied region cross the Fermi level at least two times as similar to the report of Harima and Takeghara (2003). The Fermi level is also not in between the valence and conduction region but it lies at the top of the valence band which results into enhanced DOS at the Fermi level. The enhanced value of DOS at the Fermi level indicates these compounds to be metal similar to the experimental results of analogous compounds (Meisner *et al.,* 1985). In the region above the Fermi level, the DOS is very small but not zero, this low DOS region is often

referred as pseudo-gap and is the typical characteristic of skutterudites compounds (Nouneh *et al*., 2007; Fornari & Singh 1999). We have indirect energy band gap of ~ (0.1 - 0.5) eV for EuM_4P_{12} (M = Fe, Ru and Os), which is due to the interaction of the light holes of pnictogens with the localized *f*-states in the conduction bands similar to the analogous system reported by Nordstrom and Singh (1996), Harima (1998). The study of electronic structure near the Fermi level and the presence of indirect bandgap and pseudogap above E_F indicate that these compounds are semimetal and suitable candidates for thermoelectric applications.

The spin-polarisation has significant influence on the band structures causing the splitting of bands in the spin up and down channel, which is responsible for the magnetic behaviour of the title compounds under study. As reported from the DOS plots and Stoner criteria, these compounds were ferromagnetic in its ground state similar to previous reports of Jeitschko and Braun (1977), Evers *et al*. (1995), Braun and Jeitschko (1980), Krishnamurthy *et al*. (2007). Europium has the highest contribution in the total magnetic moments, the Eu moments are antiferromagnetically coupled with the transitional elements but the coupling is negligible, that gives total ferromagnetic behaviour of the system. Our calculated magnetic moment values are lower than the experimental values (Sales *et al.*, 2003; Buschow, 2009; Sekine *et al.,* 2009; Bauer *et al*., 2004). The choice of LSDA method and the exclusion of Coulomb interaction (U) in our calculation can be responsible for the lower magnetic moment in our calculation. The LSDA method has a tendency to underestimate the intra-atomic correlation between the 4*f* electrons and hence overestimate the hybridization Kanai *et al*. (2002) between the states of Eu-*f* and M-*d* which leads to a less prominent splitting of the 4*f*-states giving rise to lower magnetic moment for Eu atoms.

The optical properties of the compounds under study are also investigated as the function of incident photon energy in the infrared to ultraviolet range. Our study shows that the significant change is not observed in the optical properties of the compounds with various combinations of central transition metal and the pnictogen elements. From the dielectric response plots it has been observed that the first critical points (absorption edge) are embedded with the Fermi level. The analyses of the optical spectra show that the photon energy close to E_F is characterised by small absorption and maximum reflectivity. Similarly, the radiation in the ultraviolet region is characterised by appreciable reflectivity with negligible absorption. The high value of static dielectric function and the static refractive index explain the metallic behaviour of the sample compounds. The high value of refractive index in the low energy radiation can be explained by using Drude theory, the material with large carrier concentration which acts as a perfect reflector and can be used in advanced optoelectronic devices. The trend obtained in our electron energy loss spectra is in contradict to the one obtained for metallic (Ag) (Pines, 1963), which also suggest our system to be semimetal. As the frequency becomes large the interband transitions dominate the free electron contribution, hence Drude term is unimportant and the material behaves as a dielectric.

The study of the transport properties of the compounds under study may give the exact picture of the thermal and magnetic behavior of the system. The effect of localized electrons of rare earth and transitional elements were also not included in our calculation. From the DOS plots it is observable that there is high chance of getting the half metallic ferromagnetic behavior of some of the compounds under study as Krishnamurthy *et al.* (2007) have already mentioned the half-metallic behavior of $EuFe_4Sb_{12}$, provided the Fermi level is inside the gap between the conduction and

valence bands. It is possible to get the Fermi level inside the gap by appropriate doping. Hence, in future work, we intend to study the thermal transport properties of this system with inclusion of effect of localized electrons and appropriate doping in our calculation.

References

References

Adroja D. T., Mcewen K. A., Park J. G., Hillier A. D., Takeda N., Riseborough P. S. and Takabatake T. (2008), Inelastic neutron scattering study of spin gap formation in heavy fermion compounds, *Jour. Optoelectronics and Adv. Mat*., **10:** 1719-1737.

Aeppli G. and Fisk Z. (1992), Kondo Insulators, *Comments Cond. Mat. Phys*., **16**: 155-170.

Amato A. (1997), Heavy-fermion systems studied by μSR technique, *Rev. Mod. Phys*., **69**: 1119-1179.

Ameri M., Boudia K., Khenata R., Bouhafs B., Rais A., Omran S. B., Abidri B. and Al-Douri Y. (2013), Structural, elastic, electronic and thermodynamic properties of the filled skutterudite $CeOs_4Sb_{12}$ determined by density functional theory, *Materials Science in Semiconductor Processing*, **16**: 1508 – 1516.

Anderson O. L. (1963), A simplified method for calculating the Debye temperature from elastic constants, *J. Phys. Chem. Solids*, **24**: 909-917.

Anisimov V. I., Zaanen J. and Andersen O. K. (1991), Band theory and Mott insulators: Hubbard U instead of Stoner I, *Phys. Rev. B*, **44:** 943-954.

Anisimov V. I., Aryasetiawan F. and Lichtenstein A. I. (1997), First-principles calculations of the electronic structure and spectra of strongly correlated systems: the LDA+U method, *J. Phys.: Condens. Matter*., **9:** 767-808.

Bannikov V.V., Shein I. R. and Ivanovskii A. L. (2007), Electronic structure, chemical bonding and elastic properties of the first thorium-containing nitride perovskite $TaThN_3$, *Phys. Status Solidi Rapid Res. Lett*., **3**: 89-91.

Bauer E., Berger St., Galatanu A., Galli M., Michor H., Hilscher G., Paul Ch., Ni B., Abd-Elmeguid M. M., Tran V. H., Grytsiv A. and Rogl, P. (2001), Crystal structure and physical properties of $Eu_{0.83}Fe_4Sb_{12}$. *Phys. Rev. B,* **63**: 224414-7.

Bauer E. D., Frederick N. A., Ho P. C., Zapf V. S. and Maple M. B. (2002), Superconductivity and heavy fermion behavior in $PrOs_4Sb_{12}$, *Phys. Rev. B,* **65:** 100506-4.

Bauer E. D., Slebarski A., Frederick N. A., Yuhasz W. M., Maple M. B., Cao D., Bridges F., Giester G. and Rogl P. (2004), Investigation of ferromagnetic filled skutterudite compounds EuT_4Sb_{12} (T = Fe, Ru, Os), *J. Phys. Condens. Matter,* **16:** 5095-5107.

Benalia S., Ameri M., Rached D., Khenata R., Rabah M. and Bouhemadou A. (2008), First-principle calculations of elastic and electronic properties of the filled skutterudite $CeFe_4P_{12}$, *Computational Materials Science*, **43**: 1022–1026.

Benalia S., Hachemaou M., Rached D., Khenata R., Bettahar N. and Benyahia M. (2009), FP-LMTO calculations of elastic and electronic properties of the filled skutterudite $CeRu_4P_{12}$, *Journal of Physics and Chemistry of Solids*, **70**: 622–626.

Blaha P., Schwarz K., Madsen G. K. H., Kvasnicka D., Luitz J., Schwarz K. (2012), *An Augmented Plane Wave plus Local Orbitals Program for Calculating Crystal*

Properties, Wien2K User's Guide, Techn. Universitat Wien, Wien.

Blochl P. E., Jepson O. and Anderson O. K. (1994), Improved tetrahedron method for Brillouin-zone integrations, *Phys. Rev. B,* **49**: 16223-16233.

Braun D. J., Jeitschko W. (1980), Preparation and structural investigations of antimonides with the $LaFe_4P_{12}$ structure, *J. Less Common Metals*, **72**: 147-156.

Brich F. J. (1938), The effect of pressure upon the elastic parameters of isotropic solids, according to Murnaghan's theory of finite strain, *Appl. Phys.,* **9**: 279-289.

Bushow K. H. J. (2009), *Handbook of magnetic materials,* Elsevier; Amsterdam, Vol. 18.

Caillat T. and Borshchevsky A. (1993), *Skutterudites: an update.* Proceedings, 7th International Conference on Thermoelctrics, ed. K. Rae, University of Texas at Arlington, p. 98.

Callaway J. (1974a), *Quantum Theory of Solids,* Academic Press: New York.

Callaway J. (1974b), *Energy Bands in Solids,* Academic Press: New York.

Cao D., Bridges F., Bushart S., Bauer E. D. and Maple M. B. (2003), X-ray-absorption spectroscopy study of the heavy-fermion superconductor $PrOs_4Sb_{12}$, *Phys. Rev. B,* **67:** 180511-4.

Chen B., Xu J.-H., Uher C., Morelli D. T. Meisner G. P., Fleurial J.-P., Caillat T. and Borshchevsky A. (1997), Low-temperature transport properties of the filled skutterudites $CeFe_{4-x}Co_x Sb_{12}$, *Phys. Rev. B,* **55**: 1476-1479.

Chen G., Dresselhaus M. S., Dresselhaus G., Fleurial J. P. and Caillat T. (2003), Recent developments in thermoelectric materials, *Int. Mater. Rev.*, **48**: 45-66.

Chen L. D., Kawahara T., Tang X. F., Goto T., Hirai T., Dyck J. S., Chen W. and Uher C. (2001), Anomalous barium filling fraction and n-type thermoelectric performance of $Ba_yCo_4Sb_{12}$, *J. Appl. Phys.*, **90**: 1864-1868.

Coleman P. (2006), Heavy Fermions: electrons at the edge of magnetism. Cond-mat/0612006 V1.

Cottenier S. (2002), *Density Functional Theory and the family of (L)APW-methods: a step-by-step introduction*, Belgium: Instituut voor Kern-en Stralingsfysica, K. U. Leuven.

Cutler M., Leavy J. F. and Fitzpatrick R. L. (1964), Electronic Transport in Semimetallic Cerium Sulfide, *Phys. Rev.*,**133**: 1143-4.

Danebrock M. E., Evers C. B. H. and Jeitschko W. (1996), Magnetic properties of alkaline earth and lanthanoid iron antimonides AFe_4Sb_{12} (A = Ca, Sr, Ba, La, Nd, Sm, Eu) with the $LaFe_4P_{12}$ structure, *J. Phys. Chem. Solids*, **57:** 381-387.

Dilley N. R., Bauer E. D., Maple M. B., Dordevic S., Basov D. N., Freibert F., Darling T. W., Migliori A., Chakoumakos B. C. and Sales B. C. (2000), Thermoelectric and optical properties of the filled skutterudite $YbFe_4Sb_{l2}$, *Phys. Rev. B,* **61**: 4608-4614.

Dordevic S.V., Dilley N. R., Bauer E. D., Basov D. N. and Degiorgi L. (1999), Optical properties of MFe_4P_{12} filled skutterudites, *Phys. Rev. B,* **60**: 321-328.

Dudarev S. L., Botton G. A., Savrasov S. Y., Humphreys C. J. and Sutton A. P. (1998), An LSDA+U study electron-energy-loss spectra and the structural stability of nickel oxide, *Phys. Rev. B*, **57**:1505-1509.

Ernst A., Henk J. and Thapa R. K. (2005), Ultrathin antiferromagnetic films on a ferromagnetic substrate: A first principle study of Mn on Fe (001), *J. Phys. Condens. Matter*, **17:** 3269-3283.

Evers C. B. H., Jeitschko W., Boonk L., Braun D. J., Ebel T. and Scholz U. D. (1995), Rare earth and uranium transition metal pnictides with $LaFe_4P_{12}$ structure, *J. Alloy. and Compds.*, **224:** 184- 189.

Feldman J. L., Singh D. J. and Kendziora C. (2003), Lattice dynamics of filled skutterudites: $La(Fe,Co)_4Sb_{12}$, *Phys. Rev. B.*, **68:** 094301-11.

Fetter A. L. and Walecka J. D. (1971), *Quantum theory of many particle systems*, McGraw-Hill, New York.

Filippi C., Umrigar C. J. and Taut M. (1994), Comparison of exact and approximate density functionals for an exactly soluble model, *J. Chem. Phys.*, **100**:1295-7.

Fornari M. and Singh D. J. (1999), Electronic structure and thermoelectric prospects of phosphide skutterudites, *Phys. Rev. B*, **59:** 9722-9727.

Fu C., Krijn K. P. C. M. and Doniach S. (1994), Electronic structure and optical properties of FeSi, a strongly correlated insulator, *Phys. Rev. B*, **49**: 2219-2222.

Georges A., Kotliar G., Krauth W., Rozenberg M. J. (1996), Dynamical mean-field theory of strongly correlated fermion systems and the limit of infinite dimensions, *Rev. Mod. Phys*., **68**: 13-20.

Goldsmid H. J. (1986), *Electronic Refrigeration*. Pion, London, p.10.

Grandjean F., Gerard A., Braum D. J. and Jeitschko W. (1984), Some physical properties of $LaFe_4P_{12}$ type compounds, *J. Phys. Chem. Solids*, **45:** 877-886.

Gross E. K. U. and Dreizler R. M. (1981), Gradient expansion of the Coulomb energy, *Z. Phys A-Atoms and Nuclei*, 302: 103-106.

Hachemaoui M., Khenata R., Bouhemadou A., Reshak A. H., Rached D. and Semari F. (2009), FP-APW + lo study of the elastic, electronic and optical properties of the filled skutterudites $CeFe_4As_{12}$ and $CeFe_4Sb_{12}$, *Current Opinion in Solid State and Materials Science,* **13**: 105–111.

Hachemaoui M., Khenata R., Bouhemadou A., Bin-Omran S., Reshak A. H., Rached D. and Semari F. (2010), Prediction study of the structural and elastic properties for the cubic skutterudites $LaFe_4A_{12}$ (A = P, As and Sb) under pressure effect, *Solid State Commun.*, **150**: 1869-1873.

Harima H. (1998), FLAPW band structure calculation and fermi surface for $LaFe_4P_{12}$, *J. Magn. Magn. Mater*., **321:** 177-181.

Harima H. and Takeghara K. (2003), Conduction bands in the filled skutterudites, *J. Phys.: Condens. Matter*, **15**: S2081-S2086.

Harima H. and Takeghara K. (2003), X-dependence of electronic band structures for $LaFe_4X_{12}$ (X = P; As; Sb), *Physica B*, **328**: 26–28.

Harima H., Takegahara K. (2003), X-dependence of electronic band structures for $LaFe_4X_{12}$ (X = P, As, Sb), *Physica B*, **328:** 26-28.

Hill R. (1952), The elastic behaviour of a crystalline aggregate, *Proc. Phys. Soc. London A*, **65:** 349-354.

Hao A., Yang X., Wang X., Zhu Y. and Liu X. J. (2010), First-principles investigations on electronic, elastic and optical properties of XC (X = Si, Ge, and Sn) under high pressure, *J. Appl. Phys.*, **108**: 063531-063537.

Hohenberg P. and Kohn W. (1964), Inhomogeneous electron gas, *Phys. Rev. B*, **136** : 864-871.

Hubbard J. (1963), Electron correlations in narrow energy bands, *Proc. Roy. Soc. London A*, **276**: 238-257.

Jamal M. (2012), Cubic-elastic, http://www.WIEN2k.at/reg_user/unsupported/ cubic-elast/(2012).

Jeitschko W. and Braun D. (1977), $LaFe_4P_{12}$ with filled $CoAs_3$-type structure and isotypic lanthanoid-transition metal polyphosphides, *Acta Crystall. B*, **33:** 3401-3406.

Jung D., Whangbo M. H. and Alvarez S. (1990), Importance of the X4 ring orbitals for the semiconducting, metallic or superconducting properties of skutterudites MX_3 and RM_4X_{12}, *Inorg. Chem.*, **29:** 2252-2255.

Kanai K., Takeda N., Nozawa S., Yokoya T., Ishikawa M. and Shin S. (2002), Electronic structure of the filled skutterudite compound $CeRu_4Sb_{12}$, *Phys. Rev. B*, **65:** 041105-041108.

Karki B. B., Stixrude L., Clark S. J., Warren M. C., Ackland G. J. and Crain J. (1997), Structure and elasticity of MgO at high pressure, *Am. Mineral*., **82:** 51-60.

Khenata R., Bouhemadou A., Reshak A. H., Ahmed R., Bouhafs B., Rached D., Al-Douri Y. and Rérat M. (2007), First-principles calculations of the elastic, electronic, and optical properties of the filled skutterudites $CeFe_4P_{12}$ and $ThFe_4P_{12}$, *Phys. Rev. B*, **75:** 195131-7.

Kihou K., Shirotani I., Shimaya Y., Sekine C. and Yagi T. (2004), High-pressure synthesis, electrical and magnetic properties of new filled skutterudites $LnOs_4P_{12}$ (Ln = Eu, Gd, Tb, Dy, Ho, Y), *Mater. Res. Bull*., **39:** 317-325.

Kjekshus A. and Pedersen G. (1961), The crystal structures of $IrAs_3$ and $IrSb_3$, *Acta Crystallogr.*, **14:** 1065-1070.

Kohn W. and Sham L. J. (1965), Self-Consistent Equations Including Exchange and Correlation Effects, *Phys. Rev. A*, **140**:1133-1138.

Kresse G. and Furthmüller J. (1996), Efficient iterative schemes for ab initio total-energy calculations using a plane-wave basis set, *Phys. Rev. B*, **54**:11169-11186.

Krishnamurthy V. V., Lang J. C., Haskel D., Keavney D. J., Srajer G., Robertson J. L., Sales B. C., Mandrus D. G., Singh D. J. and Bilc D. I. (2007), Ferrimagnetism in $EuFe_4Sb_{12}$ due to the Interplay of *f*-electron moments and a nearly ferromagnetic host, *Phys. Rev. Lett.*, **98:** 126403-4.

Lamberton G. A., Bhattacharya S., Littleton R. T., Kaeser M. A., Tedstrom R. H., Tritt T. M., Yang J. and Nolas G. S. (2002). High figure of merit in Eu-filled $CoSb_3$ based skutterudites. *Appl. Phys. Lett.,* **80:** 598- 600.

Lee K. W. and Pickett W. E. (2004), Infinite-layer $LaNiO_2$: Ni^{1+} is not Cu^{2+}, *Phys. Rev. B,* **70**: 165109-6.

Lefebvre-Devos I., Lassalle M., Wallart X., Olivier-Fourcade J., Monconduit L. and Jumas J. C. (2001), Bonding in skutterudites: combined experimental and theoretical characterization of $CoSb_3$, *Phys. Rev.B,* **63:** 125110-125116.

Leithe-Jasper A., Schnelle W., Rosner H., Senthilkumaran N., Rabis A., Baenitz M., Gippius A., Morozova E., Mydosh J. A. and Grin Y. (2003), Ferromagnetic ordering in alkali-metal iron antimonides: $NaFe_4Sb_{12}$ and KFe_4Sb_{12}, *Phys. Rev. Lett*., **91**: 037208-4. Erratum: (2004), **92:** 0899004.

Leithe-Jasper A., Schnelle W., Rosner H., Baenitz M., Rabis A., Gippius A. A., Morozova E. N., Borrmann H., Burkhardt U., Ramlau R., Schwarz U., Mydosh J. A., Grin Y., Ksenofontov V. and Reiman S. (2004), Weak itinerant ferromagnetism and electronic and crystal structures of alkali-metal iron antimonides:$NaFe_4Sb_{12}$ and KFe_4Sb_{12}, *Phys. Rev. B* ,**70:** 214418-12.

Li L. X., Liu H, Wang J. Y, Hu X. B, Zhao S. R, Jiang H. D., Huang Q. J, Wang H. H. and Li Z. F. (2001), Raman spectroscopy investigation of partially filled skutterudite, *Chem. Phys. Lett.*, **347:** 373-377.

Liechtenstein A. I., Anisimov A. I. and Zaanen J. (1995), Density-functional theory and strong interactions: orbital ordering in Mott-Hubbard insulators, *Phys. Rev. B,* **52**: R5467 – R5470.

Lougin S., French R. H., De Noyer L .K., Ching W.-Y. and Xu Y. –N. (1996), *J. Phys.D: Appl. Phys*. **1740**: 29-33.

Ma S.-K. and Brueckner K. A. (1968), Correlation energy of an electron gas with a slowly varying high density, *Phys. Rev.*, **165**: 18-31.

Mahan G. D. and Sofo J. O. (1996), The best thermoelectric, *Proc. Natl. Acad. Sci. USA*, **93**: 7436- 7439.

Maple M. B., Ho P. C., Zapf V. S., Frederick N. A., Bauer E. D., Yuhasz W. M., Woodward F. M. and Lynn J. W. (2002), Investigation of ferromagnetic filled skutterudite compounds EuT_4Sb_{12} (T = Fe, Ru, Os), *J. Phys. Soc. Jpn*.**, 71:** 23-28.

Matheiss L.F., Hamman D. R. (1993), Band structure and semiconducting properties of FeSi, *Phys. Rev. B*, **47**: 13114- 13119.

Mattesini M. (2009), Elastic properties and electrostructural correlations in ternary scandium-based cubic inverse perovskites: A first principles study, *Phys. Rev. B*, **79**: 125122-9.

Meisner G. P., Torikachvili M. S., Yang K. N., Maple M. B. and Guertin R. P. (1985). UFe_4P_{12} and $CeFe_4P_{12}$: Nonmetallic isotypes of superconducting $LaFe_4P_{12}$, *J. Appl. Phys*., **57:** 3037-3039.

Morelli D. T., Meisner G. P., Chen B. X., Hu S. Q. and Uher C. (1997), Cerium filling and doping of cobalt triantimonide, *Phys. Rev. B*, **56**: 7376- 7383.

Murnaghan F. D. (1944), The compressibility of media under extreme pressures, *Proc. Natl. Acad. Sci., USA* , **30**: 244-247.

Mutou T. and Saso T. (2004), Optical conductivity of Ce-based filled skutterudites, *J. Phys. Soc. Jpn.*, **73:** 2900-2905.

Nanba T., Hayashi M., Shirotani I. and Sekine C. (1999), Optical response of $PrRu_4P_{12}$ due to metal insulator transition, *Physica B*, **259-261:** 853-854.

Nolas G. S., Slack G. A., Caillat T. and Meisner G. P. (1996), Raman scattering study of antimony-based skutterudites, *J. Appl. Phys.* **79:** 2622-2627.

Nolas G. S., Cohn J. L. and Slack G. A. (1998), Effect of partial void filling on the lattice thermal conductivity of skutterudites, *Phys. Rev. B*, **58:** 164-170.

Nolas G. S., Morelli D. T. and Tritt, T. M. (1999), Skutterudites: A phonon-glass-electron crystal approach to advanced thermoelectric energy conversion applications, *Annu. Rev. Mater. Sci.* **29:** 89-116.

Nolas G. S., Kaeser M., Littleton IV R. T. and Tritt T. M. (2000), High figure of merit in partially filled ytterbium skutterudite materials, *Appl. Phys. Lett.*, **77:** 1855-1857.

Nolas G. S., Yoon G., Sellinschegg H., Smalley A. and Johnson D. C. (2005), Synthesis and transport properties of $HfFe_4Sb_{12}$, *Appl. Phys. Lett.*, **86**: 042111-2.

Nordstrom L. and Singh D. J. (1996), Electronic structure of Ce-filled skutterudites, *Phys. Rev. B,* **53**: 1103-1108.

Nouneha K., Reshak A. H., Auluck S., Kityk I.V., Viennois R., Benet S. and Charar S. (2007), Band energy and thermoelectricity of filled skutterudites $LaFe_4Sb_{12}$ and $CeFe_4Sb_{12}$, *J. Alloy. and Comp.*, **437**: 39–46.

Pei Y. Z., Chen L. D., Zhang W., Shi X., Bai S. Q., Zhao X. Y., Mei Z. G. and Li X. Y. (2006), Synthesis and thermoelectric properties of $K_yCo_4Sb_{12}$, *Appl. Phys. Lett.*, **89**: 221107-3.

Penn D. R. (1962), Wave-number-dependent dielectric functions of semiconductors, *Phys. Rev.***128**: 2093-7.

Perdew J. P. Zunger A. (1981), Self-interaction correction to density-functional approximations for many-electron systems, *Phys. Rev. B,* 23 : 5048–5079.

Perdew J. P. (1985), Accurate density functional for the energy: real-space cut off of the gradient expansion for the exchange hole, *Phys. Rev. Lett.***, 55**:1665–1668.

Perdew J. P., Burke K. and Ernzerhof M. (1996), Generalized gradient approximation Made Simple, *Phy. Rev. Lett.*, **77:** 3865–3868.

Pettifor D. G. (1992), Theoretical predictions of structure and related properties of intermetallics, *Materials Science and Technology*, **8:** 345–349.

Pines D. (1963), *Elemantary Excitations in Solids*. W. A. Benjamin, Inc, New York.

Prytz Ø., Saeterli R., Løvvik O.M. and Taftø J. (2006), Comparison of theoretical and experimental dielectric functions: electron energy-loss spectroscopy and density functional calculations on skutterudites, *Phys. Rev. B***, 74:** 245109-245116.

Pugh S. F. (1954), Relations between the elastic moduli and the plastic properties of polycrystalline pure metals, *Philos. Mag*. **45:** 823-843.

Qiu P. F., Yang J., Liu R. H., Shi X., Huang X. Y., Snyder G. J., Zhang W. and Chen L. D. (2011), High-temperature electrical and thermal transport properties of fully filled skutterudites RFe_4Sb_{12} (R = Ca, Sr, Ba, La, Ce, Pr, Nd, Eu, and Yb), *Jour. Appl. Phys.*, **109:** 063713-8.

Rajagopalan M. (2013), Elaectronic topological transition in Nd_3Al under compression: An *ab initio* study, *Physica B*, **413**:1-5.

Recknagel C., Reinfried N., Hohn P., Schnelle W., Rosner H., Grin Yu. and Leithe-Jasper A. (2007), Application of spark plasma sintering to the fabrication of binary and ternary skutterudites, *Science and Technology of Advanced Materials***, 8:** 357-363.

Reshak A. H. (2007). *Linear and Nonlinear Optical Properties.* Habilitation Thesis, Institute of Physical Biology, South Bohemia, Nove Hrady.

Riseborough P.S. (1992), Theory of the dynamic magnetic response of $Ce_3Bi_4Pt_3$: A heavy-fermion semiconductor, *Phys. Rev. B.,* **45**: 13984-13995.

Riseborough P.S. (2000), Heavy fermion semiconductors, *Adv. Phys*., **49:** 257-320.

Rowe D. M., McNaughton A. G., Hartman R. F., Hall W. C. and Bennett G. L. (1997), *CRC Handbook of Thermoelectrics*, CRC, Boca Raton, 441–537.

Sales B. C., Mandrus D. and Williams R. K. (1996), Filled skutterudite antimonides: A new class of thermoelectric materials, *Science,* **272:** 1325-1328.

Sales B. C., Mandrus D., Chakoumakos B. C., Keppens V. and Thompson J. R. (1997), Filled skutterudite antimonides: Electron crystals and phonon glasses, *Phys. Rev. B,* **56:** 15081-15089.

Sales B. C. (1998), Electron crystals and phonon glasses: a new path to improved thermoelectric materials, *Mater. Res. Soc. Bull.,* **23:** 15–21.

Sales B. C., Chakoumakos B. C. and Mandrus D. (2000), Thermoelectric properties of thallium-filled skutterudites, *Phys. Rev. B,* **61**: 2475-2481.

Sales B. C., Gschneidner K. A. Jr., Bunzli J. C. G. and Pecharsky V. K. (2003), *Handbook on the Physics and Chemistry of Rare Earths*, Amsterdam: Elsevier. Chapter 211, pp. 1-34.

Sanada S., Aoki Y., Aoki H. and Tsuchiya A. (2005), Exotic heavy-Fermion state in filled skutterudite $SmOs_4Sb_{12}$, *J. Phys. Soc. Jpn.,* **74:** 246-250.

Sato H., Abe Y., Okada H., Matsuda T. D., Abe K., Sugawara H., Aoki Y. (2000), Anomalous transport properties of RFe_4P_{12} (R = La, Ce, Pr, and Nd), *Phys. Rev. B,* **62:** 15125- 15130.

Schwarz K. and Blaha P. (2003), Solid state calculations using WIEN2k, *Computational Materials Science,* **28**: 259-273.

Sekine C., Uchiumi T., Shirotani I. and Yagi T. (1997), Superconductivity of $LaRu_4X_{12}$ (X = P, As and Sb) with skutterudite structure, *Phys. Rev. Lett.***, 79:** 3218-3221.

Sekine C., Uchiumi T., Shirotani I., Matsuhira K., Sakakibara T., Goto T. and Yagi T. (2000), Magnetic properties of the filled skutterudite-type structure compounds $GdRu_4P_{12}$ and $TbRu_4P_{12}$ synthesized under high pressure, *Phys. Rev. B,* **62:** 581-584.

Sekine C., Inoue M., Inaba T. and Shirotani I. (2000), Magnetic and electrical properties of the "filled skutterudite-type compound $EuRu_4P_{12}$, *Physica B,* **281&282**: 308-310.

Sekine C., Akahira K., Ito K. and Yagi T. (2009), Magnetic properties of new filled skutterudite compounds EuT_4As_{12} (T = Fe, Ru,As) synthesized under high pressure, *J. Phys. Soc. Jpn.*, **78**: 093707-04.

Shankar A., Rai D. P., Sandeep and Thapa R. K. (2013), Ground state properties of filled skutterudite $EuRu_4P_{12}$: A first principles study, *J. of Alloys Compds.,* **578:** 559-564.

Shankar A. and Thapa R. K. (2013), Electronic, magnetic and structural properties of the filled skutterudite $EuFe_4P_{12}$: LSDA and LSDA+U calculation, *Physica B,* **427:** 31-36.

Shein I. R. and Ivanovskii A. L. (2008), Elastic properties of mono-and polycrystalline hexagonal AlB_2-like diborides of *s*, *p* and *d* metals from first-principles calculations, *J. Phys. Condens. Matter*, **20:** 415218-9.

Shi X., Kong H., Li C. P., Uher C., Yang J., Salvador J. R., Wang H., Chen L. and Zhang W. (2008), Low thermal conductivity and high thermoelectric figure of merit in *n*-type $Ba_xYb_yCo_4Sb_{12}$ double-filled skutterudites, *Appl. Phys. Lett.*, **92**: 182101-3.

Shirotani I., Uchiumi T., Ohno K. and Sekine C. (1997), Superconductivity of filled skutterudites $LaRu_4As_{12}$ and $PrRu_4As_{12}$, *Phys. Rev. B*, **56**: 7866-786.

Sichelschmidt J., Voevodin V., Im H. J., Kimura S., Rosner H., Leithe-Jasper A., Schnelle W., Burkhardt U., Mydosh J. A., Grin Yu. and Steglich F. (2006), Optical pseudogap from iron states in filled skutterudites AFe_4Sb_{12} (A = Yb*;* Ca*;* Ba), *Phys. Rev. Lett.,* **96:** 037406-4.

Singh D. J. (1994), *Plane waves pseudopotential and the LAPW method*, Kluwer Academic Publishers, 02061.

Singh D. J. and Pickett W. E. (1994), Skutterudite antimonides: quasilinear bands and unusual transport, *Phys. Rev. B*, **50**: 11235-11238.

Singh D. J. and Mazin I. I. (1997), Calculated thermoelectric properties of La-filled skutterudites, *Phys. Rev. B,* **56:** 1650-1653.

Slack G. A. and Tsoukala V. G. (1994), Some properties of semiconducting $IrSb_3$, *J. Appl. Phys.*, **76:** 1665-1671.

Slack G. A. (1995), *CRC Handbook of Thermoelectrics*, ed. D. M. Rowe, CRC Press, New York, 407–440.

Snyder G. J. and Toberer E. S. (2008), Complex thermoelectric materials, *Nature Mater.*, **7:** 105-114.

Sofo J. O. and Mahan G. D. (1998), Electronic structure of $CoSb_3$: A narrow-band-gap semiconductor, *Phys. Rev. B*, **58**: 15620-15623.

Stewart G. R. (2001), Non-Fermi-liquid behavior in *d* and *f*-electron metals, *Rev. Mod.Phys.*, **73**: 797-855.

Sugawara H., Osaki S., Saha S. R., Aoki Y., Sato H., Inada Y., Shishido H., Settai R., Onuki Y., Harima H. and Oikawa K. (2002), Fermi surface of the heavy fermion superconductor $PrOs_4Sb_{12}$, *Phys. Rev. B***, 66:** 22-26.

Takeda N. and Ishikawa M. (1999), Anomalous magnetic properties of $CeRu_4Sb_{12}$, *Physica B,* **259-261:** 92-93.

Takegahara K., Harima H., Kaneta Y., Yanase A. (1993), Electronic band structures of $Ce_3Pt_3Sb_4$ and $Ce_3Pt_3Bi_4$, *J. Phys. Soci. Jpn.*, **62:** 2103-2111.

Takeda N., Ishikawa M. (2000), Superconducting and magnetic properties of filled skutterudite compounds $RERu_4Sb_{12}$ (RE=La, Ce, Pr, Nd and Eu), *J. Phys. Soc. Jpn.*, **69:** 868-873.

Takeghara K. and Harima H. (2003), FLAPW electronic band structure of the filled skutterudite $ThFe_4P_{12}$, *Physica B,* **329–333:** 464–466.

Tvergaard V. and Hutchinson J. W. (1988), Microcracking in ceramics induced by thermal expansion or elastic anisotropy, *J. Am. Ceram. Soc.*, **71:**157-166.

Uher C. (2001), Skutterudites: prospective novel thermoelectric, *Semiconduct Semimet, **68:*** 139-253.

Uher C. (2003), *Chemistry, Physics and Materials Science of Thermoelectric Materials: Beyond Bismuth Telluride,* edited by M. G. Kanatzidis and S. D. Mahanti and T. P. Hogan (Kluwer Academics, Plenum Publishers, New York, 2003), p. 121.

Varma C.M. (1976), Mixed-valence compounds, *Rev. Mod. Phys.*, **48**: 219-238.

Viennois R., Charar S., Ravot D., Haen P., Mauger A., Bentien A., Paschen S. and Steglich F. (2005), Spin fluctuations in the skutterudite compound $LaFe_4Sb_{12}$, *Eur. Phys. J. B,* **46**: 257-267.

Voigt W., Lehrbuch der Kristallphysik, Teubner, Leipzig, 1928.

Wang J. and Yip S. (1993), Crystal instabilities at finite strain, *Phys. Rev. Lett*., **71:** 4182-4185.

Wojciechowski K. T., Tobola J. and Leszczynski J. (2003), Thermoelectric properties and electronic structure of $CoSb_3$ doped with Se and Te, *J. Alloys Compd*, **361:** 19-27.

Wooten F. (1972), *Optical Properties of Solids*, Academic Press: New York.

Wu Z. and Cohen R. E. (2006), More accurate generalized gradient approximation for solids, *Phys. Rev. B*, **73**: 235116-6.

Xu B., Liang J., Li X., Sun J. F. and Yi L. (2011), Thermoelectric performance of the filled-skutterudite $LaFe_4Sb_{12}$ and $CeFe_4Sb_{12}$, *Eur. Phys. J. B*, **79:** 275-281.

Yang J., Zhang W., Bai S. Q., Mei Z. and Chen L. D. (2007), Dual-frequency resonant phonon scattering in $Ba_xR_yCo_4Sb_{12}$ (R=La, Ce, and Sr), *Appl. Phys. Lett*. **90:** 192111-3.

Zhao X. Y., Shi X., Chen L. D., Zhang W. Q., Zhang W. B. and Pei Y. Z. (2006), Synthesis and thermoelectric properties of Sr-filled skutterudite $Sr_yCo_4Sb_{12}$, *J. Appl. Phys.*, **99:** 053711-4.

Zheng J. -C. (2008), Recent advances on thermoelectric materials, *Front. Phys. China*, **3:** 269-279.